الجمهورية الجزائرية الديمقراطية الشعبية
REPUBLIQUE ALGERIENNE DEMOCRATIQUE ET POPULAIRE
وزارة التعليم العالي والبحث العلمي
MINISTERE DE L'ENSEIGNEMENT SUPERIEUR ET DE LA RECHERCHE SCIENTIFIQUE
جامعة فرحات عباس سطيف 1
UNIVERSITE FERHAT ABBAS SETIF1
UFAS1 (ALGERIE)

THESE

Présenté à la Faculté de Technologie

Pour l'Obtention du Diplôme de

Doctorat

Domaine : Science et Technologie
Filière : Electronique
Option : Electronique et commande industrielle

Par

Mr. TALBI Billel

Contribution à l'Amélioration de la Commande d'un Système de Pompage Photovoltaïque

Soutenue le : 20 / 06 / 2018 devant un jury composé de :

FERHAT-HAMIDA Abdelhak	Professeur	Univ. Sétif 1	Président
KRIM Fateh	Professeur	Univ. Sétif 1	Directeur de thèse
REKIOUA Toufik	Professeur	Univ. Bejaia	Co-Directeur de thèse
MENDIL Boubaker	Professeur	Univ. Bejaia	Examinateur
SEMECHEDDINE Samia	MCA	Univ. Sétif 1	Examinateur

Contribution to Improvement in Control of a Photovoltaic Pumping System

by

TALBI Billel

A thesis
presented to the University of Sétif 1
in fulfillment of the
thesis requirement for the degree of
Doctor of Philosophy
in
Electronics and Industrial Control

To my mother

To my Father

To my nephews Abdurrahman and Ayoub

To my sister and my brothers

Acknowledgement

*In the name of **ALLAH**, the Most Gracious and the Most Merciful. Thanks to **ALLAH** who is the source of all the knowledge in this world, for the strengths and guidance in completing this thesis.*

*I express my deep sense of gratitude and heart-felt thanks to my supervisor, Prof. **KRIM Fateh**, for his invaluable guidance, patience, kindness and consistent encouragement throughout the course of this work. I am very glad that I have pursued my doctoral studies under his excellent supervision. I would like to express my thanks to my co-supervisor, Prof. **REKIOUA Toufik**, for his comments and suggestions during the writing of this thesis.*

*I would like to express my appreciation to my thesis committee members: Prof. **FERHAT-HAMIDA Abdelhak**, Prof. **MENDIL Boubaker** and Dr. **SEMECHEDDINE Samia** for their discussions, suggestions, and feedbacks to improve my thesis.*

*I cannot forget to mention all my friends, **LEPCI** group, **LAIB Abdelbaset**, **SAHLI Abdeslem**, **FEROURA Hamza**, **BELAOUT Abdesslam**, **BOUYAHIA Semcheddine** and **ARABI Abderrazak** for their great friendship, help and support.*

TALBI Billel

Abstract

This thesis is part of the research work dedicated for exploitation of solar photovoltaic energy. Due to the increasing energy demands, the use of photovoltaic energy has increased significantly in the worldwide, especially in remote and isolation regions. Off-grid photovoltaic systems, particularly water pumping system, is becoming more widespread. The use of photovoltaic energy as an energy source for water pumping is considered as one of the most promising areas of the photovoltaic applications. The photovoltaic pumping systems are basically operated in two ways, with or without battery bank. The study presented in this thesis focuses on the improvement photovoltaic power extracting for a battery-less pumping system. In this context, many researchers are committed to invent the algorithms for extracting the maximum energy from a photovoltaic array. It is the principle named maximum power point tracking (MPPT), which is the main object of our research. In the first, various MPPT strategies based on fuzzy logic and predictive control for an off-grid photovoltaic system with resistive load have been developed to improve the performance of the perturb and observe (P&O) algorithm under sudden irradiance changes. The different MPPT strategies have been simulated and verified experimentally using a laboratory bench based on the photovoltaic emulator. Afterwards, a high-performance control scheme have been developed for a photovoltaic pumping system based on three-phase induction motor, in order to maximize the delivered power by the photovoltaic array, to protect the motor under sudden load drops, to regulate the DC-link voltage and to minimize the electromechanical losses in the conversion chain. The developed control scheme is based on fuzzy logic and predictive control. In addition, this scheme has been confirmed through simulation and real-time hardware in the loop system. Simulations presented in this thesis are performed with MATLAB/Simulink® environment, and practical implementation in real-time has been done through a dSPACE DS 1104 system.

Keywords : Photovoltaic energy; Photovoltaic pumping system; MPPT; Fuzzy logic; Predictive control.

Table of Contents

List of Figures

List of Tables

List of Acronyms

AC	Alternative current
ANN	Artificial neural network
CMPPT	Current based MPPT
DC	Direct current
DTC	Direct torque control
EPIA	European Photovoltaic Industry Association
FCS-MPC	Finite control set model predictive control
FLC	Fuzzy logic control (controller)
FOC	Field-oriented control
FOCV	Fractional open-circuit voltage
FSCC	Fractional short-circuit current
GA	Genetic algorithm
GW	Gigawatt
HIL	Hardware in the loop
IGBT	Insulated gate bipolar transistor
IM	Induction motor
IncCon	Incremental conductance
I-V	Current-voltage
MPC	Model predictive control
MPP	Maximum power point
MPPT	Maximum power point tracking
P&O	Perturb and observe
PCC	Predictive current control
PI	Proportional-integral
PID	Proportional-integral-derivative
PSO	Particle swarm optimization
PTC	Predictive and flux torque control
PV	Photovoltaic
P-V	Power-voltage
PWM	Pulse width modulation
STC	Standard test conditions

SVM	Space vector modulation
T-S	Takagi-sugeno
VSI	Voltage source inverter

List of Symbols

c_1, c_2, c_3	Constants depending on the pump geometric dimensions
C_{in}	Boost input capacitor (μF)
F	Viscose friction coefficient (N.m.s)
H	Head (m)
H_g	Geometrical height (m)
I_d	Diode current (A)
I_{inv}	Inverter input voltage (A)
I_L	Boost input current (A)
I_o	Reverse saturation current of the diode (A)
I_{ph}	Photovoltaic cell photocurrent (A)
I_{PV}	Photovoltaic array output current (A)
i_r	Rotor current vector (A)
I_r	Derived current by the shunt resistance (A)
i_s	Stator current vector (A)
I_{SC}	Photovoltaic array short-circuit current
J	Moment of inertia of the mechanical shaft (kg.m²)
k	Boltzmann constant (1.38×10^{-23} J/K)
k_p	Pump constant speed
L	Boost input inductor (mH)
L_m	Magnetizing inductances (H)
L_r	Rotor inductances (H).
L_s	Stator inductances (H).
n	Diode ideality factor
N_p	Number of cells connected in parallel
N_{pp}	Number of modules connected in parallel
N_s	Number of cells connected in series
N_{ss}	Number of modules connected in series
p	Number of pole pairs
q	Electronic charge (1.6×10^{-19} C)
Q	Flow rate (liter/s or m^3/s)
R	Boost resistive load (Ω)

R_r	Rotor resistance (Ω)
R_s	Photovoltaic cell series resistance (Ω)
R_{sh}	Photovoltaic cell shunt resistance (Ω)
R_{ss}	Stator resistance (Ω)
S	Switching signal of the Boost converter
S_a, S_b, S_c	Switching signals of the inverter.
T	Absolute temperature (K)
T_e	Electromagnetic torque (N.m)
T_L	Load torque connected to the IM (N.m)
T_s	Sample time of the MPC algorithm (μs)
v_{aN}, v_{bN}, v_{cN}	Phase-to-neutral voltages of the inverter (V)
V_C	Boost output voltage (V)
V_{DC}	DC-link voltage (V)
V_{OC}	Photovoltaic array open-circuit voltage (V)
V_{PV}	Photovoltaic array output voltage (V)
v_s	Stator voltage vector (V)
V_t	Thermal voltage (V)
w_i	The weight coefficient
θ_s	Stator flux angle (rad)
λ	Weighting factor
φ_r	Rotor flux vector (Wb)
φ_s	Stator flux vector (Wb)
φ_s^*	Complex conjugate value of the stator flux vector (Wb)
ω	Rotor electrical speed (rad/s)
ω_m	Rotor mechanical speed (rad/s)
ω_o	Angular frequency (rad/s)

Chapter 1

Introduction

1.1 INTRODUCTION TO PHOTOVOLTAICS

In recent years, electricity production from renewable energy sources has attracted great attention in both academia and industry due to the concerns about the global climate change and energy supplies. By 2016, the power generation from renewable energy sources worldwide exceeded 2017 gigawatt (GW) representing approximately 19.3% of global energy consumption [1.1]. Among all the renewable energy sources, solar photovoltaic (PV) energy is increasingly becoming mainstream and competitive with conventional sources of energy. This success is essentially due to the technological developments in solar PV energy system as well as the encouragement of governments incentive programs.

A recent study shows the potential of the solar based energy generation using the PV panel to fulfill the world's energy demand. The annual and cumulative installed PV power capacity worldwide is shown in Figure 1.1 [1.1]. The cumulative installed capacity increased exponentially from 6 GW in 2006 to 303 GW by 2016. It was anticipated on a moderate scale that the cumulative PV capacity would reach 1100 GW by 2030, according to European Photovoltaic Industry Association (EPIA) [1.2]. In 2016, approximately 75 GW of new PV power was installed, which is equivalent to the installation of more than 31000 solar panels every hour [1.1]. The PV energy industry demonstrated an excellent growth rate of more than 30% by the end of 2016. The key reason for this significant development is the increased competitiveness of PV energy because of the cost reduction of PV modules and the introduction of economic incentives or subsidies. This has made PV-generated electrical energy cost-effective and competitive in some regions of the world with good solar irradiation conditions. In addition, PV systems can range from small scale to large scale, making it possible to

implement PV systems by individuals compared to other renewable energy sources (wind, marine, geothermal, etc.) that have higher capital costs.

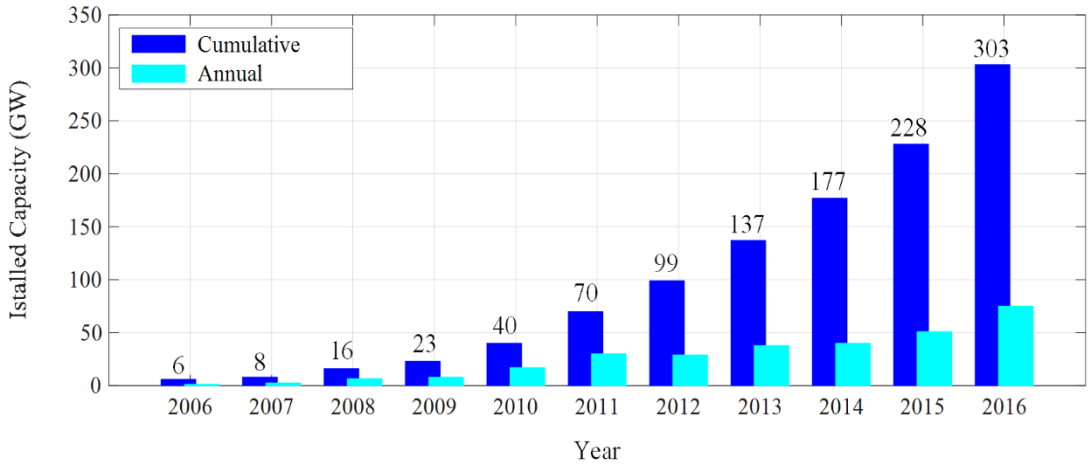

Figure 1.1: Global annual and cumulative installed PV power from 2006 to 2016.

Generally, photovoltaic systems operate in two different modes: off-grid and grid-connected [1.3-4]. Grid-connected PV energy conversion systems are designed to be able to inject a sinusoidal current into the utility grid. These systems can be grouped into two classes of applications: distributed generation or centralized power systems [1.3-4]. Distributed generation systems are installed to deliver power to a grid-connected customer or directly to the grid. On the other hand, centralized PV power systems offer bulk power in order to reduce fuel sources dependency and greenhouse gases.

Off-grid PV systems, as their name implies, are designed to function independently of the utility grid [1.3-4]. These systems are composed of several components that convert solar energy into electric energy in a controlled, reliable and efficient manner in order to supply a DC or AC loads. Off-grid PV system is one of the best options for meeting electricity demands in remote or isolation regions where utility power is unavailable or costly. Among the numerous applications of the off-grid PV systems, water pumping system is one of the most promising and attractive in various areas such as domestic and livestock water supplies, small-scale irrigation systems and fish farms.

1.2 BACKGROUNDS OF PHOTOVOLTAIC PUMPING SYSTEMS

In various remote and isolation regions, hand pumps or diesel-drive pumps are used for water supply. Diesel pumps consume fossil fuel, affect environment, need more maintenance and are less reliable [1.5]. Due to the cost reduction of PV modules and the developments in

power electronics systems technology, photovoltaic powered water pumping systems have received more and more attention and become a reliable alternative for diesel-drive pumps over the last few years.

A PV pumping system is operated independently of the utility grid and is composed of several components such as PV array, power converters, electrical motor, water pump and storage element which can be a battery bank or/and a water tank. PV pumping systems are generally installed with battery bank [1.6], and also can work without chemical storage elements. In battery-less PV pumping systems, the role of batteries is substituted by fluid storage, and steady-state operation depends on the amount of available power, in order to increase the reliability and decrease the cost of such systems (batteries are heavy and expensive and have short lifetime). PV pumping system can be designed to supply either AC or DC motors. For DC motor pumping system, DC motor can be connected directly to the PV array [1.7] or utilize single-stage DC-DC power converters such as the boost [1.8], buck [1.9], buck-boost [1.10] or Cuk [1.11-12] converters. The DC-DC power converters in such systems play a major role in changing the voltage or current level to track the maximum power point (MPP) of the PV array, as shown in Figure 1.2.

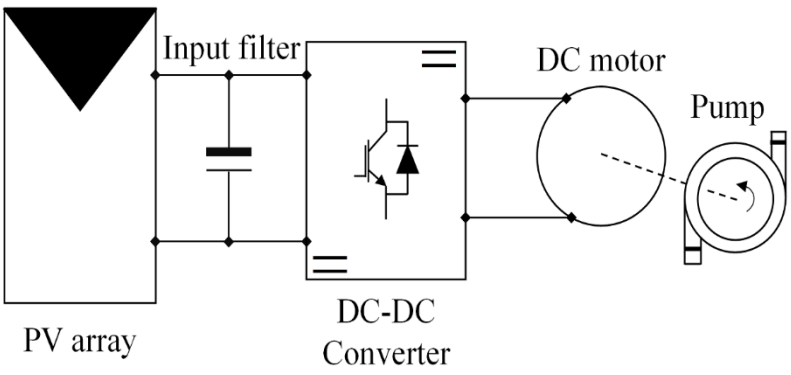

Figure 1.2: Block diagram of a single-stage PV pumping system using DC motor.

However, the problems associated with DC motors are the high cost and the regular maintenance requirement due to their commutator and brushes. On the other hand, AC motors are generally more reliable and less costly than the DC motors. Many different AC motors have been proposed in PV water pumping [1.12-28]. The main advantages and disadvantages of each of these motors are summarized in Table 1.1. In PV water pumping system driven by AC motor, the MPP is extracted from the PV array to feed the motor-pump set. Single and two stages topologies are commonly used topologies in PV pumping systems using AC motor [1.13-21].

TABLE 1.1: Advantages and disadvantages of the different types of motor used for PV water pumping system.

Motor	Advantages	disadvantages
Brushed DC [1.7-12]	• Simple speed control	• Brushes need to be changed periodically • High initial and maintenance cost
Brushless DC [1.13, 21, 25, 26, 27]	• Lower maintenance • High efficiency	• High initial cost • Possible demagnetization • Control complexity
Switched reluctance motor [1.22]	• Lower cost • Simple construction • No permanent magnets	• High iron losses • Possible mechanical resonance • Control complexity
Permanent magnet synchronous motor [1.14, 23]	• High power density • Lower maintenance cost • High efficiency • Compact volume	• High initial cost • High weight • Possible demagnetization
Open-end winding induction motor [1.18-19]	• Simple construction • Reduced losses and improved efficiency	• High initial and maintenance cost • Increased converter cost
Induction motor [1.15, 16, 17, 20, 24, 28]	• Simple and rugged in construction • Lower initial and maintenance cost • Lower torque oscillations • Available for single or three-phase supply • Inverters are designed to regulate frequency to maximize power to the motor in response to changing insolation levels • These motors can handle larger pumping requirements	• Control complexity • Less efficiency

In single-stage PV pumping system containing AC motor, the system utilizes a single conversion unit (DC-AC power inverter) to track the MPP and interface the PV system to AC motor. In this topology, PV maximum power is delivered into AC motor with high efficiency

and low cost. However, to fulfill AC motor requirements, this topology requires a step-up transformer, which reduces the system efficiency and increases cost, or a PV array with a high DC voltage, this solution is impractical for fractional kilowatt rating (< 1 kW) PV system. Moreover, inverter control is complicated because the control objectives, such as maximum power point tracking (MPPT) and reduction the electromechanical conversion losses, are simultaneously considered. Different types of DC-AC inverters have been applied to enhance and regulate the performance, such as two-level [1.13-17], multilevel [1.18-20] and Z source voltage inverters [1.21]. Figure 1.3 illustrates the block diagram of a single-stage PV pumping system using AC motor with and without a step-up transformer.

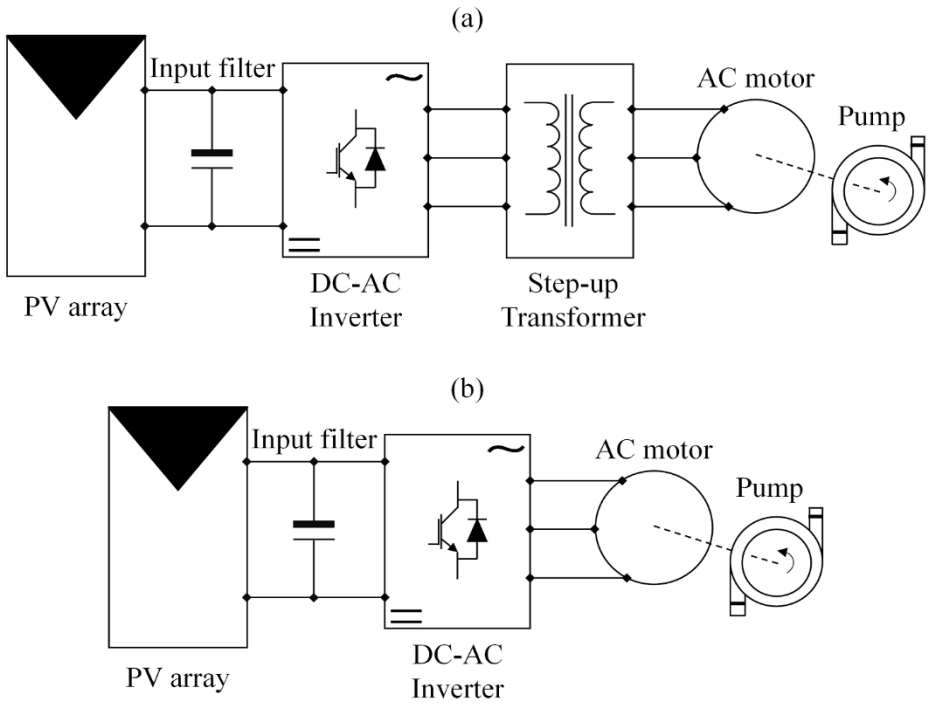

Figure 1.3: Block diagram of a single-stage PV pumping system using AC motor (a) with and (b) without a step-up transformer.

In two-stage PV pumping system containing AC motor, two conversion stages are used. The first stage uses a DC-DC converter (boost [1.23-24], buck-boost[1.25], Cuck [1.26], zeta [1.27] and push–pull [1.28]) for boosting the PV output voltage level and tracking the MPP. A DC-AC inverter is utilized in the second stage to regulate the DC-link voltage and to convert the PV power to AC power for meeting AC motor. The advantages of the two-stage topology lie in the simplicity of designing the control scheme, since the control requirements are disturbed between the two stages. A block diagram of a two-stage PV pumping system using AC motor is illustrated in Figure 1.4.

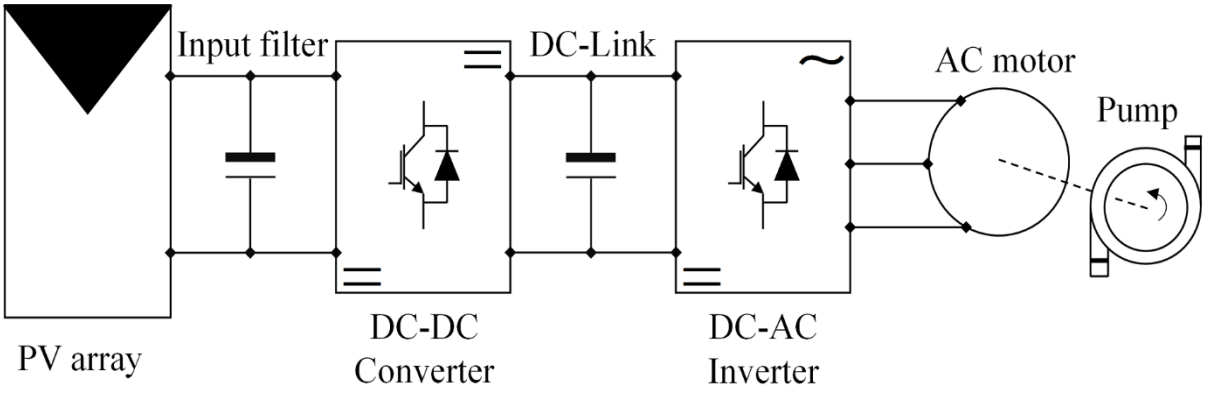

Figure 1.4: Block diagram of a two-stage PV pumping system using AC motor.

1.3 MOTIVATION

The design of an effective photovoltaic pumping system without the use of electrochemical storage elements represents a great challenge. It is necessary to deal with the effect of the different operation conditions on the entire energy conversion chain. In other words, it is required to obtain the best performance from each system component over a wide input power range.

However, the output power of a typical PV array can considerably change its position during the day due to the varying atmospheric conditions. Therefore, it is necessary to design a controller that is able to set the value of voltage or current of the PV array and always ensure the working within its maximum power point. Several MPPT controllers have been proposed throughout the literature; nevertheless, most of those controllers have certain disadvantages such as instability, steady-state power oscillation, etc; MPPT schemes that address those challenges suffer from computational burden and increased hardware costs.

Motivated by the above concerns, this thesis focuses on the formulation of new MPPT algorithms that are simple and robust to the atmospheric condition changes. The algorithms shall take into consideration all the challenges and concerns that are presented in the literature (e.g. sudden changing atmospheric conditions, tracking accuracy, etc.)

Furthermore, the electromechanical power conversion in the PV pumping system must be with minimum losses for different atmospheric conditions. Therefore, the DC-AC inverter in the system should have a good DC-link controller and high drive motor performance, which can offer fast transient response and high control accuracy. Moreover, the occurrence of load drops due to any reason might lead to increase the motor voltage in battery-less PV system, which can may damage the motor. Thus, the protection of motor will take into account in the control scheme.

1.4 THESIS ORGANIZATION

The research presented in this thesis is organized into six chapters. The work carried out in each chapter is summarized as follows:

Chapter-2: This chapter decribes the components models of an off-grid photovoltaic system for water pumping. These models are used in the following chapters for control design and simulation work.

Chapter-3: In this chapter, a review of the most widely used maximum power point algorithm for photovoltaic systems is presented. Furthermore, a short overview of the state of the art in control of three-phase induction motor is described in this chapter.

Chapter-4: Two variable current step size perturb and observe maximum power point tracking algorithms for photovoltaic systems are presented in this chapter. The proposed algorithms are employed with a model predictive current controller. Simulation and experimental results are provided to demonstrate the validity and the performance improvement of the proposed algorithms.

Chapter-5: In this chapter, a high-performance control scheme is proposed for battery-less photovoltaic pumping system based on three phase induction motor. The proposed control scheme based on the fuzzy logic and model predictive control strategies. simulations and real-time hardware in the loop implementations are provided to confirm the performance improvement of the proposed control scheme.

Chapter-6: The thesis general conclusion and the author's contributions are summarized. Possible extensions to the research presented in this thesis are suggested.

REFERENCES

[1.1] Renewable Energy Policy Network for the 21st Centuray (REN21), 2016. Renewables Global Status Report. [Online]. Available: http://www.ren21.net/.

[1.2] European Photovoltaic Industry Association (EPIA), 2012, Global Market Outlook for Photovoltaics until 2016. [Online]. Available: http://www.epia.org/.

[1.3] Ellabban, O., Abu-Rub, H., Blaabjerg F., 2014. Renewable energy resources: current status, future prospects and their enabling technology. Renew. Sustain. Energy Rev.39, 748–764.

[1.4] Madeti, S.R., Singh, S.N., 2017. Monitoring system for photovoltaic plants: A review. Renew. Sustain. Energy Rev. 67, 1180–1207.

[1.5] Periasamy, P., Jain, N.K., Singh, I.P., 2015. A review on development of photovoltaic water pumping system. Renew. Sustain. Energy Rev. 43, 918–925.

[1.6] Rahrah, K., Rekioua, D., Rekioua, T., Bacha, S., 2015. Photovoltaic pumping system in Bejaia climate with battery storage. Int. J. Hydrogen Energy 40, 13665–13675.

[1.7] Kolhe, M., Joshi, J.C., Kothari, D.P., 2004. Performance analysis of a directly coupled photovoltaic water-pumping System. IEEE Trans. Energy Convers. 19, 613–618.

[1.8] Akbaba, M., 2006. Optimum matching parameters of an MPPT unit used for a PVGpowered water pumping system for maximum power transfer. Int. J. Energy Res. 30, 395–409.

[1.9] Elgendy, M.A., Zahawi, B., Atkinson D.J., 2010. Comparison of directly connected and constant voltage controlled photovoltaic pumping systems. IEEE Trans. Sustain. Energy 1, 184–192.

[1.10] El-Khatib, M.F., Shaaban, S., El-Sebah, M.I.A, 2017. A proposed advanced maximum power point tracking control for a photovoltaic-solar pump system. Sol. Energy 158, 321–331.

[1.11] Algazar, M.M., AL-monier, Hamdy, EL-halim, H.A., Salem, M.E.E.K., 2012. Maximum power point tracking using fuzzy logic control. Int. J. Electr. Power Energy Syst. 39, 21–28.

[1.12] Mohamed, A.A.S., Berzoy, A., Mohammed, O., 2017. Design and hardware implementation of FL MPPT control of PV systems based on GA and small-signal analysis. IEEE Trans. Sustain. Energy 8, 279–290.

[1.13] Kumar, R., Bhim, S., 2016. Single stage solar PV fed brushless DC motor driven water pump. IEEE Trans. Ind. Appl. 52, 2315–2322.

[1.14] Antonello, R., Carraro, M., Costabeber, A., Tinazzi, F., Zigliotto, M., 2017. Energy-efficient autonomous solar water-pumping system for permanent-magnet synchronous motors. IEEE Trans. Ind. Electron. 64, 43–51.

[1.15] Betka, A., Attali, A., 2010. Optimization of a photovoltaic pumping system based on the optimal control theory. Sol. Energy 84, 1273–1283.

[1.16] Packiam, P., Jain, N.K., Singh, I.P., 2013. Microcontroller-based simple maximum power point tracking controller for single-stage solar stand-alone water pumping system. Progr Photovolt: Res Appl. 21, 462–471.

[1.17] Chergui, M.-I., Bourahla, M., 2013. Application of the DTC control in the photovoltaic pumping system. Energy Convers. Manage. 65, 655–662.

[1.18] Jain, S., Thopukara, A.K., Karampuri, R., Somasekhar, V.T., 2016. An integrated control algorithm for a single-stage PV pumping system using an open-end winding induction motor, IEEE Trans. Ind. Electron. 63, 956–996.

[1.19] Jain, S., Thopukara, A.K., Karampuri, R., Somasekhar, V.T., 2015. A single-stage photovoltaic system for a dual-inverter-fed open-end winding induction motor drive for pumping applications. IEEE Trans. Power Electron. 30, 4809–4818.

[1.20] Elkholy, M.M., Fathy, A., 2016. Optimization of a PV fed water pumping system without storage based on teaching-learning-based optimization algorithm and artificial neural network. Sol. Energy 139, 199–212.

[1.21] Niapour, S.A.K.H.M., Danyali, S., Sharifian, M.B.B., Feyzi, M.R., 2011. Brushless DC motor drives supplied by PV power system based on Z-source inverter and FL-IC MPPT controller. Energy Conv. Manage. 52, 3043–3059.

[1.22] Bhim, S., Kumar, R., 2016. Solar Powered Water Pumping System Employing Switched Reluctance Motor Drive. IEEE Trans. Ind. Appl. 52, 3949–3957.

[1.23] Farhat, M., Barambones, O., Fleh, A., Sbita, L., 2016. Variable structure MPP controller for photovoltaic pumping system. Trans Inst Measure Control 39, 1–10.

[1.24] Achour, A., Rekioua, D., Mohammedi, A., Mokrani, Z., Rekioua, T., Bacha, S., 2016. Application of direct torque control to a photovoltaic pumping system with sliding-mode control optimization. Electric Power Compon. Syst. 44, 172–184.

[1.25] Bhim, S., Kumar, R., 2016. Simple brushless DC motor drive for solar photovoltaic array fed water pumping system. IET Power Electron. 9, 1487–1495.

[1.26] Kumar, R., Bhim, S., 2017. Solar PV powered BLDC motor drive for water pumping using Cuk converter. IEEE Trans. Ind. Appl. 11, 222–232.

[1.27] Kumar, R., Bhim, S., 2016. BLDC motor-driven solar PV array-fed water pumping system employing zeta converter. IEEE Trans. Ind. Appl. 52, 2315–2322.

[1.28] Vitorino, M.A., de Rossiter, C.M.B., Jacobina, C.B., Lima, A.M.N., 2011. An effective induction motor control for photovoltaic pumping. IEEE Trans. Ind. Electron. 58, 1162–1170.

Chapter 2

Modeling of the Photovoltaic Pumping System Components

2.1 INTRODUCTION

Following the discussion in the previous chapter, a typical configuration of a battery-less photovoltaic (PV) water pumping system, shown in Figure 2.1, is a promising solution for an effective, economic and robust PV pumping system. The system includes a PV generation system, which is a group of series-parallel connected modules (PV array). A passive input filter, a capacitor, which is used to reduce the current and voltage ripple (and hence power) at the PV side, follows the PV array. The input filter is followed by a DC-DC boost converter, which is used to perform the maximum power point tracking (MPPT) of the PV array and elevate its voltage. The DC-DC converter is connected through DC-link (capacitor) to the three-phase two-level inverter. The inverter is used to convert the DC power to AC power and feeds the energy to the utility induction motor (IM) with high power quality. The IM is directly coupled with a centrifugal pump in order to convert the mechanical energy to hydraulic energy.

In order to control the PV pumping system, an essential step consists in modeling the installation components. Hence, this chapter presents the modeling of the proposed PV pumping system components. The mathematical models for PV array, both the boost and invert power converters, IM and centrifugal pump are explicitly developed.

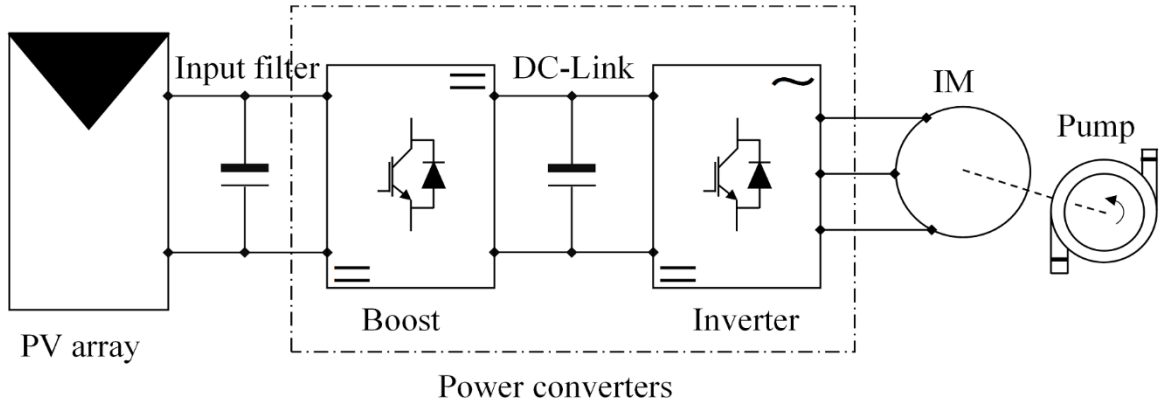

Figure 2.1: Block diagram of the proposed PV pumping system.

2.2 PHOTOVOLTAIC ARRAY MODELING

Photovoltaic arrays are made of a number of PV modules connected in series and in parallel, where the basic component within module is PV cells. The type of connection depends on the voltage and current levels at which it is desired that the power treating system dedicated to the PV array operate. Figure 2.2 represents a PV array system.

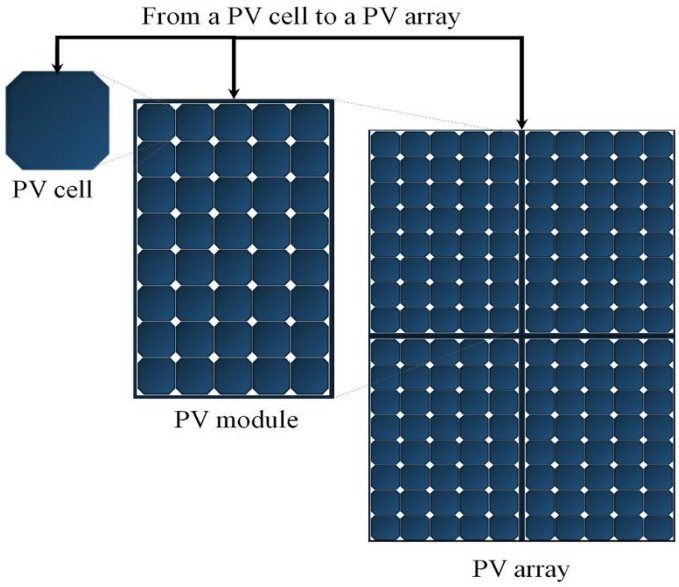

Figure 2.2: PV array system.

2.2.1 Photovoltaic Cell

The PV cell is principally a p-n junction fabricated in a thin wafer of semiconductor. The solar energy is directly converted to electricity through photovoltaic effect. The electrical characteristics of a PV cell are nonlinear and are highly dependent on solar irradiation and

temperature. Different equivalent circuit models of PV cell have been discussed in the literature [2.1-5]. For simplicity and accuracy, the single diode model is the most studied and used in this work. In this model, the PV cell can be electrically modeled by an equivalent circuit such as the one shown in Figure 2.3, with a photocurrent source in parallel with a diode, a shunt resistance R_{sh} and a series resistance R_s.

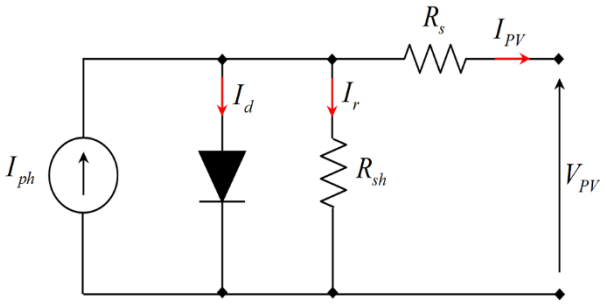

Figure 2.3: The equivalent circuit of a PV cell.

The model of Figure 2.3 can be mathematically described by the following equation [2.1]:

$$I_{PV} = I_{ph} - I_d - I_r = I_{ph} - I_o\left(e^{\frac{V_{PV}+R_s I_{PV}}{nV_t}} - 1\right) - \frac{V_{PV}+R_s I_{PV}}{R_{sh}} \tag{2.1}$$

where:

I_{PV} : is the cell output current (A).

I_{ph} : is the cell photocurrent (A).

I_d : is the diode current (Shockley equation) (A).

I_r : is the derived current by the shunt resistance (A).

I_0 : is the reverse saturation current of the diode (A).

V_{PV} : is the cell output voltage (V).

R_s : is the cell series parasitic resistance (Ω).

R_{sh} : is the cell shunt parasitic resistance (Ω).

n : is the diode ideality factor

V_t : is the thermal voltage given by:

$$V_t = \frac{kT}{q} \tag{2.2}$$

where:

k : is the Boltzmann constant (1.38×10^{-23} J/K).

T : is the absolute temperature (K).

q : is the electronic charge (1.6×10^{-19} C)

2.2.2 Photovoltaic Module

Due to low power ratings of each individual PV cell, the cells are connected in series-parallel configuration form a PV module in order to produce required power. Usually, the PV module is rated by its DC output power under standard test conditions (STC) and commercially STC is specified at an irradiance of 1000 W/m² and a 25°C PV cell temperature [2.1]. Figure 2.4 shows the equivalent circuit of a PV module. The nonlinear current-voltage characteristic of the PV module is modeled by the following equation where all cells are identical [2.1]:

$$I_{PV} = N_p I_{ph} - N_p I_o \left(e^{\frac{N_s V_{PV} + (N_s/N_p) R_s I_{PV}}{n N_s V_t}} - 1 \right) - \frac{N_s V_{PV} + (N_s / N_p) R_s I_{PV}}{(N_s / N_p) R_{sh}} \qquad (2.3)$$

where:

I_{PV} : is the module output current (A).

V_{PV} : is the module output voltage (V).

N_s : is the number of cells connected in series

N_p : is the number of cells connected in parallel

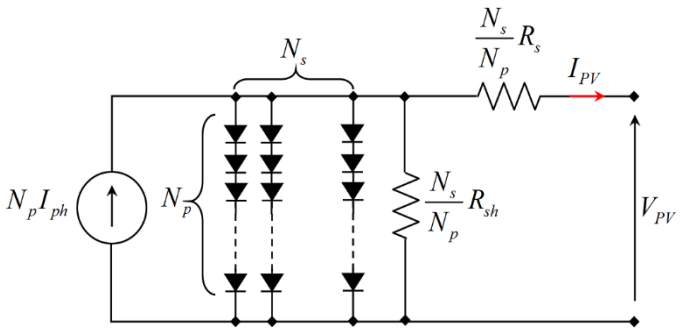

Figure 2.4: The equivalent circuit of a PV module.

The PV module considered for this thesis is pb solar BP SX 120 of 120 Wp. The electrical nominal characteristics at STC of this module are listed in Table 2.1. The power versus voltage (P-V) and the current versus voltage (I-V) characteristics of the pb solar BP SX 120 module under STC are shown in Figure 2.5. A PV module can produce the power at a point, called an operating point, anywhere on the I-V curve. Three operating points on the I-V curve are important in defining the performance of a PV module, i.e., the maximum power point, the

short-circuit current and the open-circuit voltage.

- ❖ The maximum power point (MPP) is the point on the I-V curve at which the PV module works with maximum power output.
- ❖ The short-circuit current point characterized by a zero voltage at the PV module terminals and by a short-circuit current (I_{SC}).
- ❖ The open-circuit voltage point characterized by a zero current in the PV panel terminals and by an open-circuit voltage (V_{OC}).

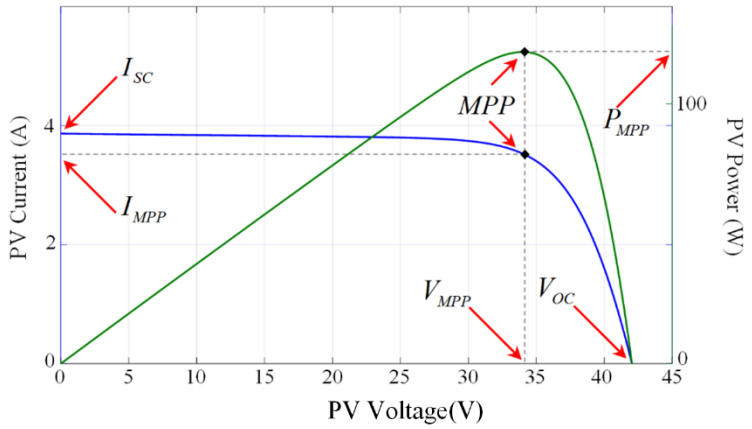

Figure 2.5: I-V and P-V characteristics of pb solar BP SX 120 module under STC.

TABLE 2.1: Nominal Operating Conditions for pb solar BP SX 120 module [2.6].

PV array	**Values (STC)**
Open-circuit voltage (V_{OC})	42.1 V
Optimum operating voltage (V_{MPP})	33.7 V
Short-circuit current (I_{SC})	3.87 A
Optimum operating current (I_{MPP})	3.56 A
Maximum power (P_{MPP})	120 Wp
Temperature coefficient of V_{OC}	-0.160 V/°C
Temperature coefficient of I_{SC}	0.065 %/°C

2.2.3 Photovoltaic Array

A PV array is made of a number of PV modules connected in series-parallel arrangement to obtain the desired voltage, current and power. The size of the PV array varies from a single PV module to any number of modules. The PV array output current and voltage can be computed from equations (2.4) and (2.5) respectively [2.7]:

$$I_{PVt} = N_{pp} I_{PV} \tag{2.4}$$

$$V_{PVt} = N_{ss} V_{PV} \tag{2.5}$$

where:

I_{PVt} : is the array output current (A).

V_{PVt} : is the array output voltage (V).

I_{PV} : is the module output current (A).

V_{PV} : is the module output voltage (V).

N_{ss} : is the number of modules connected in series

N_{pp} : is the number of modules connected in parallel

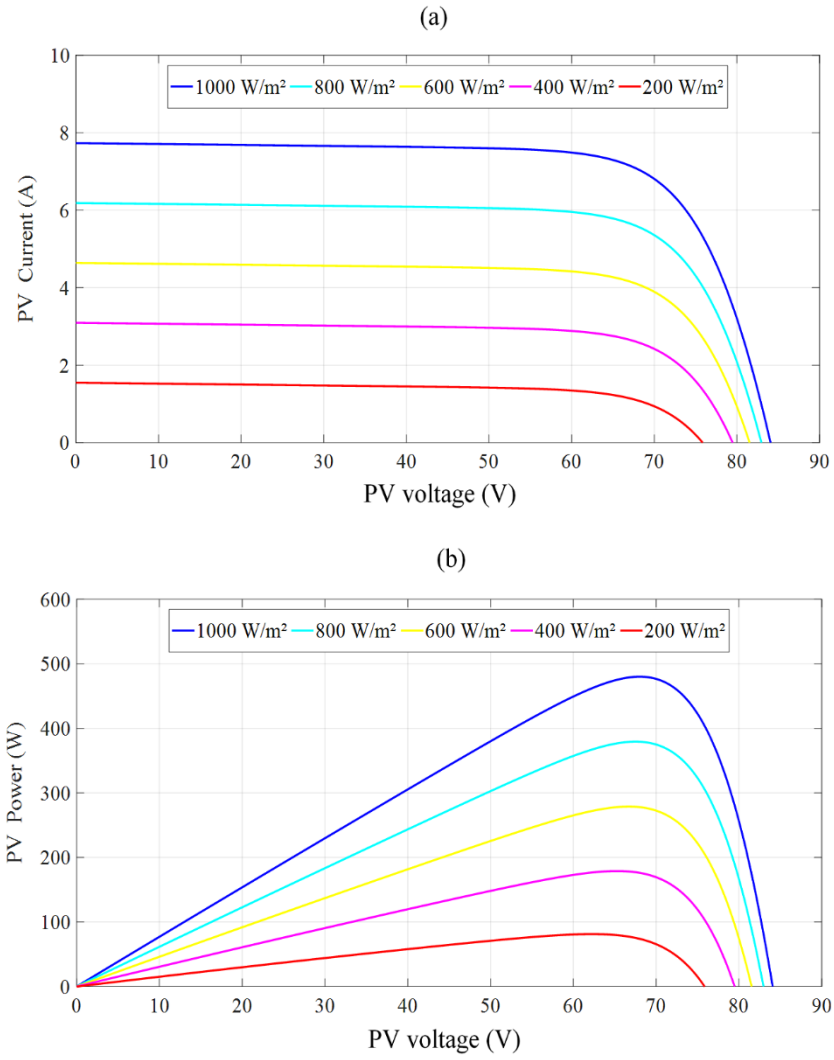

Figure 2.6: (a) I-V and (b) P-V characteristics of PV array under different levels of solar irradiation at 25°C.

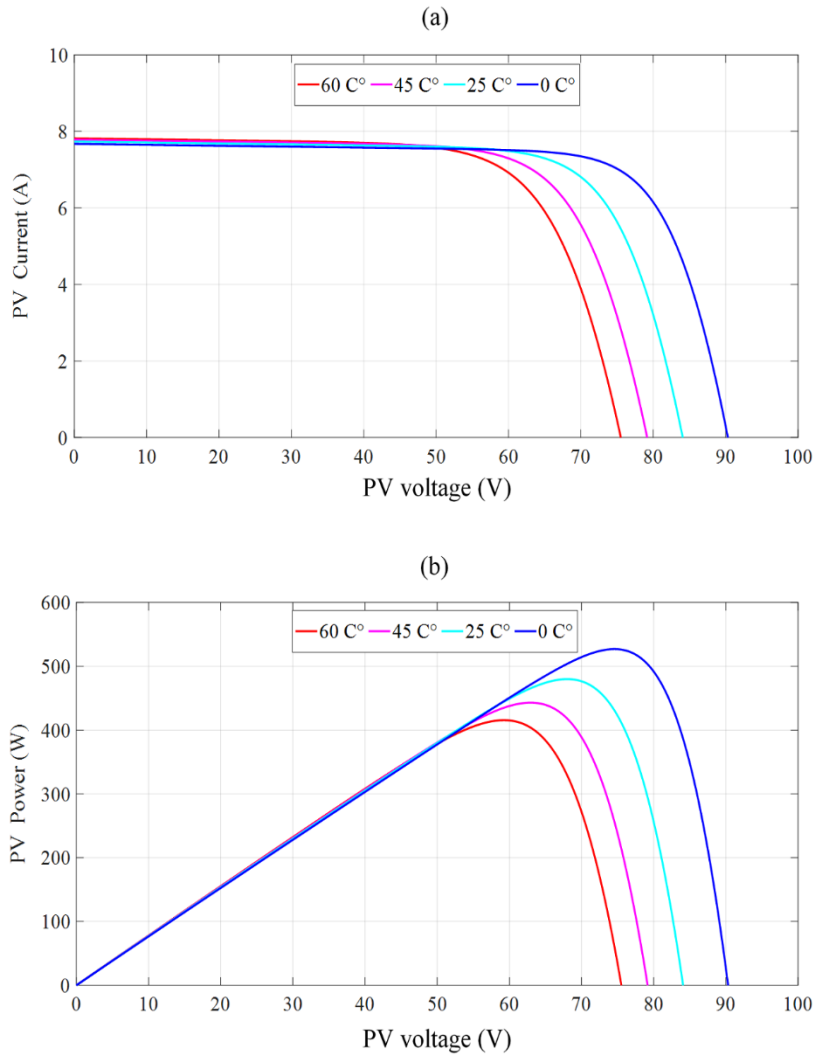

Figure 2.7: (a) I-V and (b) P-V characteristics of PV array under different temperatures at 1000 W/m².

The electrical behavior of the PV array is generally represented by the power versus voltage (P-V) and the current versus voltage (I-V) characteristics. A PV array with four pb solar BP SX 120 modules, connected 2×2 in series and parallel, is considered. Figures 2.6 and 2.7 highlighted the strong dependence of the considered PV array performances on the temperature and irradiance levels. The irradiance has a significant effect on the short-circuit current value, as shown in Figure 2.6. On the contrary, the irradiance level has a slight effect on the open-circuit current value. On the other hand, the temperature has a negligible effect on the short-circuit value but it has an important effect on the open circuit voltage value, as shown in Figure 2.7. It is worth noting that the temperature usually changes quite slowly, so that the temperature value is often considered a constant with respect to the variation the irradiation level can be subjected to during the day. This simplifying assumption will be also adopted in this thesis.

2.3 POWER CONVERTERS MODELING

The power electronic converters used in the PV system are receiving more attention due to their flexible controllability and maturing technology. For a PV array, the output power is a DC power and variable as the conditions climatic changes. It cannot be directly connected to the IM. Thus, the PV power should be maximized, and then converted to AC power, which meets the IM requirement. This process has two conversion stages: DC-DC and DC-AC, as shown in Figure 2.1.

2.3.1 DC-DC Boost Converter

The device responsible for maintaining the PV array on the maximum power point, MPP, is the DC/DC converter. Among several options, it was chosen the boost converter. This converter is very simple in structure, design and control and is capable of elevating voltage and controlling the MPPT also, it offers a continuous current at the input. The boost converter can be found implemented with an inductor, a power electronic switch (IGBT), a diode and capacitor [2.8-9]. The equivalent boost circuits during switch-on and switch-off intervals for ideal switch are shown in Figure 2.8.

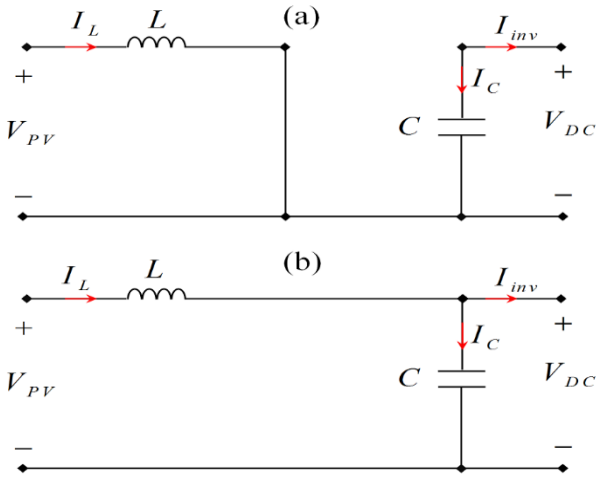

Figure 2.8: Equivalent boost circuits: (a) switching on and (b) switching off.

When the switch is considered as closed (Figure 2.8(a)), the boost converter operation can be described by the well-known system of equations as follows:

$$\frac{d}{dt} I_L = \frac{1}{L} V_{PV} \tag{2.6}$$

$$\frac{d}{dt} V_{DC} = -\frac{1}{C} I_{inv} \tag{2.7}$$

In case of the open switch (Figure 2.8(b)), the previous equation system can be expressed as:

$$\frac{d}{dt}I_L = \frac{1}{L}(V_{PV} - V_{DC}) \tag{2.8}$$

$$\frac{d}{dt}V_{DC} = \frac{1}{C}(I_L - I_{inv}) \tag{2.9}$$

The aforementioned equations (Eq. 2.6 to 2.9) can be expressed as follows:

$$\frac{d}{dt}I_L = -(1-S)\frac{1}{L}V_{DC} + \frac{1}{L}V_{PV} \tag{2.10}$$

$$\frac{d}{dt}V_{DC} = (1-S)\frac{1}{C}I_L - \frac{1}{C}I_{inv} \tag{2.11}$$

where:

I_L : is the boost input current (A).

V_{PV} : is the boost input voltage (V).

V_{DC} : is the boost output voltage (V).

I_{inv} : is the boost output current (A).

L : is the boost input inductor (mH).

C : is the boost output capacitor (μF).

S : is the switching signal taking value from the discrete set $S = [1, 0]$.

2.3.2 DC-AC Converter

The power circuit of the two-level voltage source inverter (VSI) is presented in Figure 2.9. It uses six bidirectional switches to connect the three-phase IM directly. Each bidirectional switch is composed of an IGBT with a parallel diode, as shown in Figure 2.9. The two switches of each inverter leg must operate in a complementary mode to avoid the short-circuit of the DC-link. It is assumed that the switches and diodes are ideal devices. The inverter output voltages can be expressed in terms of DC-link voltage and switching states as follows [2.10-11]:

$$v_{aN} = S_a V_{DC} \tag{2.12}$$

$$v_{bN} = S_b V_{DC} \tag{2.13}$$

$$v_{cN} = S_c V_{DC} \tag{2.14}$$

where:

v_{aN}, v_{bN}, v_{cN} : are the phase-to-neutral (N) voltages of the inverter (V).

S_a, S_b, S_c : are the switching signals of the inverter.

V_{DC} : is the inverter input voltage (V).

Considering the unitary vector *a*, which represents the 120° phase displacement between the phases, the output voltage vector *v* can be defined as [2.10-11]:

$$v = \frac{2}{3}(v_{aN} + a v_{bN} + a^2 v_{cN}) \tag{2.15}$$

where:

$$a = e^{j2\pi/3} = -\frac{1}{2} + j\frac{\sqrt{3}}{2} \tag{2.16}$$

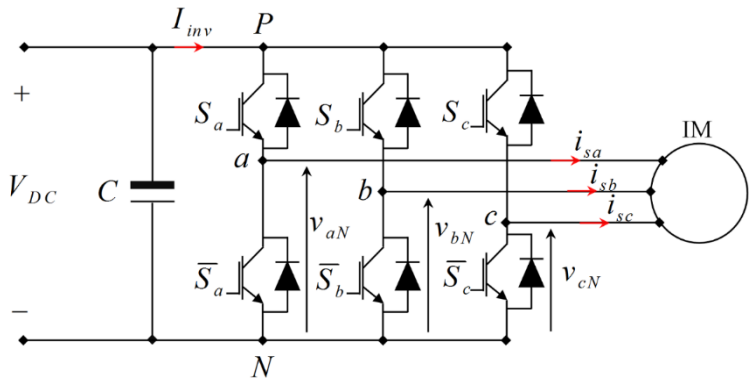

Figure 2.9: Two-level inverter topology.

The possible number of combinations for the gating signals (S_a, S_b and S_c) becomes eight (2^3), and consequently eight voltage vectors for the inverter are obtained. A space vector diagram that contains these eight combinations is shown in Figure 2.10.

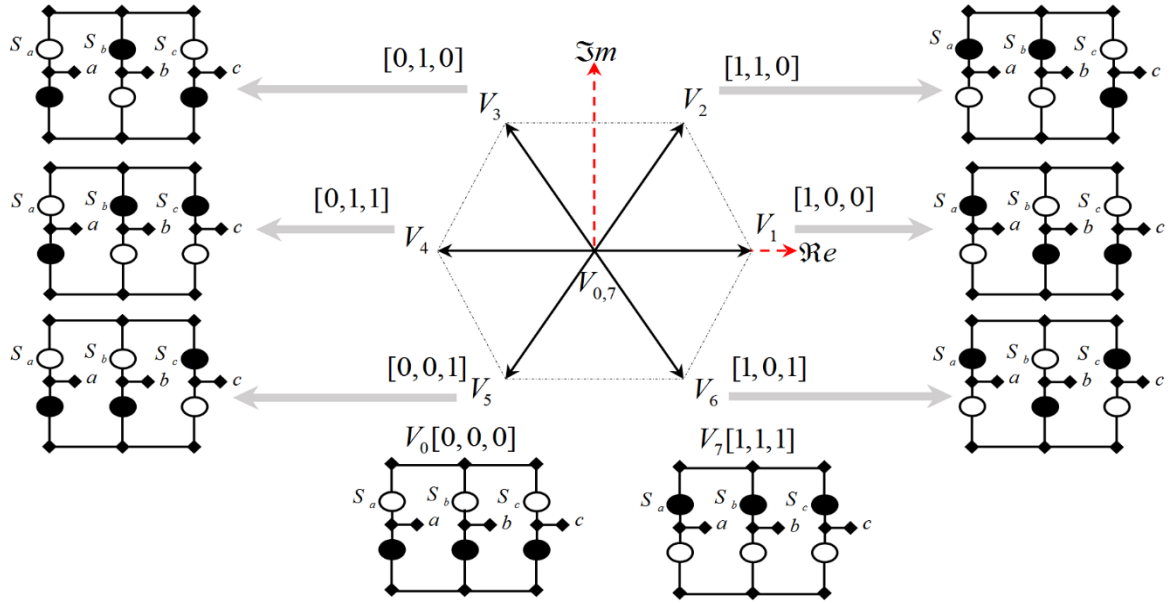

Figure 2.10: Voltage vectors in the complex plane

2.4 INDUCTION MOTOR MODELING

The attractiveness of induction motors (IM) is due to their robustness and operation reliability. They are small in volume and weight, do not require much maintenance, and are of reasonable cost compared to the DC motor. The IM are classified into two types, wound and squirrel-cage, which describes the form of the rotor winding. The squirrel-cage rotor is more mostly applied and it has the rotor winding connection as a short-circuit without any external connections [2.12-13]. The IM considered in this thesis is the squirrel-cage type.

IM contains two main components in its structure: stator winding and rotor winding. The three-phase windings have a spatial phase shift of 120°and suppling by an AC power source, which will create a rotating magnetic field, the so-called stator flux. Then, the constantly changing flux will cause a current induced in the rotor winding, afterward this induced current will generate a magnetic field, the so-called rotor flux. Since both fluxes are opposite to each other, a rotational force is generated to accelerate the rotor until the magnetizing torque is balanced to the load torque [2.13].

To model and analyze such a motor, space vectors as complex state variables should be used because of their convenience and efficiency. In power electronic system, a three-phase current system can be represented by a three-axis coordinate system, as presented in Figure 2.10(a). This three-phase system can be described by using a complex reference frame. Figure 2.10(b) illustrates the equivalent representation.

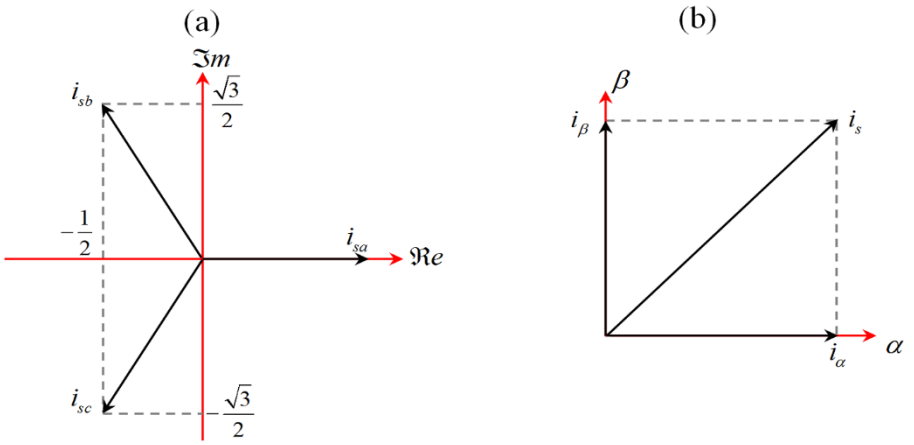

Figure 2.11: Coordinate transformation. (a) Current System in a three axis coordinate (a,b,c). (b) Currents expressed in a complex reference frame $\alpha\beta$.

A three-phase stator currents system, with angular frequency ω_o, can be defined in a fixed three-phase coordinate frame:

$$i_{sa} = I\sin(\omega_o t) \tag{2.17}$$

$$i_{sb} = I\sin\left(\omega_o t + \frac{2\pi}{3}\right) \tag{2.18}$$

$$i_{sb} = I\sin\left(\omega_o t + \frac{4\pi}{3}\right) \tag{2.19}$$

The transformation from a three- to a two-phase system of the stator currents is presented by:

$$i_s = \frac{2}{3}(i_{sa} + a i_{sb} + a^2 i_{sb}) \tag{2.20}$$

$$a = e^{j2\pi/3} = -\frac{1}{2} + j\frac{\sqrt{3}}{2} \tag{2.21}$$

$$a^2 = e^{j4\pi/3} = -\frac{1}{2} - j\frac{\sqrt{3}}{2} \tag{2.22}$$

The same coordinate transformation aforementioned is used for the electromagnetic variables. Therefore, the equations of an induction motor can be described in any arbitrary reference frame rotating at an angular frequency ω_k [2.13]:

$$v_s = R_{ss} i_s + \frac{d}{dt}\varphi_s + j\omega_k \tag{2.23}$$

$$0 = R_r i_r + \frac{d}{dt}\varphi_r + j(\omega_k - \omega)\varphi_r \tag{2.24}$$

$$\varphi_s = L_s i_s + L_m i_r \tag{2.25}$$

$$\varphi_r = L_r i_r + L_m i_s \tag{2.26}$$

$$T_e = \frac{3}{2} p\Im m(\varphi_s^* \cdot i_s) \tag{2.27}$$

where:

L_s, L_r and L_m : are the stator, rotor, and magnetizing inductances, respectively (H).

R_{ss} and R_r : are the stator and rotor resistances (Ω).

v_s and i_s : are the stator voltage and current vectors.

i_r : is the rotor current vector (A).

φ_s and φ_r : are the stator and rotor flux vectors (Wb).

ω : is the rotor electrical speed (rad/s)

T_e : is the electromagnetic torque (N.m).

p : is the number of pole pairs.

φ_s^* : is the complex conjugate value of the stator flux vector.

For $\omega_k = 0$ the coordinate system is stator-fixed, i.e., the coordinates are given in the $\alpha\beta$ system. The mechanical rotor speed dynamics are given as:

$$J\frac{d}{dt}\omega_m = T_e - T_L - F\omega_m \tag{2.28}$$

where:

ω_m : is the rotor mechanical speed (rad/s).

T_L : is the load torque connected to the IM (N.m).

J : is the moment of inertia of the mechanical shaft (kg.m²).

F : is the viscous friction coefficient (N.m.s).

The electrical rotor speed ω is related to the mechanical rotor speed ω_m as demonstrated below:

$$\omega = p\omega_m \tag{2.29}$$

2.5 CENTRIFUGAL PUMP MODELING

A centrifugal pump is one of the most used pump type in water pumping applications, due to its advantage such as suitable for small to high head, less torque to start, large flow rates, low cost and high efficiency compared to other pump types [2.14-15]. The centrifugal pump is used for converting the mechanical energy into hydraulic energy. As it has been previously mentioned, it is coupled directly to the IM and opposes a load torque T_L [2.14]:

$$T_L = k_p\omega_m^2 \tag{2.30}$$

where:

k_p : is the pump constant speed.

ω_m : is the rotor mechanical speed (rad/s).

The centrifugal pump is characterized by its head-flow rate performance curve at the nominal speed. The head-flow curves at different speeds are commonly estimated using the affinity laws (similarity laws) of the pump [2.14-16]. These laws state that the flow rate is directly proportional to the pump speed, the head is proportional to the square of the speed, and the hydraulic power is proportional to the cube of the speed. The head-flow characteristics of a

centrifugal pump, Figure 2.12, driven at a rotor speed ω_m can be described by Peleider-Peterman model [2.16]:

$$H = c_1\omega_m^2 + c_2\omega_m Q + c_3 Q^2 \tag{2.31}$$

where:

H : is the head (m).
Q : is the flow rate (liter/s or m^3/s).
c_1, c_2 and c_3 : are constants depending on the pump geometric dimensions.

The pump performance is estimated by specifying a load curve; the head-flow characteristic of the pipe network can be given by [2.16]:

$$H = H_g + \psi Q^2 \tag{2.32}$$

where:

H_g : is the geometrical height, which is the difference between the free level of the water to pump and the highest point of the canalization (m).

ψ : is a constant depending on conduit diameter and on all frictional losses of the pipe network.

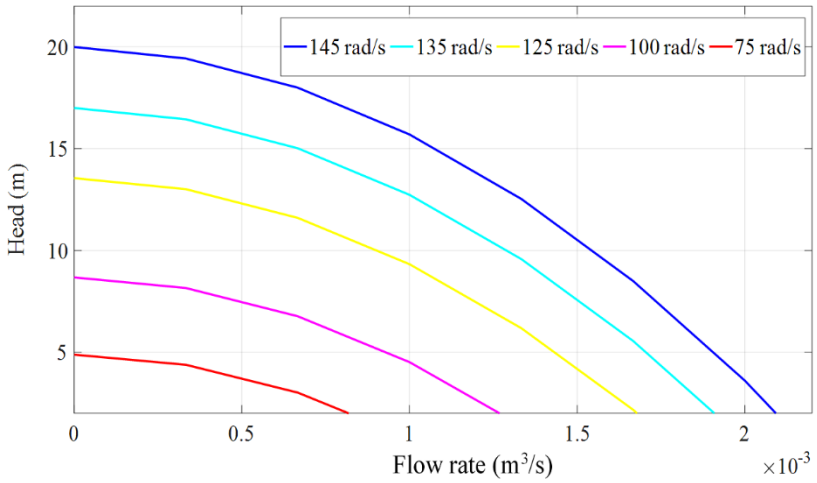

Figure 2.12: Head-flow pump characteristics under different rotor speeds.

2.6 CONCLUSION

The aim of this chapter is to describe the components models of the proposed battery-less photovoltaic pumping system, which will be used in the following chapters for the system control and simulation work. First, the photovoltaic cell, module and array, and their characteristic curves have been described. Additionally, the power converters used in the proposed pumping system were presented to illustrate their power circuit and to model

mathematically. Moreover, the induction motor is modeled in a complex reference frame to facilitate and understand the operation of motor control. Finally, the centrifugal pump model and their head-flow characteristics under different rotor speeds were presented.

REFERENCES

[2.1] Villalva, M.G., Gazoli, J.R., Filho, E.R., 2009. Comprehensive approach to modeling and simulation of photovoltaic arrays. IEEE Trans. Power Electron. 24, 1198– 1208.

[2.2] Farivar, G., Asaei, B., 2011. A new approach for solar module temperature estimation using the simple diode model. IEEE Trans. Energy Convers. 26, 1118–1126.

[2.3] Rekioua, D., Matagne, E., 2012. Optimization of Photovoltaic Power Systems. Springer Verlag.

[2.4] Bishop, J.W., 1988. Computer simulation of the effects of electrical mismatches in photovoltaic cell interconnection circuits. Solar Cells 25, 73–89.

[2.5] Kassis, A., Saad, M., 2010. Analysis of multi-crystalline silicon solar cells at low illumination levels using a modified two-diode model. Solar Energy Materials and Solar Cells 94, 2108–2112.

[2.6] BP Solar Arrays Datasheet, 2001. [Online]. Available: http://www.eastcountysolar. com/pdf/BPSX120.pdf.

[2.7] Alajmi, B., 2013. Design and control of photovoltaic systems in distributed generation. PhD. thesis, University of Strathclyde.

[2.8] Abu-Rub, H., Malinowski, M., Al-Haddad, K., 2014. Power electronics for renewable Energy systems, transportation and industrial applications. John Wiley & Sons.

[2.9] Luo, F. L., Ye, H., 2004. Advanced DC-DC converters. CRC Press Boca Raton.

[2-10] Rodriguez, J., Pontt, J., Silva, C.A.C.A., Correa, P., Lezana, P., Cortes, P., Ammann, U., 2007. Predictive current control of a voltage source inverter. IEEE Trans. Ind. Electron. 54, 495–503.

[2.11] Cortes, P., Ortiz, G., Yuz, J.I., Rodriguez, J., Vazquez, S., Franquelo, L.G., 2009. Model predictive control of an inverter with output filter for UPS applications. IEEE Trans. Ind. Electron. 56, 1875–1883.

[2.12] Giri, F., 2013. AC Electrical Motors Control. John Wiley & Sons.

[2.13] Rodriguez, J., Cortes, P., 2012. Predictive Control of Power Converters and Electrical

Drives. John Wiley & Sons.

[2.14] Betka, A., Attali, A., 2010. Optimization of a photovoltaic pumping system based on the optimal control theory. Sol. Energy 84, 1273–1283.

[2.15] Betka, A., Attali, A., 2004. Performance optimization of a photovoltaic induction motor pumping system. Renew. Energy 29, 2167–2181.

[2.16] Achour, A., Rekioua, D., Mohammedi, A., Mokrani, Z., Rekioua, T., Bacha, S., 2016. Application of direct torque control to a photovoltaic pumping system with slidingmode control optimization. Electric Power Compon. Syst. 44, 172–184.

Chapter 3

Literature Review

3.1 INTRODUCTION

The efficiency of solar photovoltaic (PV) energy conversion to electrical energy is relatively low, and the characteristics of the PV array are highly nonlinear and are dependent on the environmental conditions. Therefore, a maximum power point tracker (MPPT) is essential to solve these issues and to ensure that the PV pumping system operate at its maximum power point (MPP). On the other hand, electromechanical power conversion in the proposed PV pumping system is provided by a three-phase induction motor (IM) fed by a two-level inverter. Assuming that the PV system is operating at the MPP during different operating conditions, it is necessary also to ensure electromechanical power conversion with minimum loss at all operating points.

In this chapter, the basic concepts of MPPT algorithms are described and analyzed; these concepts include the fractional open-circuit voltage (FOCS) and short-circuit current (FSCC) methods, perturb and observe (P&O) algorithm, incremental conductance (IncCon) algorithm, and an overview on other advanced concepts is presented. In addition, this chapter gives a short review of the state of the art in electrical IM drive systems control and highlights known problems in these methods.

3.2 MAXIMUM POWER POINT TRACKING ALGORITHMS

The MPPT unit is a power conversion system with a suitable control algorithm that allows extracting the maximum power from a PV array. The maximization of the delivered power can be achieved by regulating the current drawn from the PV array or the voltage across it to yield

operation at or close to the MPP. Numerous MPPT Algorithms with different levels of complexity, accuracy, efficiency and implementation difficulty have been proposed for maximizing the energy utilization efficiency of the PV arrays in the literature [3.1-5].

3.2.1 Basic MPPT Algorithms

3.2.1.1 Fractional open-circuit voltage and short-circuit current methods

These methods have the advantage of simplicity, where only multiplication is needed to set the reference voltage or current using the occasional measurement of one voltage or one current [3.1-5].

The fractional open-circuit voltage (FOCV) algorithm is based on the fact that the operating voltage at MPP of the PV array (V_{MPP}) is approximately linearly proportional to the open-circuit voltage of PV array (V_{OC}) with varying solar irradiation and temperature levels, as expressed in the equation below:

$$V_{MPP} = k_{OC} V_{OC} \tag{3.1}$$

where:

k_{OC} : is a proportional constant and depends on the characteristics of the PV array being used. The factor k_{OC} is generally found to be between 70 to 82% [3.5].

The FOCV algorithm can be implemented with the flowchart presented in Figure 3.1(a). The PV array is periodically disconnected to allow measurement of its open-circuit voltage. Afterward, The MPP is updated based on the relation given in Eq. 3.1 and the operating voltage of the PV array is adjusted to the new optimum voltage point. This method has the advantages of simplicity and easy implementation. Nevertheless, Eq.3.1 is an approximation then the PV array will never perfectly match the MPP. In addition, a striking disadvantage of the FOCV method is that the PV array needs to be periodically disconnected from the MPPT for a very short time (to measure the open-circuit voltage). This results in considerable energy losses in the long run. This issue can be avoided by using a separate pilot PV cell [3.6-7]. However, this solution comes at an additional cost and the mismatch between the characteristics of the reference pilot PV cell and the actual PV array can cause a steady-state error in the MPPT.

The fractional short-circuit current (FSCC) algorithm is similar to FOCV method and utilizes the fact that the current corresponding to the MPP of the PV array (I_{MPP}) is approximately linearly proportional to the short-circuit current of the PV array (I_{SC}), under various solar irradiance and temperature levels as given in the following equation:

$$I_{MPP} = k_{SC} I_{SC} \tag{3.2}$$

where:

k_{SC}: is a proportional constant. Just like in the FOCV technique, k_{SC} has to be determined according to the PV array in use. Typically, the value of k_{SC} varies from 85 and 95% [3.5].

In a similar way to the FOCV algorithm, the FSCC method might be applied by measuring periodically the short-circuit current instead of the open-circuit voltage, therefore, to force the PV array to operate at the optimum current point which is set from Eq. 3.2. As illustrated in Figure 3.2 (b), the flowchart of the FSCC algorithm is similar to that of the FOCV algorithm. Therefore, this method offers the same advantages and disadvantages as the FOCV algorithm.

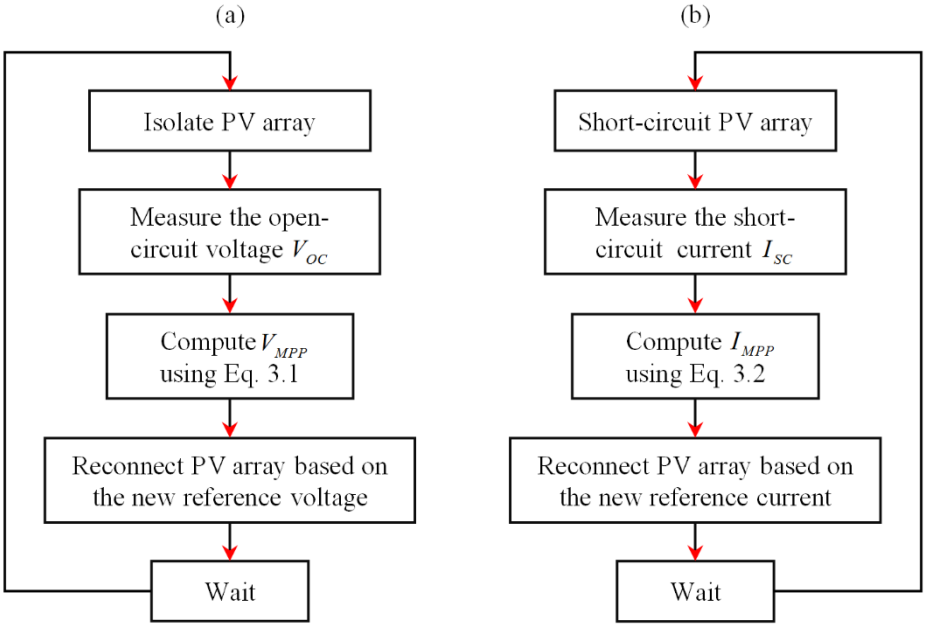

Figure 3.1: (a) Flowchart of the FOCV method, (b) flowchart of the FSCC method.

3.2.1.2 Perturb and observe algorithm

A frequently used class of MPPT algorithms operates by continuously perturbing the operating point of the PV arrays and observing the corresponding variation in the output power in order to determine the next variation that leads to the MPP; therefore they are known as Perturb and Observe (P&O) algorithms [3. 8-10].

In P&O algorithm, a fixed perturb value is utilized to produce a reference signal for the outer control loop. The perturbation variable can be the reference value for the PV array terminal voltage or the PV panel output current or the duty cycle signal of the interfacing DC-

DC converter. The basic flowchart of the P&O algorithm is represented in Figure 3.2(a). This algorithm is based on scanning the voltage-current-power characteristic curves in search for a determined condition that signals the MPP. As shown in Figure 3.2(b), if the operating power point is on the left side of the MPP, the algorithm must move it to the right to be nearer to the MPP, and vice versa if it is on the opposite side (on the right side), as depicted in Figure 3.2(c).

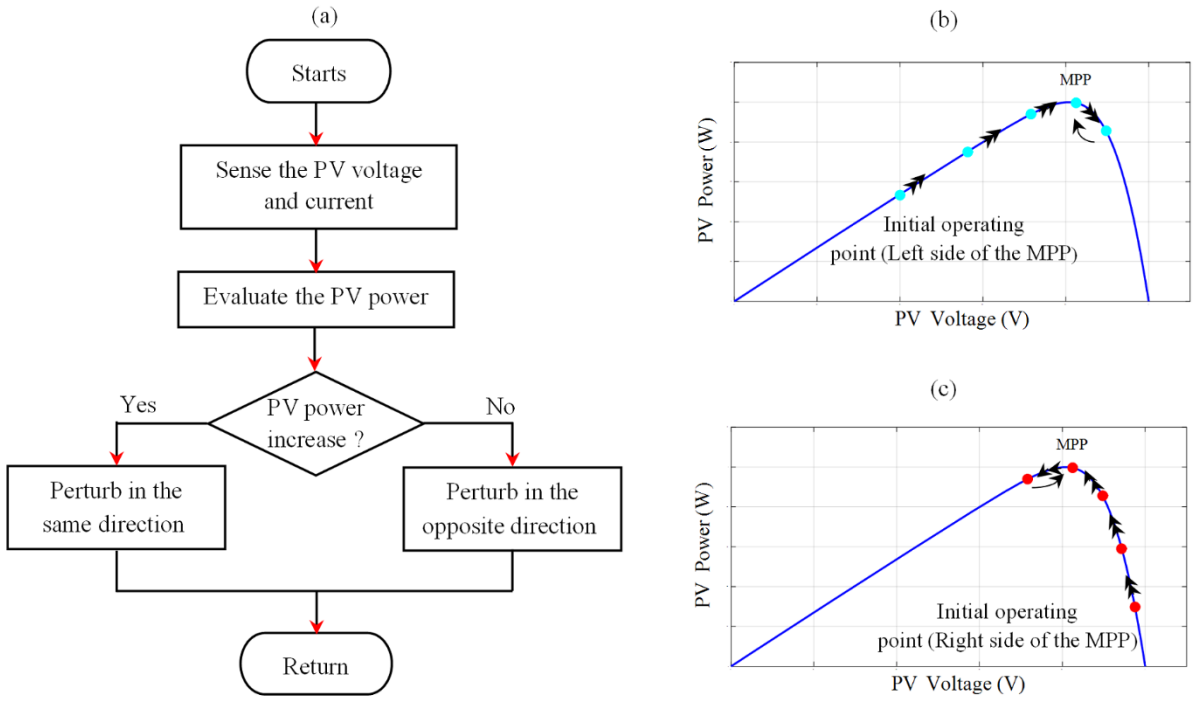

Figure 3.2: (a) Flowchart of the P&O algorithm, (b) and (c) power-voltage characteristics of the PV operating points using the P&O algorithm.

The P&O algorithm is broadly used in the commercial products of PV systems for extracting the MPP because of its simplicity, ease of implementation, few measured parameters and low cost. Nevertheless, the fixed perturb step is determined according to the system designer, and consequently the solution provided by this algorithm is not standard and system dependent. When a large perturb step is considered, the tracking is fast and the power oscillations are significant. On the contrary, if a small perturb step is considered, slower tracking is achieved with decreased power oscillations. In addition, the P&O is not very accurate in the case of rapidly changing environmental conditions, where the algorithm reacts as if the increase occurred as a result of the previous perturbation [3.11].

In general, a proportional-integral (PI) or hysteresis controller following the MPPT is employed to control the power converter. A review of research related to the fixed step P&O is shown in Table 3.1.

TABLE 3.1: Conventional P&O with fixed perturb step from research survey.

Authors	Year	Control Variable/ Converter Type	Controller Implementation	*MPPT performances*
Femia et al. [3.10]	2005	Duty cycle/Boost Converter	-	Good tracking Large steady-state oscillations Low complexity and easy implementation
Kim et al. [3.12]	1996	PV current (Hysteresis)/Boost Converter	Mixed analog and digital electronics	Good tracking Medium steady-state oscillations Low complexity and easy implementation
Chomsuwan et al. [3.13]	2002	PV current (PI)/ Two switch Buck-Boost Converter	ADMC331 Microcontroller	Good tracking Medium steady-state oscillations Low complexity and moderate effort for implementation
Femia et al. [3.14]	2008	PV voltage (PI)/Boost Converter	-	Improved tracking in partial shading Medium steady-state oscillations Low complexity and moderate effort for implementation
Figueres et al. [3.15]	2009	PV voltage (PI)/Inverter Converter	TMS320F281 Microcontroller	Slow tracking Medium steady-state oscillations Low complexity and moderate effort for implementation
Patel et al. [3.16]	2010	PV voltage (PI)/Boost Converter	-	Slow tracking Medium steady-state oscillations Low complexity and moderate effort for implementation

3.2.1.3 Incremental conductance algorithm

The incremental conductance (IncCon) algorithm is similar to the P&O method and was proposed to improve the tracking accuracy and dynamic performance in rapidly changing atmospheric conditions [3.11, 17-18]. The IncCon algorithm is derived from the power-voltage curve of a PV array, Figure 3.3, where the slope of the curve is positive on the left side of the

MPP, negative on the right side of the MPP and zero at the MPP. The slope of the power-voltage curve can be expressed as:

$$\frac{dP_{PV}}{dV_{PV}} = \frac{dI_{PV}V_{PV}}{dV_{PV}} = I_{PV} + V_{PV}\frac{dI_{PV}}{dV_{VP}} \tag{3.3}$$

Therefore, the basic equations of this method are as follows:

$$\frac{dI_{PV}}{dV_{VP}} = -\frac{I_{PV}}{V_{VP}}, \quad \text{at MPP} \tag{3.4}$$

$$\frac{dI_{PV}}{dV_{VP}} \succ -\frac{I_{PV}}{V_{VP}}, \quad \text{at left of MPP} \tag{3.5}$$

$$\frac{dI_{PV}}{dV_{VP}} \prec -\frac{I_{PV}}{V_{VP}}, \quad \text{at right of MPP} \tag{3.6}$$

where:

dI_{PV} / dV_{PV} : is the incremental conductance.

I_{PV} / V_{PV} : is the conductance.

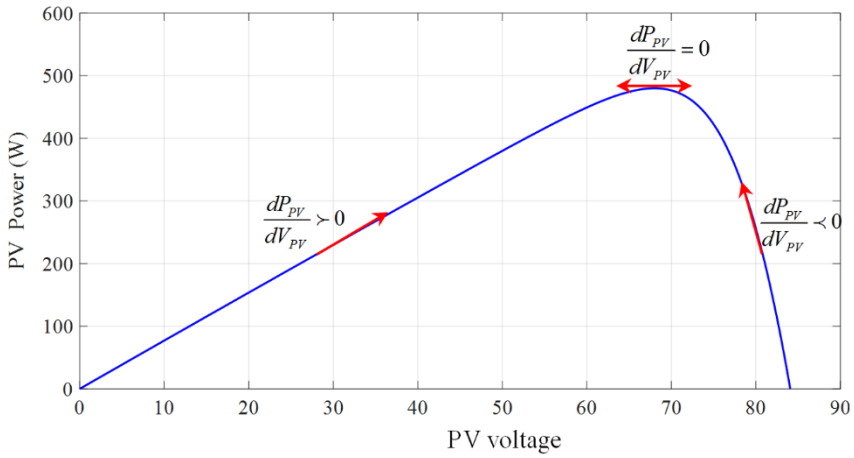

Figure 3.3: Basic idea of the IncCon algorithm on a Power-Voltage curve of a PV array.

The derivative of the current with respect to the derivative of voltage can be estimated as the difference between the actual values and the previous instant values in that iteration process. Therefore, by comparing the conductance I_{PV}/V_{PV} to the incremental conductance dI_{PV}/dV_{PV} as shown in Figure 3.4, the algorithm can track the MPP and stay there until a change of dI_{PV} or dV_{PV} occurs as a result of a change in atmospheric condition.

However, the MPP is rarely obtained by Eq. 3.4 in practical implementation, consequently, power oscillations around the MPP are presented even in stable atmospheric conditions as the

P&O algorithm. In order to solve this issue, a small error (ε) can be added to the maximum power condition (Eq. 3.4) [3.17].

$$\frac{dI_{PV}}{dV_{VP}} + \frac{I_{PV}}{V_{VP}} = \varepsilon \tag{3.7}$$

The size of this permissible error determines the sensitivity of the system. This error is selected with respect of the tradeoff between the problem of not operating exactly at the MPP and the possibility of oscillating around it. With this approximation, the IncCon algorithm presents the same disadvantages as P&O algorithm. In addition, the execution time of the IncCon algorithm is longer than the P&O due to extra and more complex arithmetic computations.

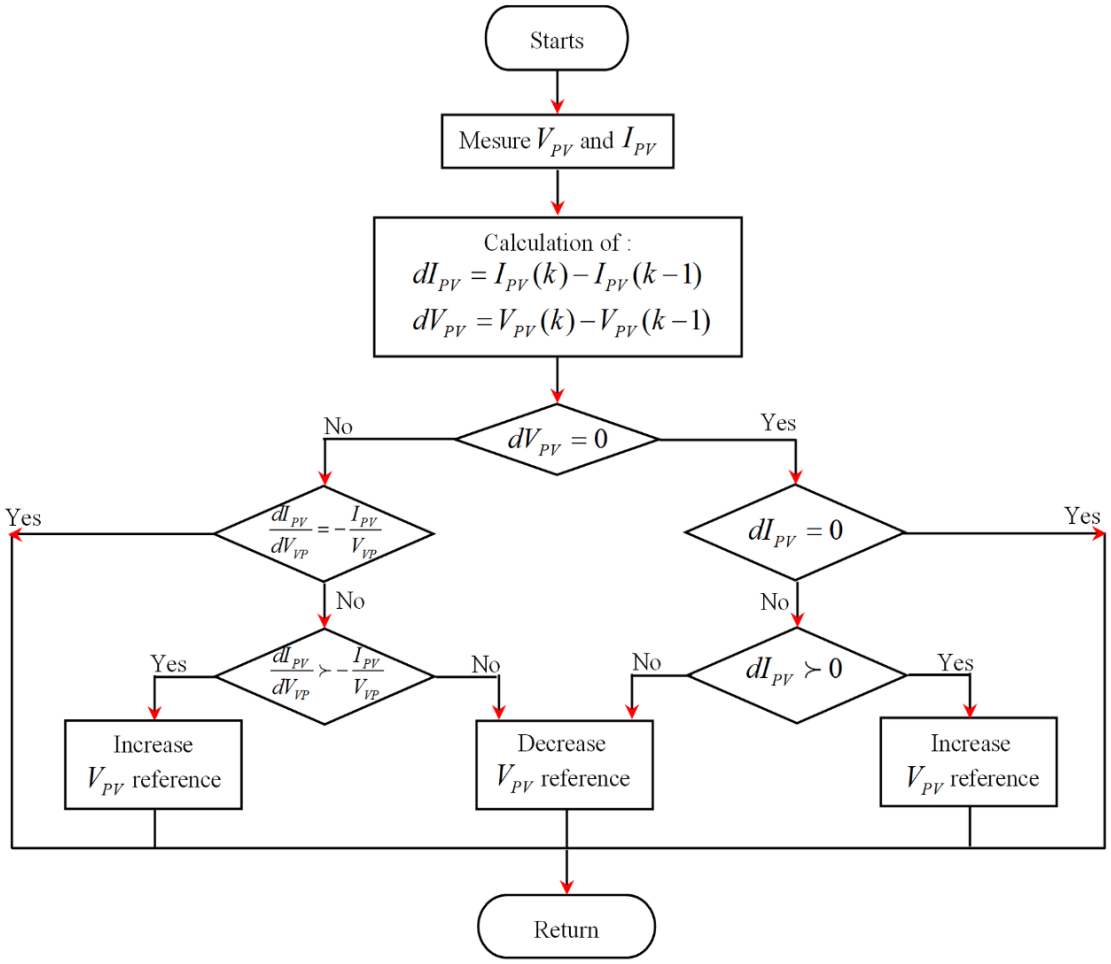

Figure 3.4: Flowchart of the IncCon algorithm.

3.2.2 Fuzzy Logic based MPPT

Numerous control strategies [3.19-24] have been proposed that use the fuzzy logic control (FLC) in MPPT applications for PV systems either independently or along with other methods.

The main advantages of such controllers are no needing to use accurate mathematical model to implement, ability of working with imprecise inputs and handling nonlinearity. The FLC parameters can be changed quickly in response to changes in the system dynamics without parameter estimation. When the environmental conditions change, the performance of a fuzzy based MPPT algorithm is strong, however, their strength depends a lot on the controller design. In FLC design, one must identify the main control variables and determine the sets that define the values of each linguistic variable. FLC consists generally of three stages, called fuzzification, rule base, defuzzification. In the first FLC stage, the numerical input variables are converted into linguistic variables based on a membership function similar to Figure 3.5. The triangular membership functions are used in this case with seven fuzzy variables, i.e., NB (Negative Big), NM (Negative Medium), NS (Negative Small), ZE (Zero), PS (Positive Small), PM (Positive Medium) and PB (Positive Big).

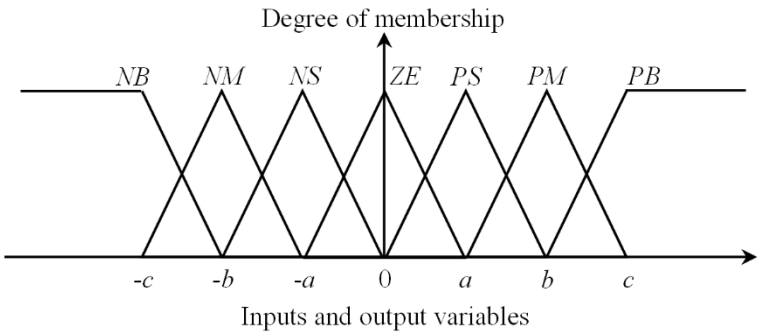

Figure 3.5: Membership function for inputs and output of fuzzy logic controller.

In most fuzzy-based MPPT algorithms, the MPP is tracked by using the slope of the power-voltage characteristic (e) and the slope change (Δe) as input variables of the FLC.

$$e = \frac{P_{PV}(k) - P_{PV}(k-1)}{V_{PV}(k) - V_{PV}(k-1)} \tag{3.8}$$

$$\Delta e = e(k) - e(k-1) \tag{3.9}$$

Once input variables are calculated and converted to the linguistic variables, the output of the fuzzy controller, which is usually the change in duty cycle (ΔD) of the power converter, can be looked up in a rule base table such as Table 3.2 [3.24]. The linguistic variables assigned to the output for the different combinations of inputs are based on the power converter being used and also on the knowledge of the user. FLC output is converted from a linguistic variable (still using a membership function as in Figure 3.5) to a numerical variable in the defuzzification stage, and offers an analog signal that will drive the power converter to the MPP.

Compared to conventional algorithms, The FLC MPPT methods possess some advantages such as better performance, good stability and fast response. Nevertheless, the implementation of these MPPT is limited in real time due to high computational burden of the fuzzy controller and the memory requirement.

TABLE 3.2: The forty-nine fuzzy rules of the fuzzy MPPT [3.24].

				Δe(k)			
e(k)	**NB**	**NM**	**NS**	**ZE**	**PS**	**PM**	**PB**
NB	ZE	ZE	ZE	NB	NB	NB	NB
NM	ZE	ZE	ZE	NM	NM	NM	NM
NS	NS	ZE	ZE	NS	NS	NS	NS
ZE	NM	NS	ZE	ZE	ZE	PS	PM
PS	PM	PS	PS	PS	ZE	ZE	ZE
PM	PM	PM	PM	ZE	ZE	ZE	ZE
PB	PB	PB	PB	ZE	ZE	ZE	ZE

3.2.3 Artificial Neural Network based MPPT

Similar to Fuzzy logic controller, the artificial neural network (ANN) have become popular and expanded in MPP tracking for PV systems with the development in soft computing technology [3.25-28]. The architecture of an ANN consists of three layers input, hidden, and output layers and the number of nodes in each layer vary and are user dependent as shown in Figure 3.6. The input variables can be the PV array current and voltage, the PV array parameters like open-circuit voltage V_{OC} and short-circuit current I_{SC}, the atmospheric data like the temperature and irradiance or any combination of these variables. The output is generally the duty cycle signal that drives the power converter to operate at or close to the MPP based on the algorithm used in the hidden layer. The link between nodes i and j is considered as having a weight of w_{ij} in Figure 3.6. The ANN technique is based on weighting the links between nodes based on some training process, where the PV parameters are tested and recorded over months or years to get the right weight for every node.

However, the major drawback of this method is that ANN has to be trained for the PV array in use and therefore cannot be generalized to work on several types at the same time unless trained to. In addition, the characteristics of a PV array change with time, implying a periodical training of the artificial neural network to track accurately the MPP. Such a limitation has been overcome in [3.29-31] by combining the ANN and fuzzy logic to achieve a suitable MPP tracker. This technique requires a costly microprocessor to implement and therefore is not suitable for small applications.

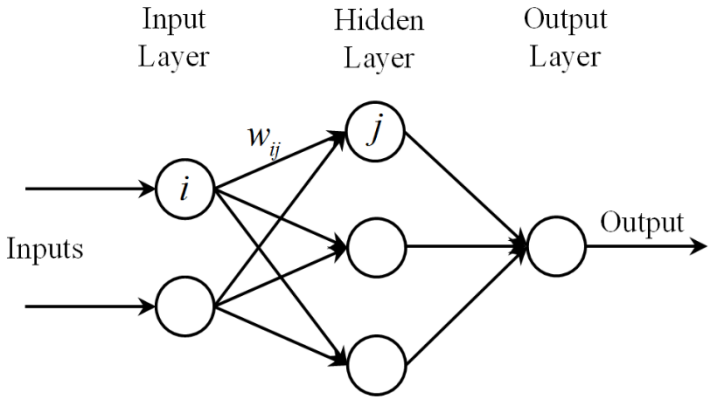

Figure 3.6: Example of artificial neural network.

3.2.4 Other MPPT Algorithms

Other different MPPT algorithms [3.31-36] have been proposed in literature; they use different control strategies in terms of complexity, efficiency and implementation costs. Examples of these MPPT algorithms include the ones based on genetic algorithm (GA) [3.31-32] and particle swarm optimization (PSO) [3.33-36]. These approaches are capable of improving the tracking performance, even when the PV system operates under partially shading conditions, compared with conventional methods. Unfortunately, several parameters in these approaches are selected on a trial and error basis, essentially depending on the designer experience. In addition, most of these techniques have a limited field of practical applicability because they require expensive hardware resources.

3.3 INDUCTION MOTOR DRIVES

Recently, important progress has been made in the induction motor drives. These drives can employ different speed control methods that include scalar (volts/hertz or *v/f*) control, field-oriented control (FOC), direct torque control (DTC) and other techniques [3.37]. The following subsections give a brief overview of the state of the art in control of electrical IM drive systems.

3.3.1 Scalar Control

Scalar control is the simplest way for controlling the induction motor. The basic idea of this technique is to keep the ratio between the stator voltage magnitude and frequency constant in order to avoid magnetic flux saturation and maximize the available torque of the IM [3.37]. Based on the constant *v/f* principle, both the open and closed-loop control of the speed of an IM can be implemented. When accuracy in the speed response is not mandatory, the open-loop speed control is used, for example in ventilation and air conditioning. The closed loop speed by slip regulation, which is an enhancement for the open-loop *v/f* control, is presented in Figure 3.6. The slip reference ω_{sl}^* is externally generated by a PI-speed controller with a limiter. The slip is added to the feedback rotor speed to produce the slip frequency reference ω_e^*. Therefore, the frequency reference generates the voltage reference through a *v/f* calculator and applied to the inverter using pulse width modulation (PWM).

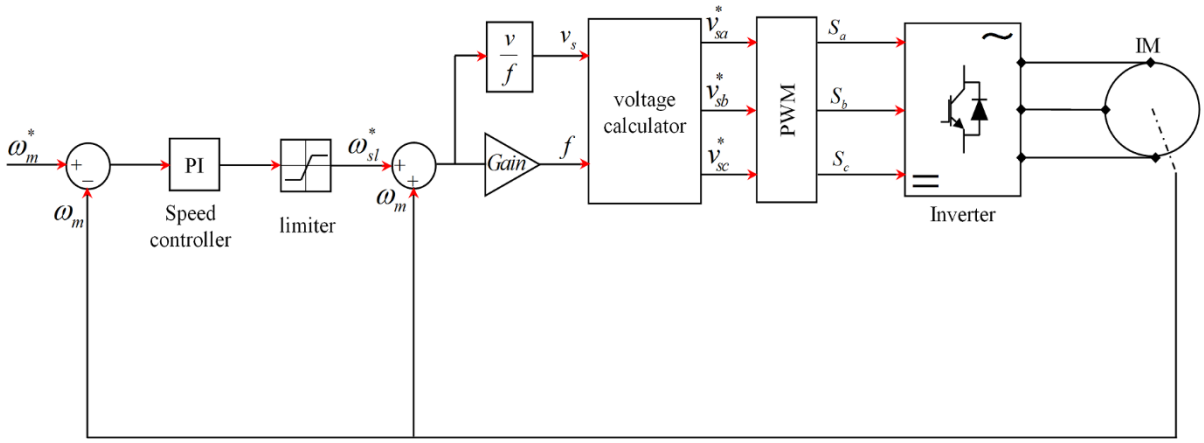

Figure 3.7: Bloc diagram of the *v/f* technique.

Scalar control strategy is generally simple, low cost, well implementable and does not require the parameter of an IM. However, *v/f* control law does not satisfy the dynamic characteristics of drive systems for critical loads since it is based on steady-state behavior of IM. Moreover, *v/f* control law does not guarantee efficient operation of IM.

3.3.2 Field-Oriented Control

Field-oriented control is identified as one of the conventional drives for controlling the speed and torque of IM. FOC method is broadly adopted to achieve high dynamic performance in the drive systems. The basic idea of FOC is to use a proper coordinate system that allows to control independently the magnitude of the rotor flux $\|\varphi_r\|$ and the electromagnetic torque T_e, which means that the torque variation is achieved with constant flux and vice-versa.

Consequently, the system will be linear and easy to control, similar to a separately excited DC machine [3.37-39]. This can be reached by aligning the coordinate system with the rotor flux. The relation between the stationary $\alpha\beta$ and rotating reference frame dq, which is aligned with the rotor flux vector φ_r, is represented in Figure 3.8. The corresponding angle that allows a complete decoupling is the rotor flux angle θ.

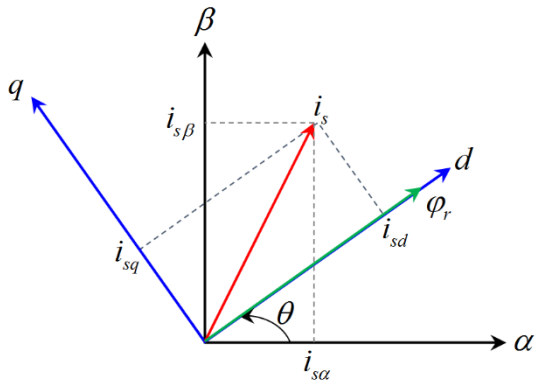

Figure 3.8: Reference frame orientation in FOC.

Once the controlled variables are expressed in a rotating coordinates frame, the rotor flux magnitude can be controlled via the real part of the stator current i_{sd}, and the electromagnetic torque is controlled via the imaginary component of the stator current i_{sq}.

A block diagram of the basic FOC structure is presented in Figure 3.9. As for normal machine operation, the sum of all three-phase stator currents is equal to zero, it is sufficient to measure only two-phase currents. The reference current i_{sq}^* is achieved by the PI-speed controller and i_{sd}^* is achieved by the rotor flux control loop, where the rotor flux estimation is based on the two-phase stator current measurements and IM model. The stator current errors are controlled using linear PI controllers. These deliver the stator reference voltages v_{sd}^* and v_{sq}^*. Then these voltages are converted into the three phase reference frame, after two further transformations from dq to $\alpha\beta$ and then to abc coordinates, and applied to the inverter using a PWM modulator.

High-performance IM control can be realized using FOC strategy. However, the main complexity in implementation of FOC is that a coordinate transformation is necessary, it implies to obtain the angle of the rotor flux, which cannot be directly measured from the IM terminals. Hence, it is required to implement an encoder, estimators or observers, which are based on IM model. Unfortunately, these estimations are very sensitive to the parameters of IM, and then the variation of IM parameters influences the accuracy of these estimations that leads to performance degradation of IM.

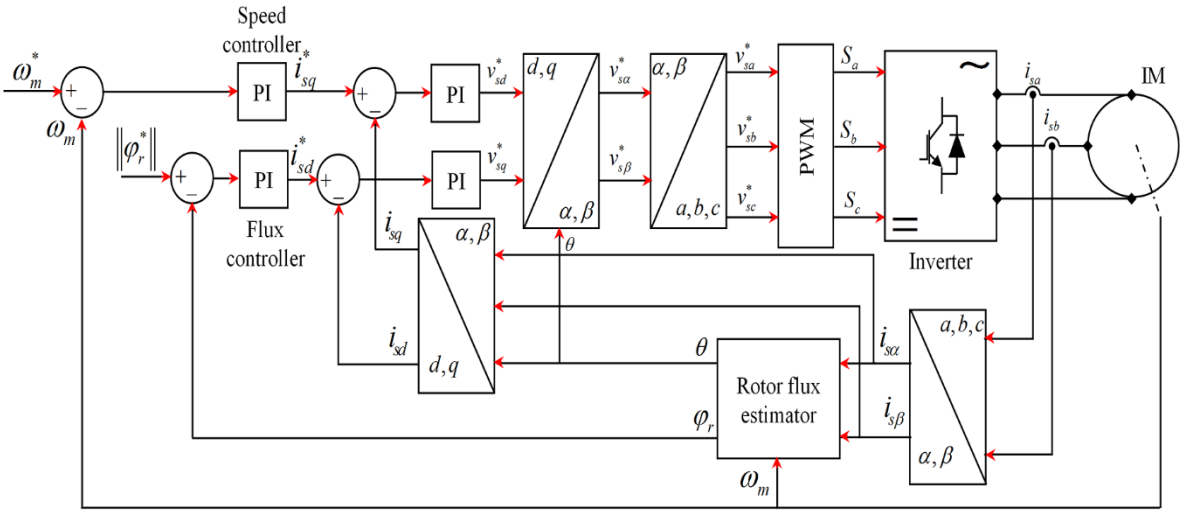

Figure 3.9: Bloc diagram of the FOC technique.

3.3.3 Direct Torque Control

Another control technique for IM, known as direct torque control has become widespread recently due to its instantaneous dynamic control that can produce similar performance obtained in DC motors [3.39-40]. DTC technique can be considered as an alternative drive to the well-known FOC strategy due to its excellent torque response and its simple control algorithm and its robust to variation of IM parameters. The control structure of DTC technique is much simpler than the FOC strategy due to the absence of PWM modulator, current controllers and coordinate transformation.

The DTC drive is based on two fundamental principles [3.39], the first one is related to neglect the voltage drop caused by the stator resistance R_{ss} in the stator voltage equation. Therefore, the stator flux φ_s can be modified by the application of a given inverter voltage vector during a sampling step. The second one is related to the fact that the rotor flux dynamics are slower than the dynamics of the stator flux. Then, the rotor flux φ_r can be considered as invariant, during a sampling step. Hence, the electromagnetic torque T_e can be changed by changing the stator flux angle by applying an appropriate voltage vector.

Figure 3.10 shows a block diagram of the basic DTC structure. The basic idea of the DTC is to replace PI controllers by faster hysteresis controllers for both the stator flux magnitude $||\varphi_s||$ and electromagnetic torque T_e and according to the output of these hysteresis controllers, the inverter switching state can be selected from a predefined look-up table. The torque reference T_e^* is achieved by a linear PI-speed controller, while the reference of the stator flux magnitude is constant $||\varphi_s^*||$. The torque and stator flux estimations are based on the IM model. Torque and flux errors are controlled using the hysteresis controllers. The output of these

controllers, hT and $h\varphi$ and the stator flux angle θ_s are the inputs of the switching selection table of the voltage vector. The selected voltage vector is directly applied to the inverter and a modulator is not necessary.

However, the major problem with DTC drive is the presence of ripples in the torque and stator flux. There are generally two main techniques to reduce the torque ripples. The first one is to use a multilevel inverter [3.41], which will provide more precise control of torque and flux. However, the cost and complexity of the controller increase proportionally. The other method is to use space vector modulation (SVM) [3.42]. The inverter switching frequency in SVM strategies is constant and usually much higher than for direct switching strategies.

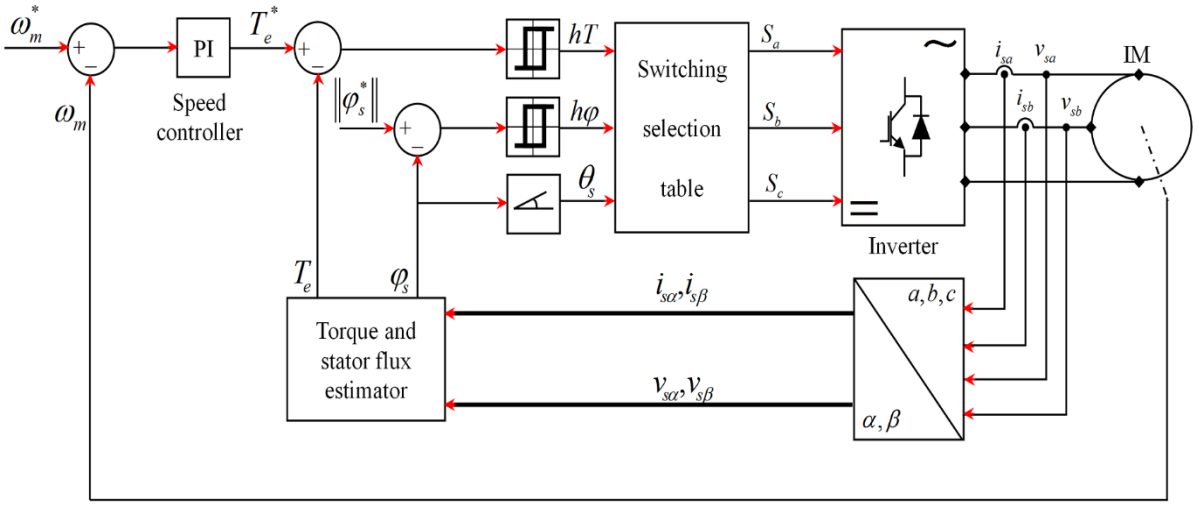

Figure 3.10: Bloc diagram of the DTC technique.

3.3.4 Other Drives

Many IM drives have been proposed in the literature that combining the conventional drives with modern control techniques, such as sliding mode [3.43], fuzzy logic [3.44], artificial neural network [3.45] and neuro-fuzzy [3.46]. These techniques have been used by the researchers for the minimization of the torque and flux ripples as well as increase the robustness to variation of motor parameters and load disturbances. However, the implementation of these techniques is limited in real-time due to complexity and high computational burden of these controllers. Nevertheless, during the last few years the model predictive control (MPC), especially finite control set model predictive control (FCS-MPC) got a rapid expansion as of this technique simplicity that is very intuitive, easy to understand and to implement [3.47]. High-performance control strategies for IM drives based on FCSMPC have been proposed in the literature such as predictive and flux torque control (PTC) [3.48] and predictive current

control (PCC) [3.48]. Compared to the conventional control techniques, these techniques eliminate the need for linear PI controllers and the modulation stage, and offers a conceptually different approach to control the inverter.

3.4 CONCLUSION

In this chapter, the state of the art of maximum power point tracking (MPPT) algorithms for photovoltaic (PV) systems are reviewed, and followed by a brief overview of the induction motor (IM) control techniques. The implementation and operating principle of different control techniques for MPPT algorithms are presented. The issues and challenges related to different algorithms, such as the tracking accuracy, the power oscillations, and the computational burden are discussed. In addition, the most extensively used high-performance control strategies for IM drives as scalar control, field-oriented control (FOC), direct torque control (DTC) and other techniques are described, along with their main advantages and disadvantages. The analysis presented in this chapter favors the P&O algorithm and DTC strategy to achieve high-performance operation for the PV pumping system based on IM.

REFERENCES

[3.1] Esram, T., Chapman, P.L., 2007. Comparison of photovoltaic array maximum power point tracking techniques. IEEE Trans. Energy Conver. 22, 439–449.

[3.2] Eltawil, M.A., Zhao, Z., 2013. MPPT techniques for photovoltaic applications. Renew. Sustain. Energy Rev. 25, 793–813.

[3.3] de Brito, M.A.G., Galotto, L., Sampaio, L.P., e Melo, G.A., Canesin, C.A., 2013. Evaluation of the main MPPT techniques for photovoltaic applications. IEEE Trans. Ind. Electron. 60, 1156–1167.

[3.4] Mohanty, P., Bhuvaneswari, G., Balasubramanian, R., Dhaliwal, N.K., 2014. MATLAB based modeling to study the performance of different MPPT techniques used for solar PV system under various operating conditions. Renew. Sustain. Energy Rev. 38, 581–593

[3.5] Karami, N., Moubayed, N., Outbib, R., 2017. General review and classification of different MPPT Techniques. Renew. Sustain. Energy Rev. 68, 1–18.

[3.6] Hart, G.W., Branz, H.M., Cox, C.H., 1984. Experimental tests of open loop maximum-power-point tracking techniques. Solar Cells 13, 185–195.

[3.7] Salameh, Z., Dagher, F., Lynch, W., 1991. Step-down maximum power point tracker for photovoltaic systems.Sol. Energy 46, 279–82.

[3.8] Eftichios, K., Kostas, K., Voulgaris, N., 2001. Development of a microcontroller-based, photovoltaic maximum power point tracking control system. IEEE Trans. Power Electron. 16, 46–54.

[3.9] Femia, N., Petrone, G., Spagnuolo, G., Vitelli, M., 2012. Power Electronics and Control Techniques for Maximum Energy Harvesting in Photovoltaic Systems. CRC Press.

[3.10] Femia, N., Petrone, G., Spagnuolo, G., Vitelli, M., 2005. Optimization of perturb and observe maximum power point tracking method. IEEE Trans. Power Electron. 20, 963–973.

[3-11] Hussein, K.H., Muta, I., Hoshino, T., Osaka, M., 1995. Maximum photovoltaic power tracking: an algorithm for rapidly changing atmospheric conditions. IEE Proc. Gener. Transnm. Distrib. 142, 59–64.

[3.12] Kim, Y., Jo, H., Kim, D., 1996. A new peak power tracker for cost effective photovoltaic power systems. IEEE Proceedings 3, 1673–1678.

[3.13] Chomsuwan, K., Prisuwanna, P., Monyakul, V., 2002. Photovoltaic grid-connected inverter using two-switch buck-boost converter. In: Proceedings of the photovoltaic specialists conference, 1527–1530.

[3.14] Fermia, N., Lisi, G., Petrone, G., Spagnuolo, G., Vitelli, M., 2008. Distributed maximum power point tracking of photovoltaic arrays: novel approach and system analysis. IEEE Trans. Ind. Electron. 55, 2610–2621.

[3.15] Figueres, E., Garcera, G., Sandia, J., Gonzalez-Espín, F., Calvo, J., 2009. Sensitivity study of the dynamics of three-phase photovoltaic inverters with an LCL grid filter. IEEE Trans. Ind. Electron. 56, 706–717.

[3.16] Patel, H., Agarwal, V., 2010. Investigations into the performance of photovoltaics based active filter configurations and their control schemes under uniform and non-uniform radiation conditions. IET Renew. Power Gener. 4, 12-22.

[3.17] Safari, A., Mekhilef, S., 2011. Simulation and hardware implementation of incremental conductance MPPT with direct control method using cuk converter. IEEE Trans. Ind. Electron. 58, 1154–1161.

[3.18] Tey, K.S., Mekhilef, S., 2014. Modified incremental conductance MPPT algorithm to mitigate inaccurate responses under fast-changing solar irradiation level. Sol. Energy 101, 333–342.

[3.19] Gounden, N.A., Ann Peter, S., Nallandula, H., Krithiga, S., 2009. Fuzzy logic controller with MPPT using line-commutated inverter for threephase grid-connected photovoltaic systems. Renew. Energy 34, 909–915.

[3.20] Alajmi, B.N., Ahmed, K.H., Finney, S.J., Williams, B.W., 2011. Fuzzy-logic-control approach of a modified hill-climbing method for maximum power point in microgrid standalone photovoltaic system. IEEE Trans. Power Electron. 26, 1022–1030.

[3.21] Al Nabulsi, A., Dhaouadi, R., 2012. Efficiency optimization of a DSP-based standalone PV system using fuzzy logic and dual-MPPT control. IEEE Trans. Ind. Informa. 8, 573–584.

[3.22] Bendib, B., Belmili, H., Krim, F., 2015. A survey of the most used MPPT methods: Conventional and advanced algorithms applied for photovoltaic systems. Renew. Sustain. Energy Rev. 45, 637–648.

[3.23] Altin, Necmi, Ozdemir, Saban, 2013. Three-phase three-level grid interactive inverter with fuzzy logic based maximum power point tracking controller. Energy Convers. Manage. 69, 17–26.

[3.24] Hasan, M., Mekhilef, S., Metselaar, I.H., 2013. Photovoltaic system modeling with fuzzy logic based maximum power point tracking algorithm. Int. J. of Photoenergy, 1-10.

[3.25] Whei-Min, L., Chih-Ming, H., Chiung-Hsing, C., 2011. Neural-network based MPPT control of a stand-alone hybrid power generation system. IEEE Trans. Power Electron. 26, 3571–3581.

[3.26] Liu, Y.-H., Liu, C.-L., Huang, J.-W., Chen, J.-H., 2013. Neural-network based maximum power point tracking methods for photovoltaic systems operating under fast changing environments. Sol. Energy 89, 42–53.

[3.27] Rizzo, S.A., Scelba, G., 2013. ANN based MPPT method for rapidly varible shading conditions. Appl. Energy 145, 124–132.

[3.28] Punitha, K., Devaraj, D., Sakthivel, S., 2013. Artificial neural network based modified incremental conductance algorithm for maximum power point tracking in photovoltaic system under partial shading conditions. Energy 62, 330–340.

[3.29] Chaouachi, A., Kamel, R.M., Nagasaka, K., 2010. A novel multi-model neuro-fuzzy-based MPPT for three-phase grid-connected photovoltaic system. Sol. Energy 84, 2219–2229.

[3.30] Chikh, A., Chandra, A., 2014. Adaptive neuro-fuzzy based solar cell model. IET Renew. Power Gener. 8, 679–686.

[3.31] Chikh, A., Chandra, A., 2015. An optimal maximum power point tracking algorithm for PV systems with climatic parameters estimation. IEEE Trans. Sust. Energy 6, 644–652.

[3.32] Larbes, C., Ait Cheikh, S.M., Obeidi, T., Zerguerras, A., 2009. Genetic algorithms optimized fuzzy logic control for the maximum power point tracking in photovoltaic system. Renw. Energy 34, 2093–2100.

[3.33] Shaiek, Y., Smida, M.B., Sakly, A., Mimouni, M.F., 2013. Comparison between conventional methods and GA approach for maximum power point tracking of shaded solar PV generators. Sol. Energy 90, 107–122.

[3.34] Ishaque, K., Salam, Z., Amjad, M., Mekhilef, S., 2012. An improved particle swarm optimization (PSO)–based MPPT for PV with reduced steady-state oscillation. IEEE Trans. Power Electron. 27, 3627–3638.

[3.35] Yi-Hwa, L., Shyh-Ching, H., Jia-Wei, H., Wen-Cheng, L., 2012. A particle swarm optimization-based maximum power point tracking algorithm for PV systems operating under partially shaded conditions. IEEE Trans. Energy Convers. 27, 1027–1035.

[3.36] Lian, K.L., Jhang, J.H., Tian, I.S., 2014. A maximum power point tracking method based on perturb-and-observe combined with particle swarm optimization. IEEE J. Photovoltaics 4, 626–633.

[3.37] Reza, C.M.F.S., Islam, M.D., Mekhilef, S., 2014. A review of reliable and energy efficient direct torque controlled induction motor drives. Renew. Sustain. Energy Rev. 37, 919–932.

[3.38] Holtz, J., 1994. Pulse width modulation for electronic power conversion. Proc. IEEE 82, 1194–1214.

[3.39] Rodriguez, J., Cortes, P., 2012. Predictive Control of Power Converters and Electrical Drives. John Wiley & Sons.

[3.40] Takahashi, I., Noguchi, T., 1986. A new quick-response and high-efficiency control strategy of an induction motor. IEEE Trans. Ind. Appl. 5, 820–827.

[3.41] Kouro, S., Bernal, R., Miranda, H., Silva, C.A., Rodriguez, J., 2007. High performance torque and flux control for multilevel inverter fed induction motors. IEEE Trans. Power Electron. 22, 116–123.

[3.42] Casadei D., Angelo, T., 2000. Implementation of a direct torque control algorithm for induction motors based on discrete space vector modulation. IEEE Trans. Power Electron. 15, 769–777

[3.43] Barambones, O., Alkorta, P., 2011. A robust vector control for induction motor drives with an adaptive sliding-mode control law. J. Frankl. Inst. 348, 300–314.

[3.44] Uddin, M.N., Hafeez, M., 2012. FLC-based DTC scheme to improve the dynamic performance of an IM drive. IEEE Trans. Ind. Appl. 48, 823–831.

[3.45] Zhang, D., Li, H., 2008. A Stochastic-based FPGA controller for an induction motor drive with integrated neural network algorithms. IEEE Trans. Ind. Electron. 55, 551–561.

[3.46] Durgasukumar, D.G., Pathak, M.K., 2012. Comparison of adaptive neuro fuzzy-based spacevector modulation for two-level inverter. Int. J. Elect. Power Energy Syst. 38, 9–19.

[4.47] Rodriguez, J., Kazmierkowski, M.P., Espinoza, J.R., Zanchetta, P., Abu-Rub, H., Young, H.A., Rojas, C.A., 2013. State of the art of finite control set model predictive control in power electronics. IEEE Trans. Ind. Informa. 9, 1003–1016.

[4.48] Wang, F., Li, S., Mei, X., Xie, W., Rodriguez, J., Kennel, R.M., 2015. Model based predictive direct control strategies for electrical drives: an experimental evaluation of PTC and PCC methods. IEEE Trans. Ind. Informa. 11, 671–681.

Chapter 4

Maximum Power Point Tracking Employing Model Predictive Control

4.1 INTRODUCTION

Maximum power point tracking (MPPT) techniques play an essential role in efficiency improvement of photovoltaic (PV) systems. The perturb and observe (P&O) technique is the most popular MPPT algorithm for industry applications due to the good balance between complexity, accuracy and reliability. This algorithm is based on scanning the voltage-current-power characteristic curves in search for a determined condition that indicates the maximum power point (MPP). However, the P&O usually presents some drawbacks such as slow response speed, steady-state power oscillation around the MPP and the poor tracking under sudden irradiance changes [4.1-4].

In this context, the present chapter documents modified P&O algorithms to minimize the problems mentioned above. The modified P&O algorithms are designed to ensure an optimal reference of photovoltaic current under any environmental conditions. Moreover, the MPPT schemes are employed with a model predictive current controller to control the power converter.

4.2 STATE OF THE ART OF MODIFIED PERTURB AND OBSERVE ALGORITHM

Different modified P&O algorithms have been documented to solve the P&O issues. The authors in [4.5] proposed a P&O algorithm with reference voltage perturbation to maximize the power of a PV pumping system for slowly and rapidly changing weather conditions. The control method has been implemented based on a proportional-integral (PI) controller and compared with a direct duty ratio perturbation technique. A variable step size P&O algorithm has been reported in [4.6], which uses the derivate of PV power to voltage for determining the variable duty cycle size, in order to accelerate the tracking operation of MPP as well as to reduce the PV power oscillation. The authors in [4.7] suggested a modified P&O algorithm based on an adaptive duty cycle step with an optimal proportional-integral-derivative (PID) controller tuned by genetic algorithms. The optimal PID controller is used to optimize the variable step size necessitated for the P&O algorithm. An improved P&O algorithm has been proposed in [4.8]. The proposed algorithm reduced the oscillation in steady-state by using a variable step size and asserted the right direction of MPP tracking by adding an instruction set. In [4.9], a modified P&O algorithm that avoids the drift phenomena in case of a sudden increase in irradiance level has been reported. The main idea of the presented algorithm is the insertion of an extra condition to the conventional P&O algorithm. In [4.10], a predictive voltage compensation loop is used to interface a current-based controller with a P&O MPPT for ensuring the right control algorithm operation as well as reducing the power oscillation. An adaptive P&O method has been designed to capture the optimal PV current by the authors in [4.11]. The designed MPPT uses a fractional short-circuit current (FSCC) method incorporated with the conventional P&O algorithm based on a current perturbation instead of voltage perturbation to accelerate the tracking performance, according to the linear relationship of PV current and irradiance level. The algorithm applied the reference current of a PI controller that generates the control signal. A real-time implementation of the PV system using a P&O algorithm providing the reference current for model predictive current controller has been discussed in [4.12]. Here the proposed current controller uses the system model for predicting the error at the next sampling time. Therefore, the switching state of the DC-DC converter that minimizes this error is selected and applied in the next sampling time. A P&O-based current MPPT strategy is presented in [4.13]. The approach employs with a sliding mode (SM) inner current loop for ensuring a high robustness to sudden irradiance changes. The authors in [4.14] proposed a zero-oscillation adaptive-step P&O MPPT using the PI voltage controller, followed by a (inner loop) current controller. In this MPPT, the perturbation is reduced to zero when the steady-state oscillation

is detected. Moreover, considering the mentioned discussions, a comparison of different MPPT schemes is summarized in Table 4.1.

TABLE 4.1: Modified P&O from research survey.

Authors	Year	Control Variable/ Converter Type	Controller Implementation	MPPT performances
Elgendy et al. [4.5]	2012	PV voltage/Boost Converter	TMS320F2812 DSP	Good tracking Medium steady-state oscillations Low complexity and moderate effort for implementation
Pandey et al. [4.6]	2008	Duty cycle/Buck Converter	ADuC831 Microcontroller	Good tracking Small steady-state oscillations Low complexity and easy implementation
Harrag et al. [4.7]	2015	Duty cycle/Boost Converter	Software implementation (Matlab/Simulink)	Good tracking Small steady-state oscillations High complexity and difficult implementation
Ahmed et al. [4.8]	2015	PV voltage/Buck-Boost Converter	Software implementation (Matlab/Simulink)	Good tracking Small steady-state oscillations Low complexity and moderate effort for implementation
Killi et al. [4.9]	2015	Duty cycle/SEPIC Converter	Arduino Atmega 2560	Good tracking Large steady-state oscillations Low complexity and easy implementation
Kakosimos et al. [4.10]	2013	PV voltage/Boost Converter	TMS320F2812 DSP	Good tracking Low steady-state oscillations Low complexity and moderate effort for implementation
Kollimalla et al. [4.11]	2014	PV current/Boost Converter	dSPACE DS 1104	Good tracking Small steady-state oscillations Low complexity and moderate effort for implementation
Shadmand et al. [4.12]	2014	PV current/Flyback Converter	dSPACE DS1103	Good tracking Small steady-state oscillations Low complexity and easy implementation
Bianconi et al. [4.13]	2013	PV current/Boost Converter	-	Good tracking Small steady-state oscillations Low complexity and moderate effort for implementation
Paz et al. [4.14]	2014	PV voltage/Boost Converter	TI C2000 Microcontroller	Good tracking Small steady-state oscillations Low complexity and moderate effort for implementation

On the other hand, fuzzy logic control offers many advantages. In particular, it does not need the mathematic model of the control process, being it is simple to understand and to apply in a variety of systems. Furthermore, application of fuzzy logic for maximization of the PV power can lead to better performance of the PV systems, and can offer good responses during

the variation in operating conditions. There are numerous modified P&O MPPT methods based on fuzzy logic controllers (FLC) for PV systems [4.15-22]. Nevertheless, the controllers investigate with a high number of rules, which will increase the computational burden, as well as increasing the controllers cost.

4.3 SYSTEM CONFIGURATION

The synoptic scheme of the PV system configuration studied in this chapter is shown in Figure 4.1. The PV array is coupled directly to a passive filter (capacitor) and followed by a boost converter, which is used to realize the MPPT operation with resistive load. The MPPT algorithm uses only the PV voltage and current measurements to generate the PV output current reference. The model predictive control (MPC) current controller is aimed to regulate the PV current according to the current reference, by controlling the average input current of the boost converter.

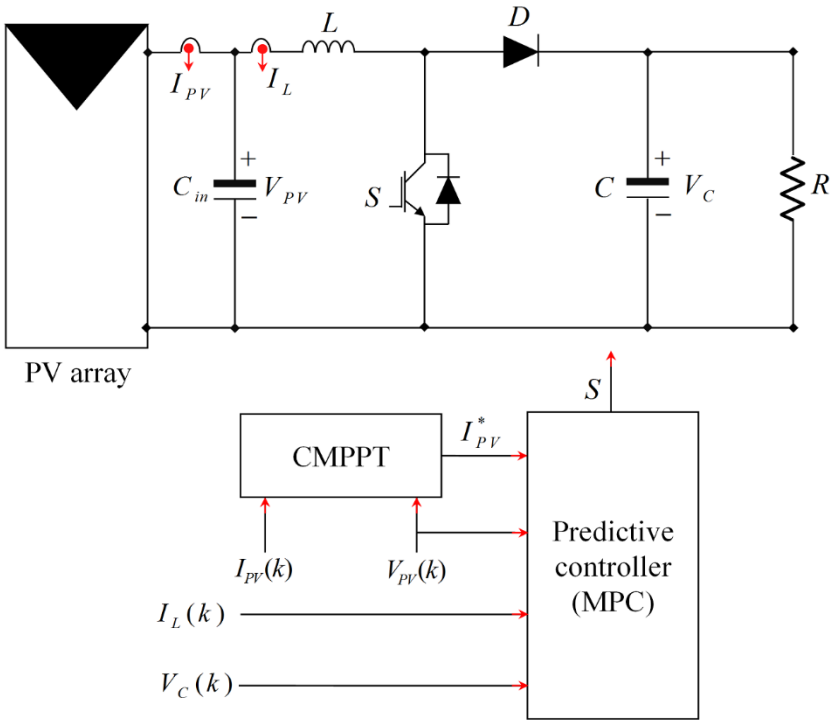

Figure 4.1: Proposed control scheme for the PV system.

4.4 MPPT ALGORITHMS

The largest part of the MPPT algorithms presented in the literature are voltage-based (VMPPT), because the logarithmic dependency of the PV voltage on the irradiation level makes the MPPT algorithm less sensible to the irradiance variation [4.1, 23]. In fact, the linear

dependency of the PV current on the irradiance level would be very useful for a fast MPPT, but the occurrence of irradiance drops might lead to the failure of the MPPT algorithm [4.23]. In this section, the different current-based MPPT (CMPPT) algorithms with a simple solution for this issue, are discussed and further explained.

4.4.1 Current Perturb and Observe Algorithm

The current perturb and observe algorithm uses the concept of a conventional P&O algorithm, nevertheless, it considers current perturbation instead of voltage or duty cycle perturbation to speed up the tracking performance. Figure 4.2 shows a flowchart for this algorithm.

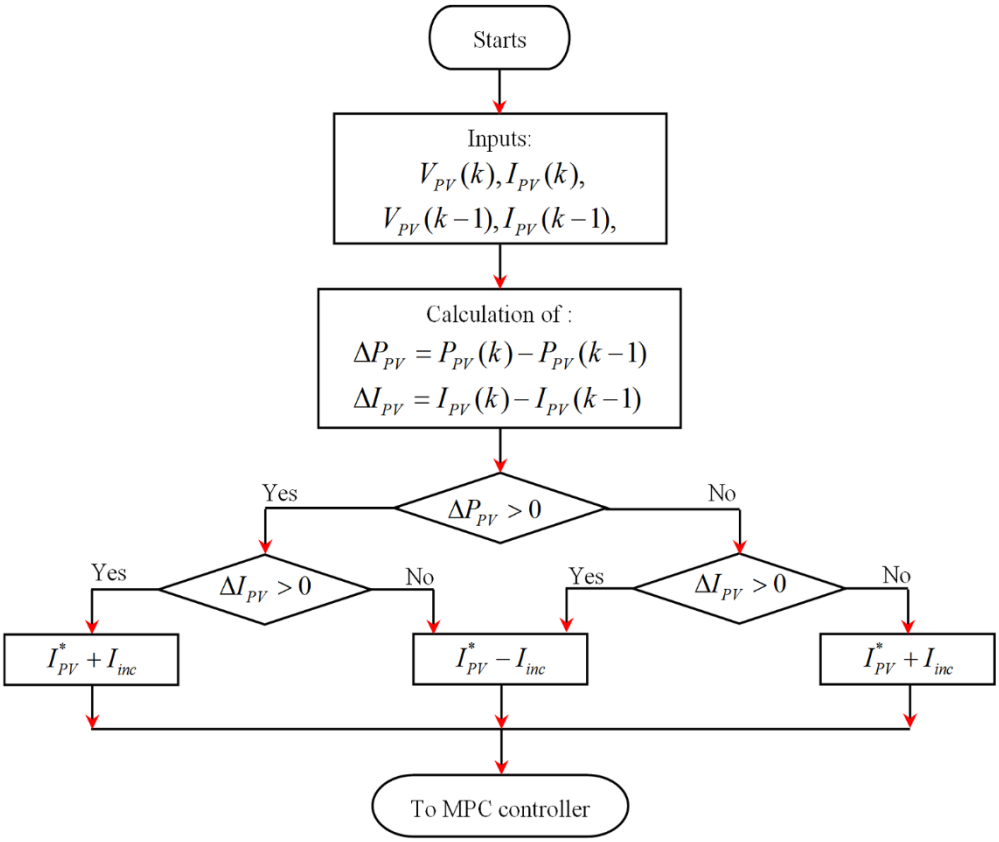

Figure 4.2: Flowchart of the current P&O algorithm.

As shown in Figure 4.2, when PV power and PV current increase at the same time and vice versa, a fixed current perturbation step size I_{inc}, will be added to the reference current I_{PV}^{*} to generate the next cycle of perturbation in order to force the operating point moving towards the MPP. When PV power increases and PV current decreases and vice versa, the perturbation step will be subtracted for the next cycle of perturbation. This process is repeated until the system reaches the MPP and oscillates around it.

4.4.2 Variable Current Step Size Perturb and Observe Algorithm

The current step size for the P&O MPPT determines how fast the MPP is achieved. Fast tracking can be achieved with bigger current increments, but excessive steady-state oscillations. This situation is inverted when the MPPT is operating with a smaller current increment. Therefore, a satisfying tradeoff between the dynamics and oscillations has to be made for the fixed step size MPPT. The variable current step size increment can solve the earlier design issue. In this chapter, the derivative of PV power to voltage (dP_{PV}/dV_{PV}), as shown in Figure 4.3, is introduced as a suitable parameter for regulating the variable increment for the P&O algorithm to determine the variable current increment for the P&O algorithm. The variable current step size method introduced to solve the problem discussed previously is given as follows:

$$I_{in} = N\left|\frac{dP_{PV}}{dV_{PV}}\right| \tag{4.1}$$

where:

N: is the scaling factor that is tuned by the design to adjust the current step size.

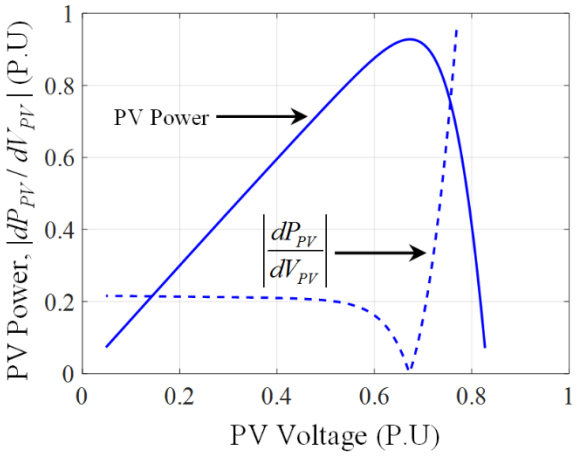

Figure 4.3: The normalized PV power and its derivative variation.

4.4.3 Fuzzy Perturb and Observe Algorithm

The fuzzy perturb and observe (FP&O) algorithm based on fuzzy logic is designed to take advantages of P&O method and eliminate its disadvantages. The flowchart of the FP&O algorithm is given in Figure 4.4. The suggested MPPT offers a variable current step size in order to improve the speed tracking of the MPP with the minimum possible of power fluctuation and to increase the stability under fast changing irradiance. The difference in this algorithm is

to replace comparison and switching methods by a fuzzy logic controller. In this chapter, the developed FLC represents MPPT controller for PV systems. Figure 4.5 shows the block diagram of the proposed FLC. The input data consists of the differential PV power ΔP_{PV} and the differential PV current ΔI_{PV} (the same inputs for P&O algorithm based on current perturbation), as shown in the following equations:

$$\Delta P_{PV} = P_{PV}(k) - P_{PV}(k-1) \tag{4.2}$$

$$\Delta I_{PV} = I_{PV}(k) - I_{PV}(k-1) \tag{4.3}$$

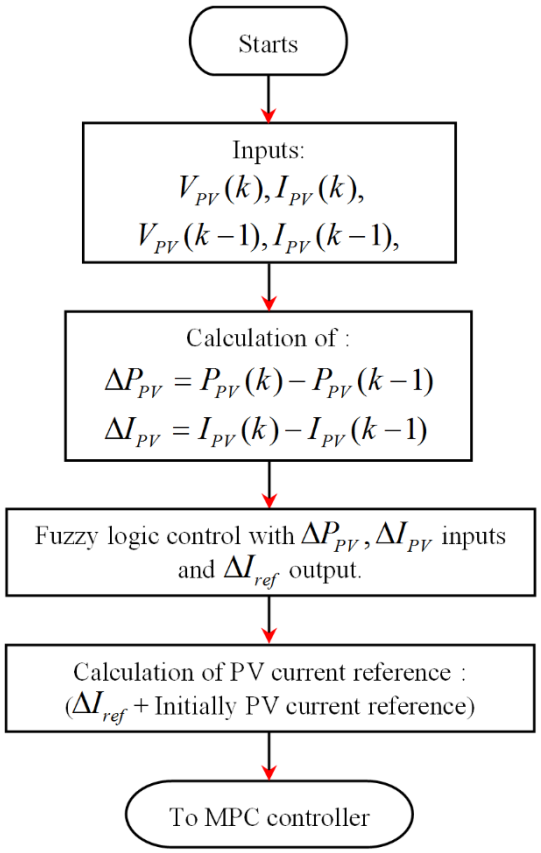

Figure 4.4: Flowchart of the FP&O algorithm.

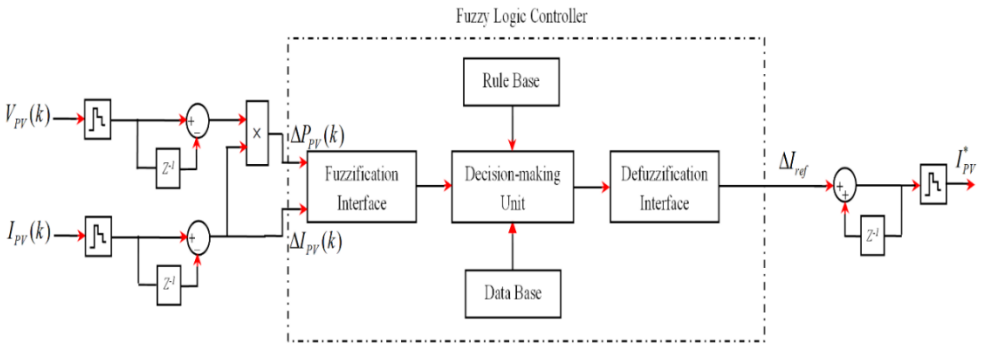

Figure 4.5: Block diagram of the proposed FLC for the FP&O algorithm.

The output controller gives the change of the PV reference current ΔI_{ref}, for computing the PV current reference. The current control is chosen to speed-up the tracking performance and to follow the right direction of the MPP under irradiance changing; due to the linear relationship between PV current and irradiance levels.

The membership functions of inputs for the FP&O algorithm are defined as trapezoidal functions in order to reduce the computational burden. The membership functions are constant in the output of the FP&O method (zero-order Takagi-Sugeno model). In Figure 4.6, membership functions for the inputs and output controller consist of four fuzzy variables with NB (Negative Big), NS (Negative Small), PS (Positive Small) and PB (Positive Big) being the linguistic labels and μ being the degree of membership. The proposed FLC is used with Takagi-Sugeno method due to its advantages (easy structure and simple design).

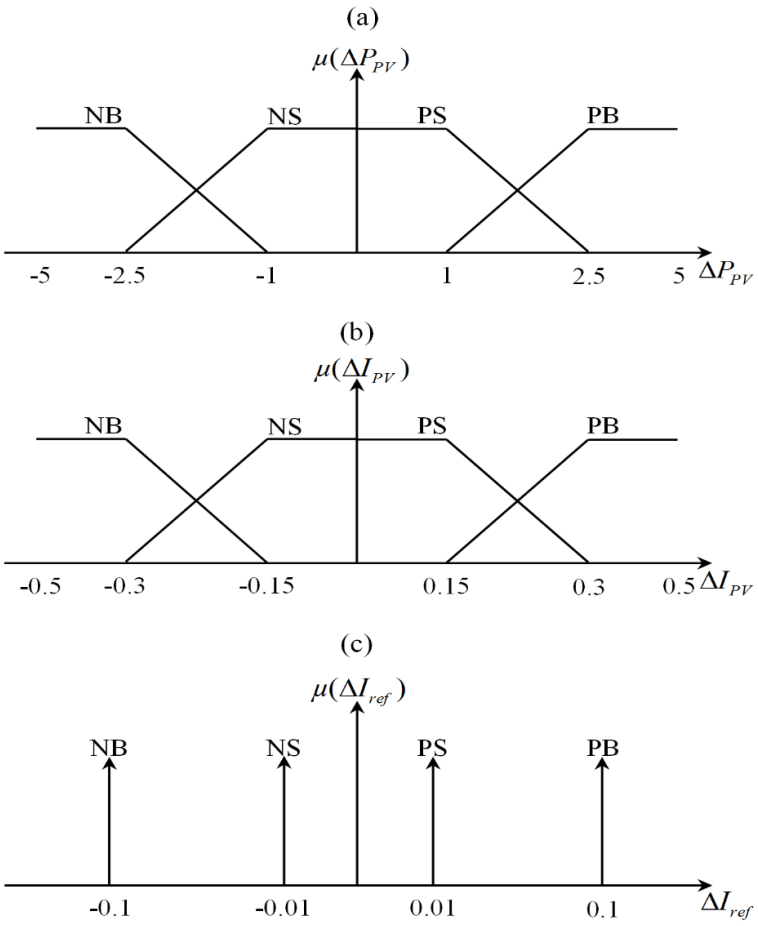

Figure 4.6: Membership function for variables of the FP&O algorithm: (a) and (b) inputs, (c) output.

The fuzzy rules are based on regulation of P&O algorithm and designed to track the MPP of the PV system under changing climatic conditions. The fuzzy rule consists of a set of if-then

statements, which guarantees all information about the controlled parameters. The details of the 16 proposed rules are shown in Table 4.2 and in the following equations:

If ΔP_{PV} is NB **AND** ΔI_{PV} is NB **THEN** ΔI_{ref} is PB.

If ΔP_{PV} is NS **AND** ΔI_{PV} is NS **THEN** ΔI_{ref} is PB.

……..

……..

……..

If ΔP_{PV} is PB **AND** ΔI_{PV} is PS **THEN** ΔI_{ref} is PB.

If ΔP_{PV} is PB **AND** ΔI_{PV} is PB **THEN** ΔI_{ref} is PB.

TABLE 4.2: Fuzzy rules base for FP&O.

	ΔI_{PV}			
ΔP_{PV}	**NB**	**NS**	**PS**	**PB**
NB	PB	PB	NB	NB
NS	PS	PS	NS	NS
PS	NS	NS	PS	PS
PB	NB	NB	PB	PB

The defuzzification is the last stage in fuzzy logic controller, where the center weighted average method is used to convert the output controller into crisp value.

$$\Delta I_{ref} = \frac{\sum_{i=1}^{n} w_i \mu_i(\Delta I_{ref})}{\sum_{i=1}^{n} w_i} \tag{4.4}$$

where:

n: is the number of rules.

w_i: is the is the weight coefficient for the rule consequent in rule i. The weight coefficient are computed by the minimum between the degree memberships of inputs:

$$w_i = \min\left[\mu_i(\Delta P_{PV}), \mu_i(\Delta I_{PV})\right] \tag{4.5}$$

4.4.4 Instability of the Current Based MPPT Algorithms and the Proposed Solution

In the case of sudden decrease in the solar irradiance, the current-based MPPT algorithm moves the operating point far from the new MPP, which can cause a system instability because the PV voltage be went to zero, while the PV current obtains almost instantaneously the short-circuit current value of the new irradiance level [4.1], as shown in Figure 4.7. The only way to avoid this voltage drop is to employ an extremely quick MPPT algorithm that must be able to change the current reference value very quickly.

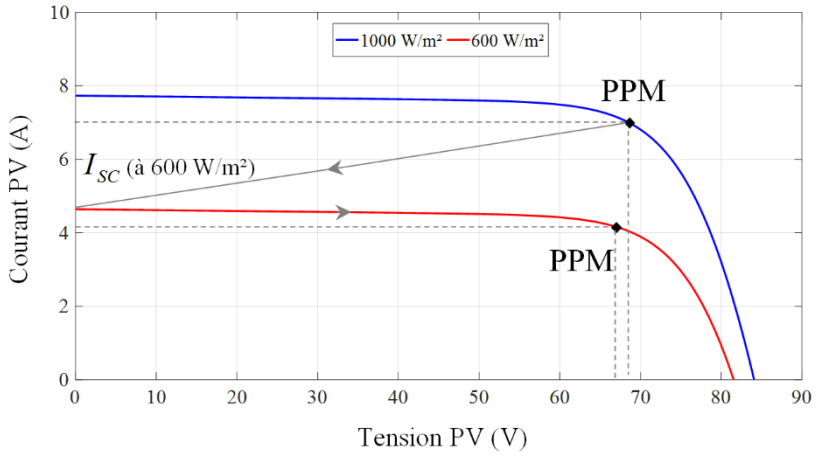

Figure 4.7: PV system behavior with CMPPT algorithm under sudden irradiance decrease.

In this context, a capacitor mounted at the PV array terminals to delay the system voltage variation under sudden irradiance decreases. Moreover, a simple solution to the instability of CMPPT algorithm is presented in this work as shown in Figure 4.8.

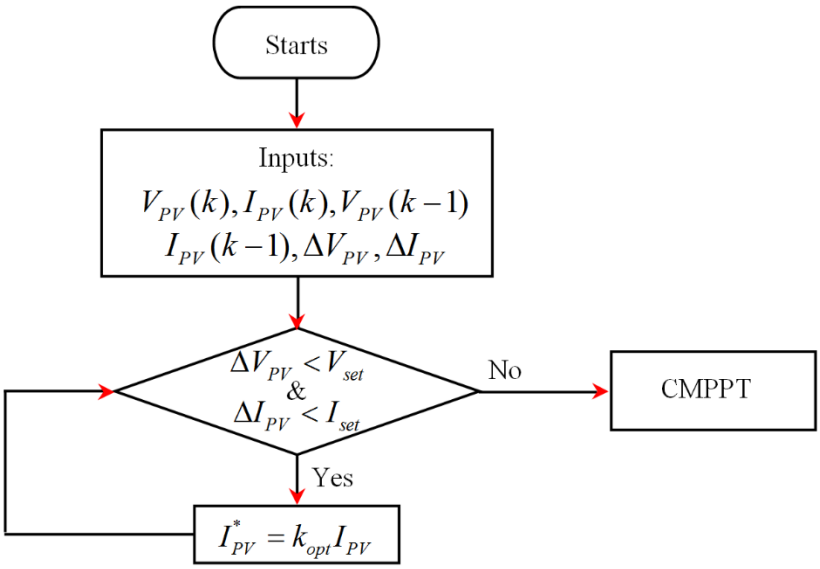

Figure 4.8: Proposed solution for CMPPT algorithm under sudden irradiance decrease.

The outline of this solution is done by checking the sudden decrease in the irradiance and if it occurs, then the MPPT scheme changes the current reference instantly, as indicated in Figure 4.8. Where V_{set} and I_{set} are the predetermined parameters used to detect the sudden irradiance decrease. k_{opt} is a proportionality constant and it is used to obtain an approximate value of the MPP current. This parameter is equal to the optimal proportionality constant that used in fractional short-circuit current (FSCC) method.

4.5 MODEL PREDICTIVE CURRENT CONTROLLER

In general, the boost converter is used as an adaptation stage to realize the MPPT for PV systems. In such systems, the boost converter offers a continuous current at the input. The control of the PV current can be achieved in an easy way if the MPC strategy is used to control the average input current of the boost converter.

4.5.1 Basic Operating of Model Predictive Control

During the last few years, the model predictive control (MPC), especially finite control set model predictive control (FSC-MPC) has rapid expansion as of this technique simplicity that is very intuitive and easy to understand. Moreover, micro-electronics and microprocessor developments has facilitated the implementation of this methodology [4.24-25].

The MPC is an advanced optimal control strategy that has been recently applied to power converters. The operating principle of MPC is summarized in Figure 4.9. The future values of the states of the system are predicted until a predefined horizon in time $k + N$ using the system model and the available information (measurements) until time k. The control action is computed by minimizing the cost function and the first element of this sequence is applied. This whole process is repeated again for each sampling instant considering the new measured data.

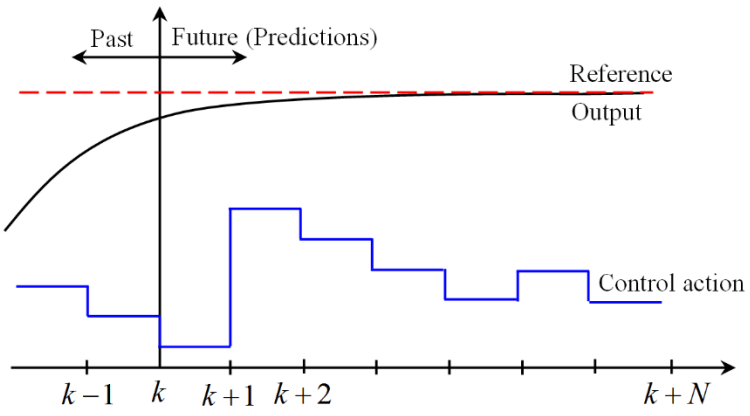

Figure 4.9: Operating principle of MPC.

4.5.2 Control Algorithm

The flowchart of the MPC algorithm is presented in Figure 4.10. The proposed MPC current controller calculates the future behavior of the controlled variable in advance. In the predictive algorithm, the input current of the boost, $I_L(k+1)$ must be calculated.

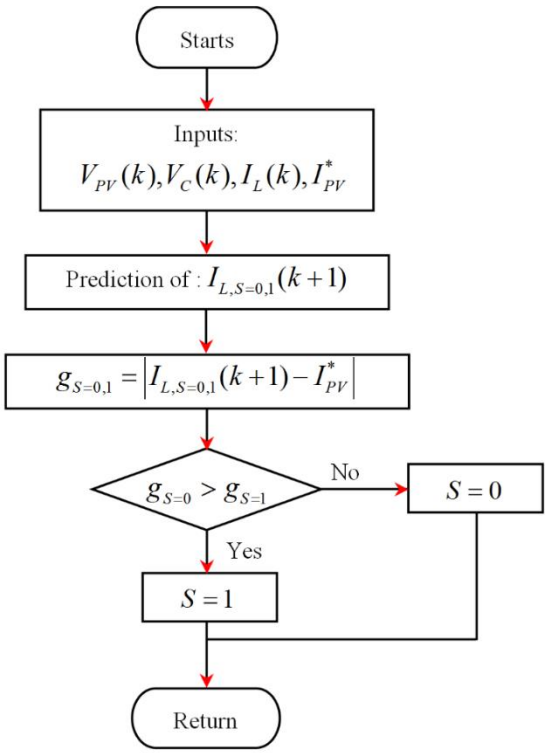

Figure 4.10: Flowchart of the MPC current controller.

The dynamic model of the boost converter with resistive load can be expressed as follows:

$$\frac{d}{dt} I_L = -(1-S)\frac{1}{L} V_C + \frac{1}{L} V_{PV} \tag{4.5}$$

$$\frac{d}{dt} V_C = (1-S)\frac{1}{C} I_L - \frac{1}{RC} V_C \tag{4.6}$$

where:

I_L : is the boost input current (A).

V_{PV} : is the boost input voltage (V).

V_C : is the boost output voltage (V).

R : is the boost resistive load (Ω).

L : is the boost input inductor (mH).

C : is the boost output capacitor (μF).

S : is the switching signal taking value from the discrete set $S = [1, 0]$.

To predict the inductor current, the Euler discretization method is considered:

$$\frac{dx(t)}{dt} \approx \frac{x(k+1)-x(k)}{T_s} \tag{4.7}$$

Therefore, the boost input current can be calculated as follows:

$$I_L(k+1) = I_L(k) - (1-S)\frac{T_s}{L}V_C(k) + \frac{T_s}{L}V_{PV}(k) \tag{4.8}$$

where:

T_s : is the sample time of the MPC algorithm.

In the proposed MPC algorithm, a cost function is evaluated for each possible switching state of the boost converter. The switching state whose current prediction $I_L(k+1)$ is close to the expected current reference I_{PV}^* is applied to the boost at the next sampling instant. In other terms, the switching state that minimizes the following cost function will be selected:

$$g_{S=0,1} = \left| I_{L,S=0,1}(k+1) - I_{PV}^* \right| \tag{4.9}$$

4.6 SIMULATION RESULTS

To verify the performance of the proposed algorithms based on MPC current controller, numerical simulations of the PV system shown in Figure 4.1 are developed and implemented in MATLAB/Simulink® software. The PV array consists of four PV modules (pb solar BP SX 120) of 120 Wp (connected in a 2 (series) × 2 (parallel)) with the current-voltage and power-voltage characteristics of the PV array illustrated in Figure 2.6. Table 4.3 lists the parameters of the boost converter components. Sampling time for the MPPT algorithms is 1 ms, and for MPC algorithm is 50 µs. The temperature is considered constant (25°C).

TABLE 4.3: Parameters of the boost converter.

Boost converter	**Nominal values**
Input capacitance (C_{in})	1110 μF
Inductance (L)	10 mH
Capacitance (C)	1110 μF
Load resistive (R)	50 Ω

4.6.1 Sudden Irradiance Changes

In this test, the irradiance level changes suddenly from 1000 W/m² to 800 W/m², 800W/m² to 400W/m² and then increases from 400 W/m² to 600 W/m², as shown in Figure 4.11, in order to investigate the performance of the system under sudden irradiance changes.

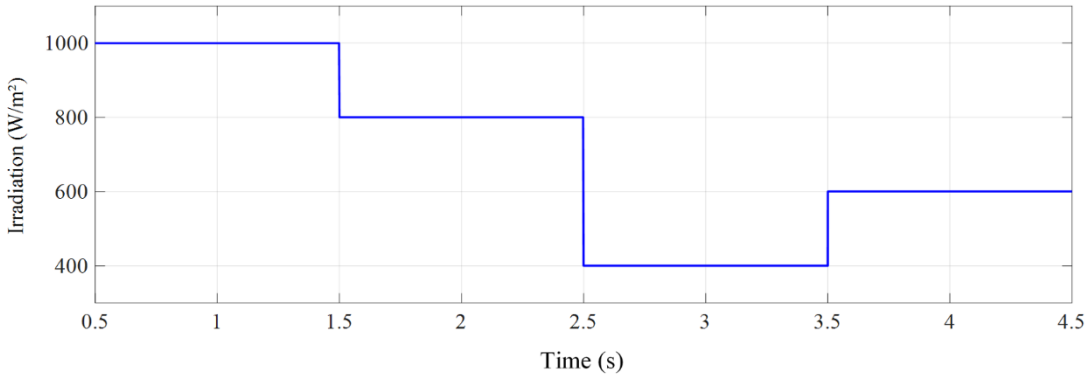

Figure 4.11: Solar irradiance profile for sudden irradiance changes test.

Figures 4.12 to 4.15 illustrate the results of the simulation of Figure 4.1 with the conventional P&O algorithm, the current P&O based on MPC, the variable current step size P&O based on MPC, and the FP&O employing MPC.

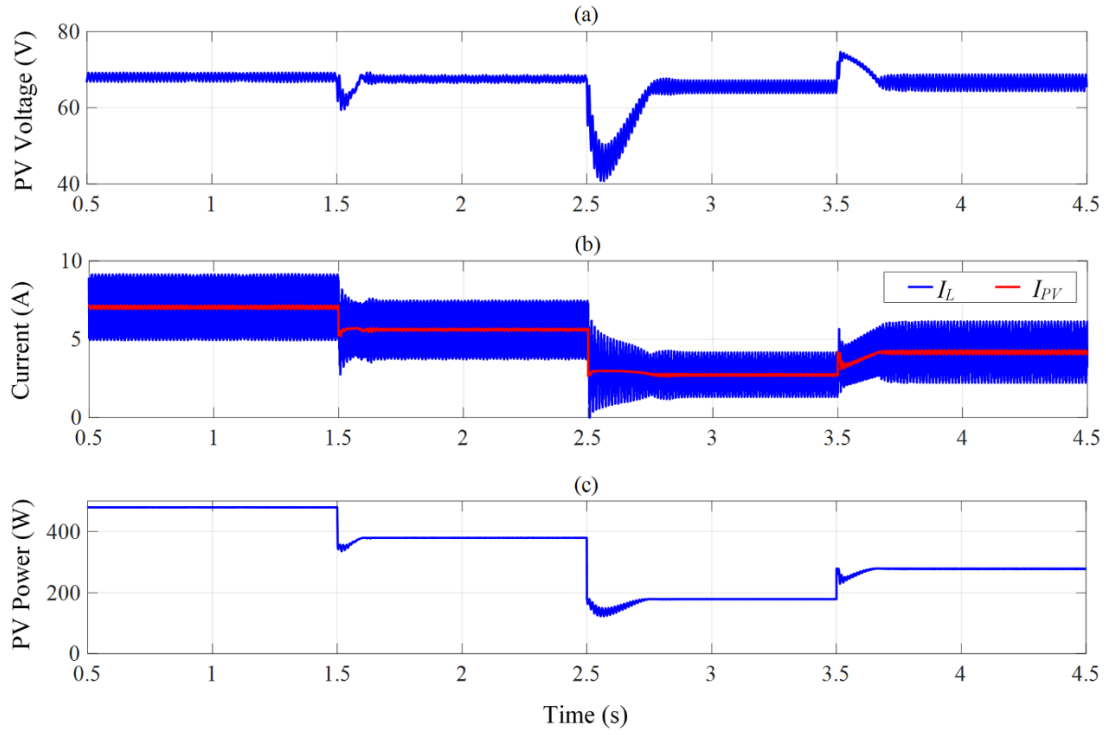

Figure 4.12: Simulation results of the system of Figure 4.1 with the conventional P&O algorithm.

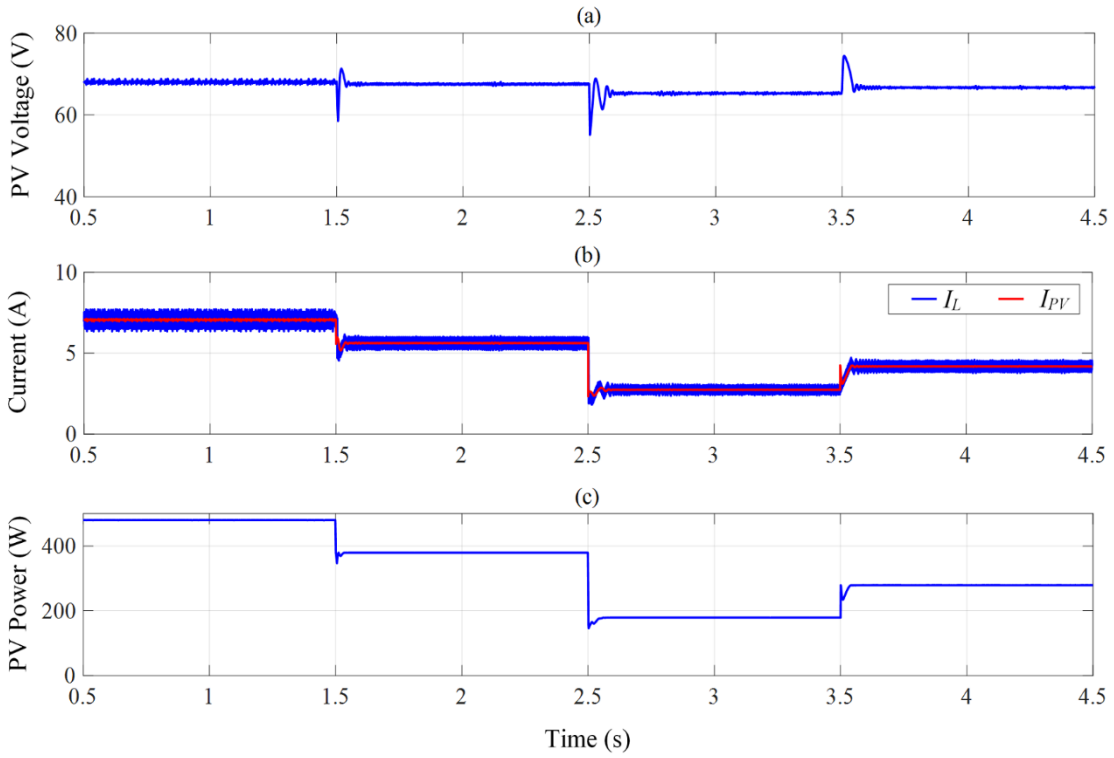

Figure 4.13: Simulation results of the system of Figure 4.1 with the current P&O algorithm based on MPC.

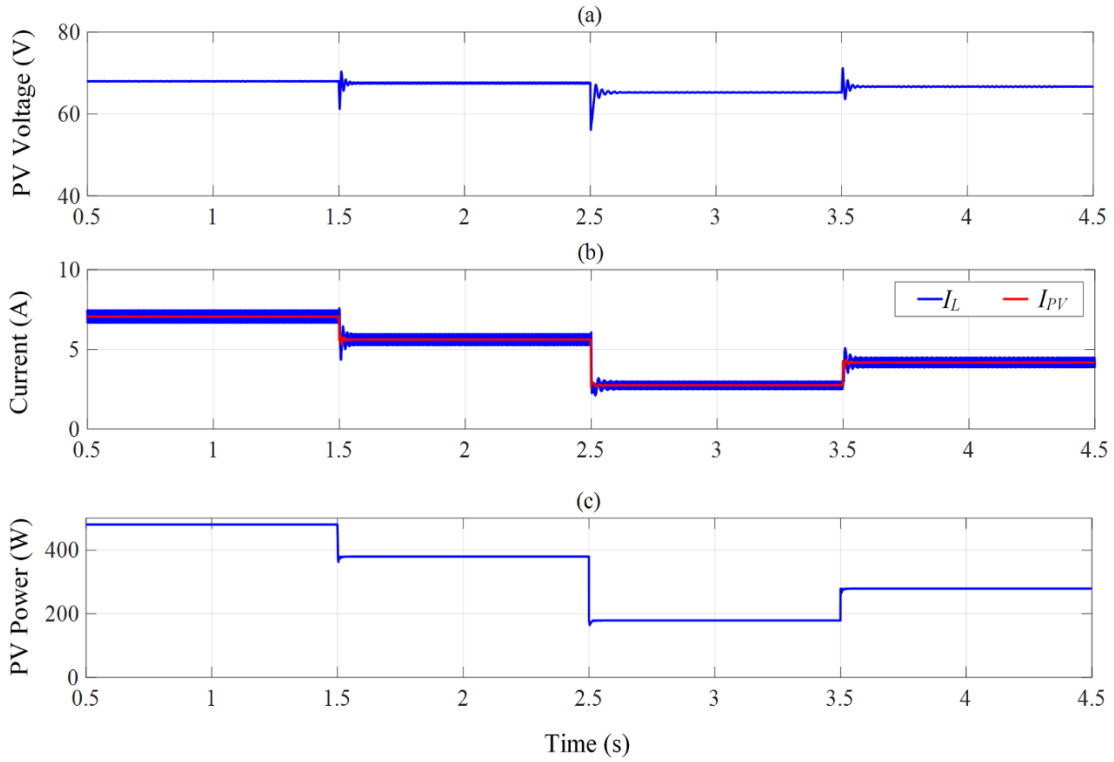

Figure 4.14: Simulation results of the system of Figure 4.1 with the variable current step size P&O algorithm based on MPC.

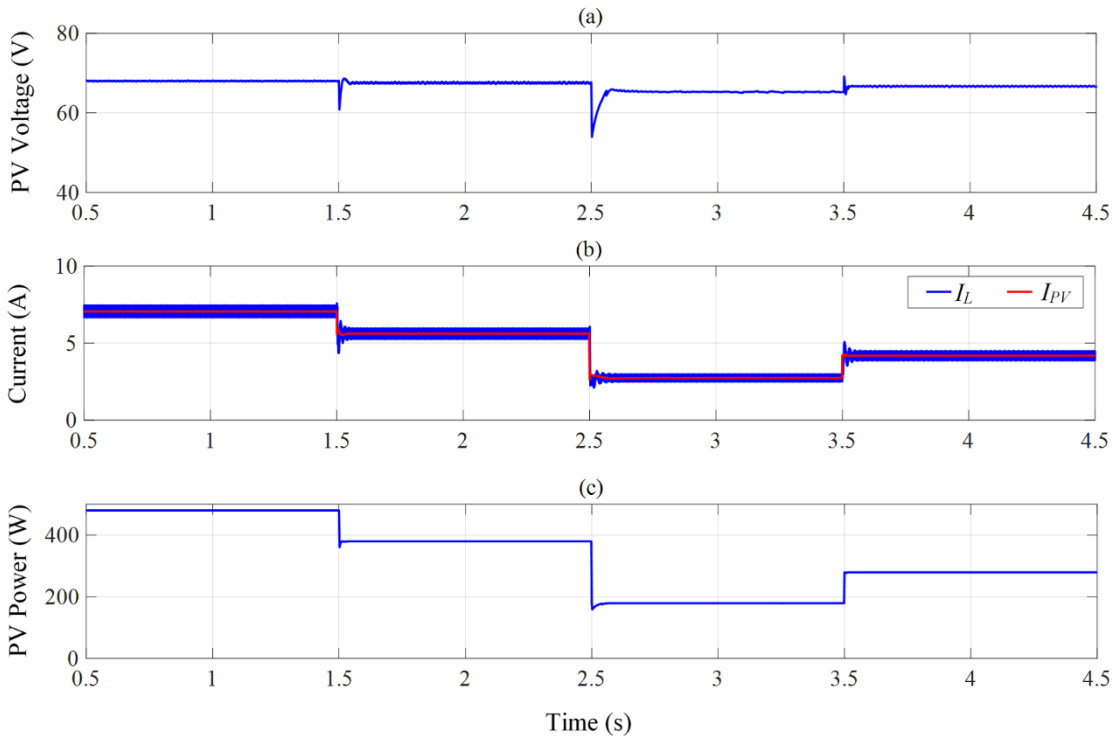

Figure 4.15: Simulation results of the system of Figure 4.1 with the FP&O algorithm based on MPC.

The comparison between the different MPPT algorithms is illustrated in Figure 4.16. Initially, the irradiance level is set to 1000 W/m² and the different MPPT algorithms work at the MPP. Next, an abrupt decrease in solar irradiance occurs at t = 1.5 s from 1000 W/m² to 800 W/m², the variable current step size P&O and FP&O algorithms show the better performance in terms of the speed tracking and the power fluctuation compared to the MPPT techniques. Where, the conventional P&O algorithm reaches the MPP at t = 0.115 s and the PV power is fluctuating around MPP (378.63-379.4 W). However, when using the conventional P&O through current perturbation based on MPC algorithm, the MPP is tracked at t = 0.034 s and the PV power is oscillating around the MPP (379.17-379.4 W). Moreover, for the variable current step size P&O and FP&O, the MPP is rapidly extracted at t = 0.018 s and t = 0.019 s respectively, and the PV power oscillation is less than 0.04 W for both methods. After, the irradiance is decreased suddenly again from 800 W/m² to 400 W/m² at t = 2.5 s. As shown in Figure 4. 16, the variable current step size P&O and FP&O methods perform better than the P&O algorithm and the P&O based on MPC algorithm. Finally, a sudden increase in the solar irradiance at t = 3.5 s from 400 W/m² to 600 W/m² is occurred. Therefore, the variable current step size P&O and FP&O algorithms can significantly be fasters, with no PV power oscillation

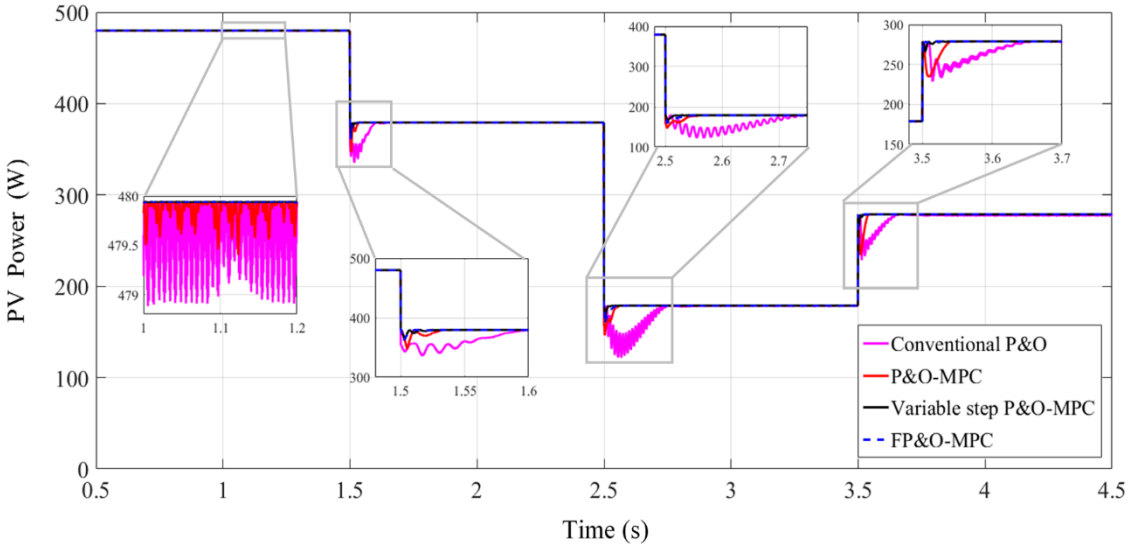

Figure 4.16: PV Output power waveforms for different MPPT algorithms under sudden irradiance changes.

in steady-state, and the MPP is directly achieved despite the sudden variation of solar irradiance level. The average tracking time of the variable current step size P&O and F&PO based on MPC algorithm under sudden changes in the irradiance is 0.0253 s and 0.026 s respectively. But with the conventional P&O algorithm requires 0.186 s (seven times lower than the FP&O MPPT) and the P&O based on MPC requires 0.0513 s (two times lower than the FP&O MPPT). A comparative table with the main values obtained in simulation for different MPPT is presented in Table 4.4.

TABLE 4.4: Summary of simulation results for sudden irradiance changes.

Technique	**Step decrease in irradiance 1000→800 W/m²**		**Step decrease in irradiance 800→400 W/m²**		**Step increase in irradiance 400→600 W/m²**	
	Tracking speed time (s)	Power oscillation (W)	Tracking speed time (s)	Power oscillation (W)	Tracking speed time (s)	Power oscillation (W)
Conventional P&O	0.115	1.18	0.268	0.77	0.175	0.98
Current P&O	0.034	0.45	0.063	0.23	0.57	0.35
Variable step size P&O	0.018	Less than 0.04	0.044	Less than 0.04	0.014	Less than 0.04
FP&O	0.019	Less than 0.04	0.047	Less than 0.04	0.012	Less than 0.04

4.6.2 Ramp Irradiance Changes

The objective of the ramp test is to quantify the ability of the MPPT to track the maximum power under ascending and descending irradiance trapezoidal with various slopes values. Figure 4.17 shows the irradiance profile used in this test.

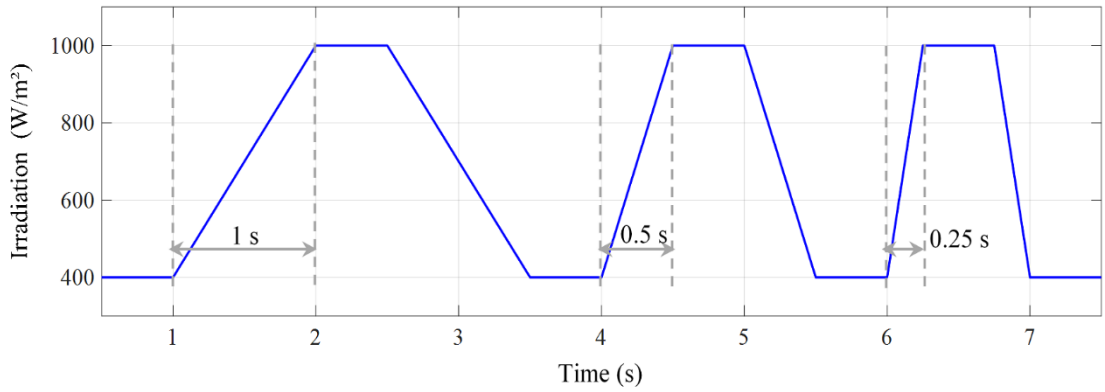

Figure 4.17: Solar irradiance profile for ramp irradiance changes test.

Figure 4.18 presents the simulation results of the power tracking performance for the different MPPT algorithms. It can be seen that the conventional P&O algorithm has more poor tracking performance if the slope of the ramp is increased with significate power fluctuations in steady-state. On the other hand, the MPPT algorithms employing MPC controllers perform better and track efficiently the maximum power at any condition, especially the variable current step size P&O and FP&O algorithms.

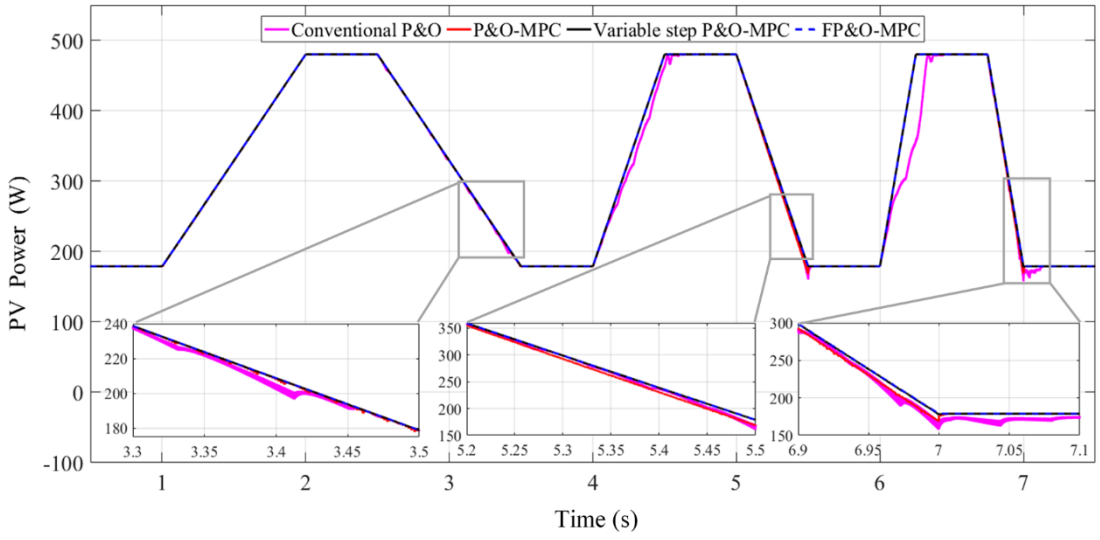

Figure 4.18: PV Output power waveforms for different MPPT algorithms under ramp irradiance changes.

4.7 EXPERIMENTAL RESULTS

A laboratory prototype of a PV system has been implemented in order to validate the studied algorithms. The experimental test bench, shown in Figure 4.19, consists of a programmable power supply (APS-1102A GW Instek) to emulate the PV array, a Semikron inverter with its control board used as a boost converter, a resistive load, a dSPACE DS 1104 system, current and voltage sensors. The control scheme has been implemented in real-time via dSPACE DS 1104 system through the Matlab/Simulink®. The system parameters (PV module and Boost converter) used in the experiment are the same as those used in the simulation, as stated in the Tables 2.1 and 4.3. The sampling time of the different MPPT algorithms is 1 ms. The sampling frequency of the MPC algorithm is set to 20 kHz. The experimental results are recorded using a 500 MHz Instek oscilloscope. The experimental system is tested under different irradiance changes (sudden and ramp), while the temperature is considered constant (25°C).

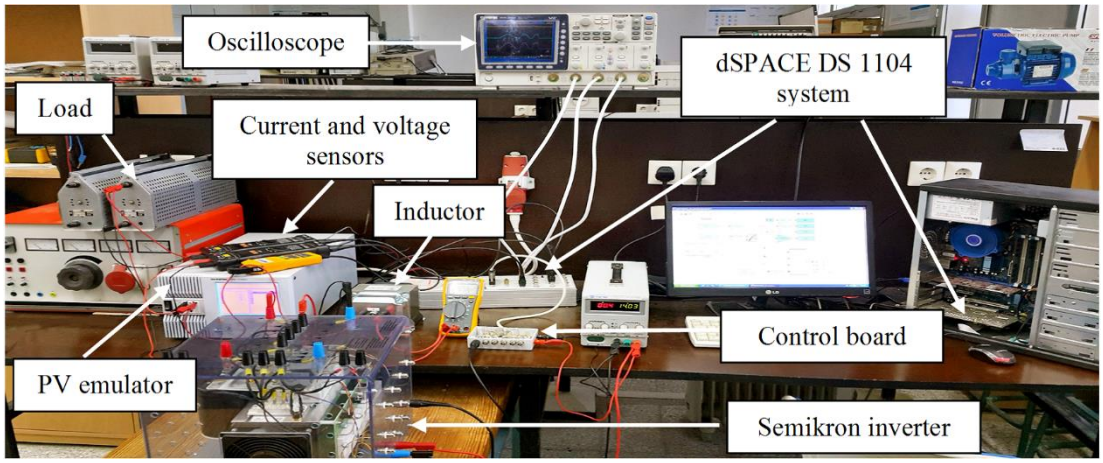

Figure 4.19: Snapshot of the experimental test bench.

4.7.1 Sudden Irradiance Changes

The performance of different MPPT algorithms is evaluated in this section under various sudden irradiance changes. A variable irradiance profile over a time period of 10 s is considered to ensure sudden decreasing and increasing in irradiance level during the experiments.

The experiment waveforms for the voltage, current and power of the PV emulator obtained with the conventional P&O are shown in Figure 4.20. The conventional P&O is implemented with the same parameters as used in the simulation results. From Figure 4.21, it is observed that for sudden decrease and increase in irradiance level, the PV power has a slow dynamic response and large power oscillation in steady state, which leads to power loss in the PV system.

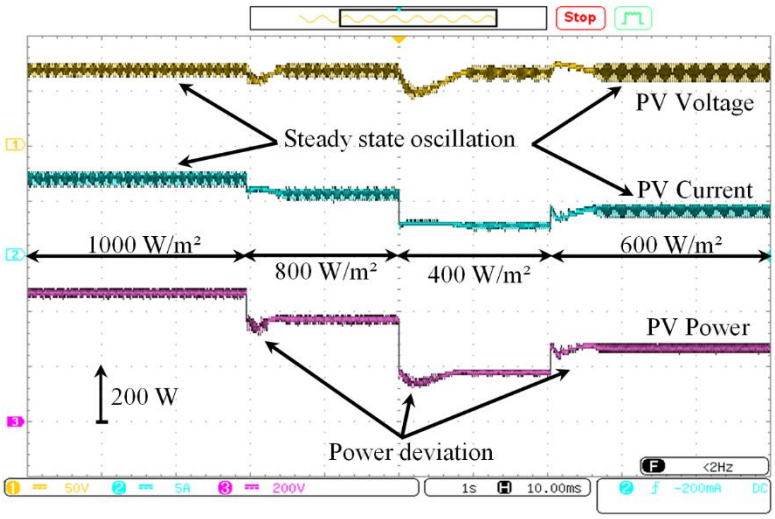

Figure 4.20: Experimental waveforms of the PV voltage, current and output power for sudden irradiance changes, using the conventional P&O.

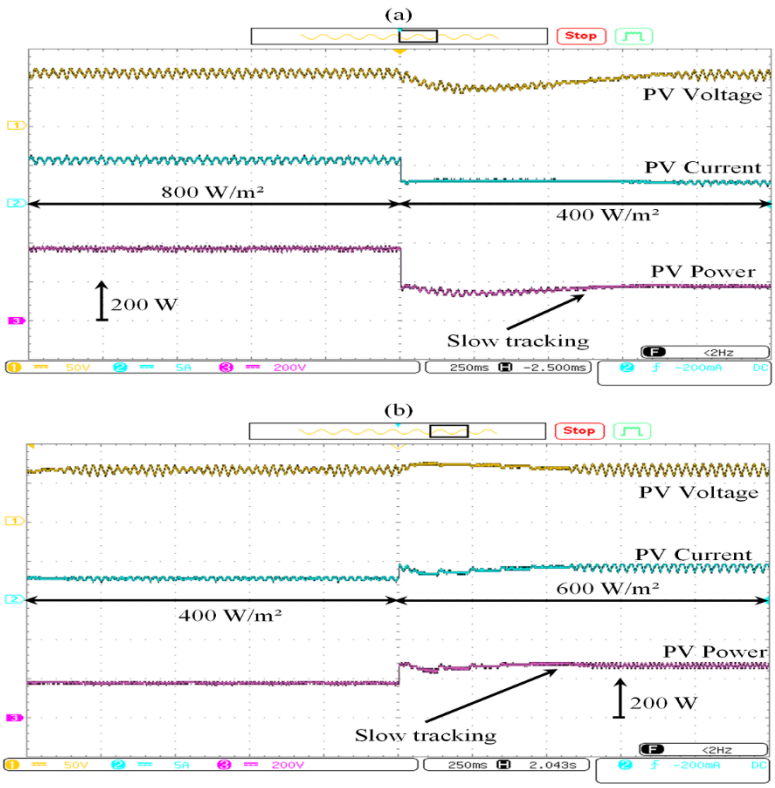

Figure 4.21: Zoom-in view of Figure 5.20 during (a) step decrease in the irradiance level (800 W/m²–400 W/m²) and (b) step increase in the irradiance level (400 W/m²–600 W/m²).

As shown in Figure 4.22, the P&O with current perturbation performed by an MPC current controller provides a better performance than the conventional P&O for sudden increasing and decreasing in irradiance. It is clear that the PV power response of P&O based on MPC is faster and lesser power oscillation than classic P&O as shown in Figure 4.23.

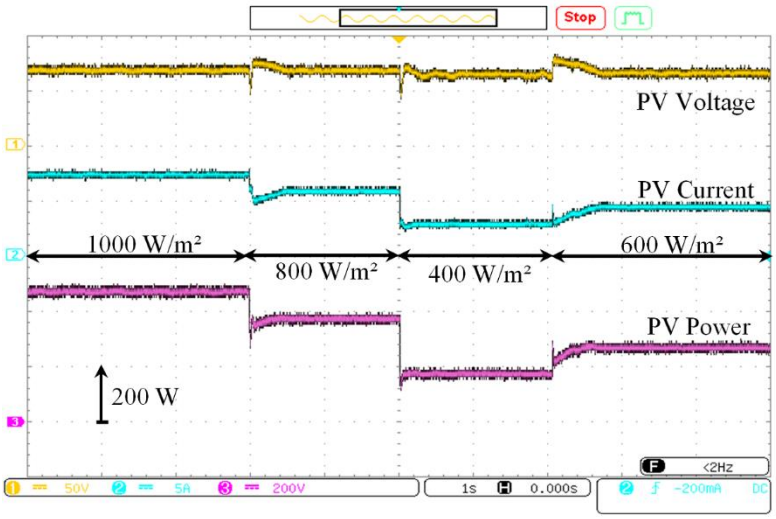

Figure 4.22: Experimental waveforms of the PV voltage, current and output power for sudden irradiance changes, using the current P&O based on MPC.

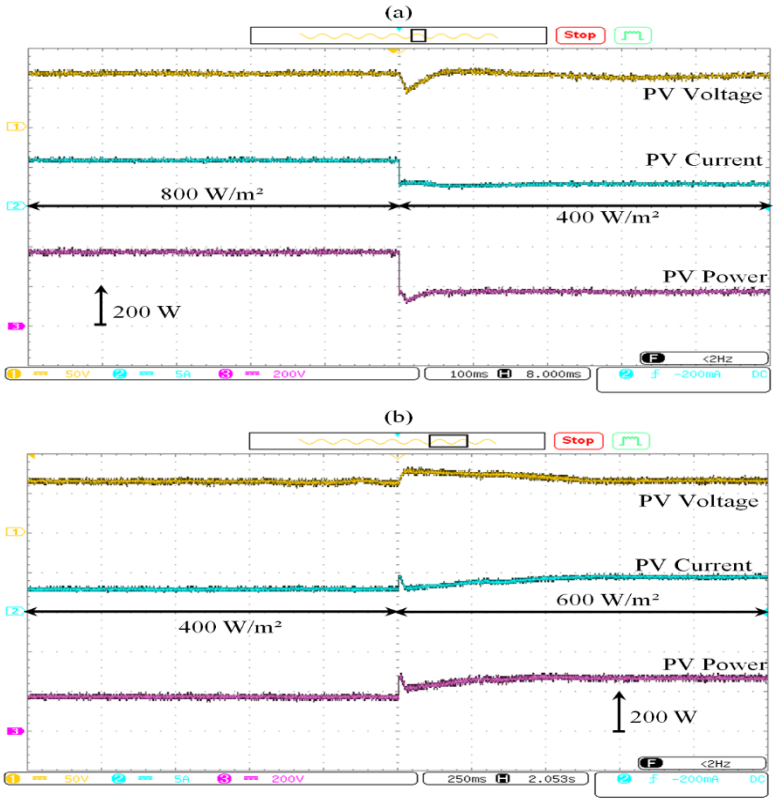

Figure 4.23: Zoom-in view of Figure 5.22 during (a) step decrease in the irradiance level (800 W/m²–400 W/m²) and (b) step increase in the irradiance level (400 W/m²–600 W/m²).

In Figure 4.24 and 4.26, the variable current step size P&O and FP&O algorithms show a high accuracy of tracking regardless of the irradiance changes, where the MPP is straightly achieved despite the sudden variation in irradiance level. As shown in Figures 4.25 and 4.27,

these algorithms are achieved rapidly the MPP during sudden decrease or increase in irradiance level. Moreover, the power oscillation in steady-state is small using these MPPT algorithms.

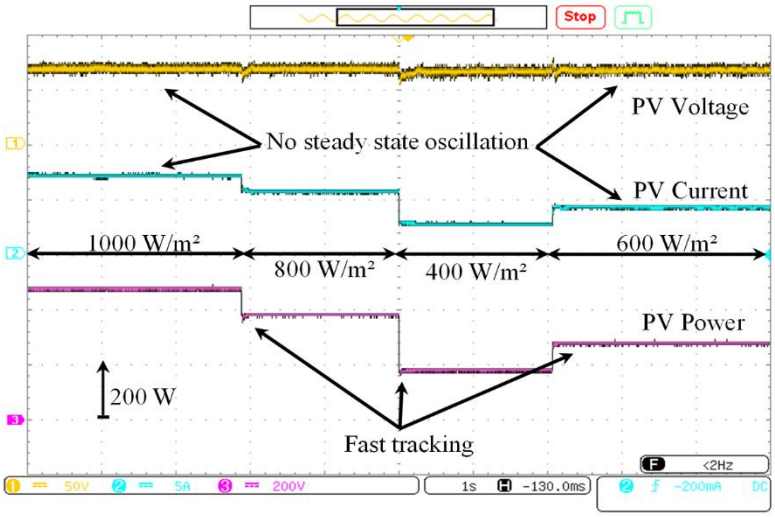

Figure 4.24: Experimental waveforms of the PV voltage, current and output power for sudden irradiance changes, using the variable current step size P&O based on MPC.

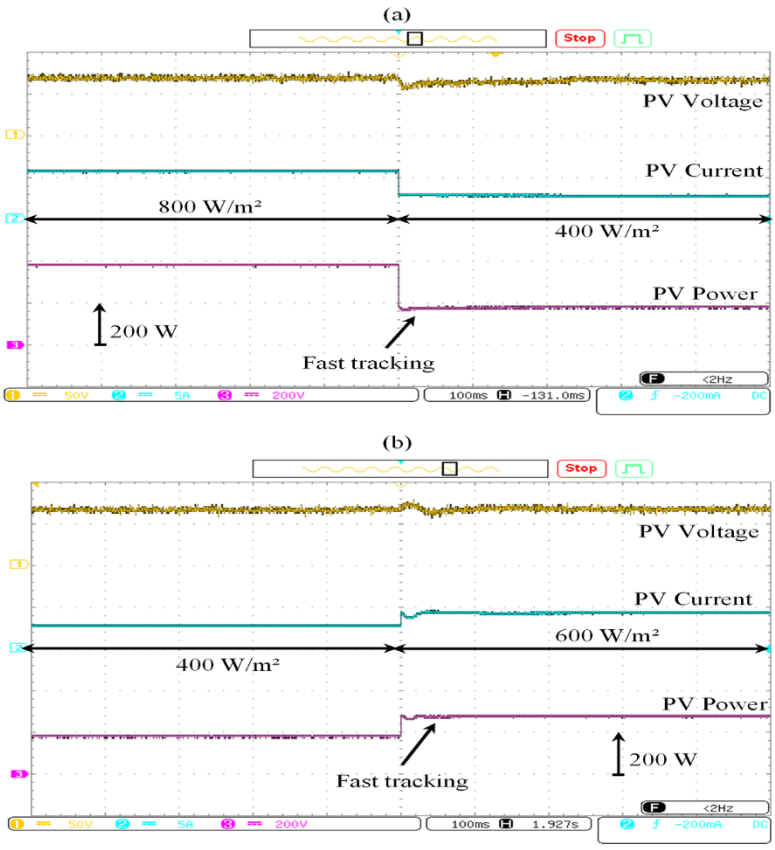

Figure 4.25: Zoom-in view of Figure 5.24 during (a) step decrease in the irradiance level (800 W/m²–400 W/m²) and (b) step increase in the irradiance level (400 W/m²–600 W/m²).

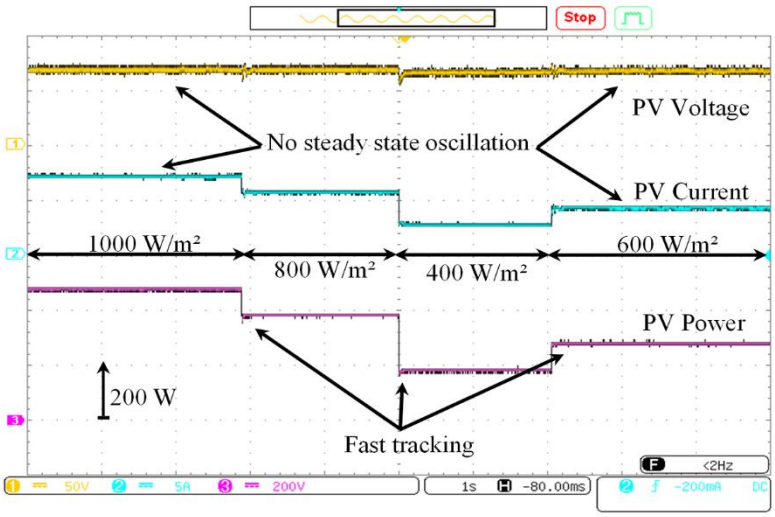

Figure 4.26: Experimental waveforms of the PV voltage, current and output power for sudden irradiance changes, using the FP&O based on MPC.

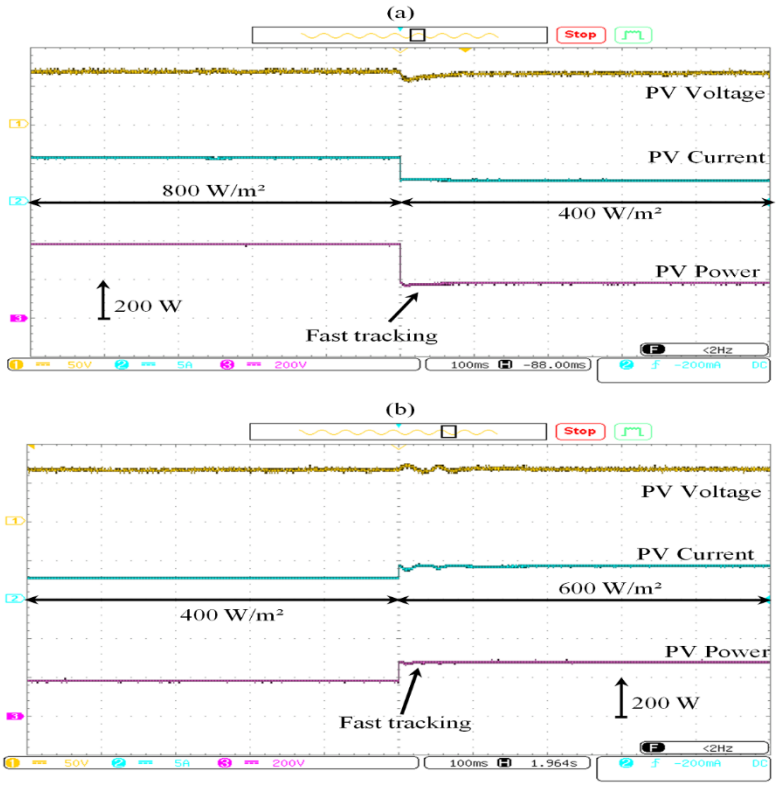

Figure 4.27: Zoom-in view of Figure 5.26 during (a) step decrease in the irradiance level (800 W/m²–400 W/m²) and (b) step increase in the irradiance level (400 W/m²–600 W/m²).

4.7.2 Ramp Irradiance Changes

Figures 4.28, 5.29, 5.30 and 5.31 show the experimental results for the different MPPT algorithms during the ramp irradiance changes, where the results are similar to those in the

simulation. These results show that the MPPT algorithms employing MPC current controller are considerably improved the poor instantaneous efficiencies corresponding to the conventional P&O method.

Table 4.5 summaries a comparison between the four MPPT methods in terms of tracking speed, power oscillation in steady-state, tracking accuracy and facility of implementation. The use of the variable current step size P&O and FP&O algorithms have reduced the tracking time. In addition, the power oscillation have also been minimized in the response with these algorithms.

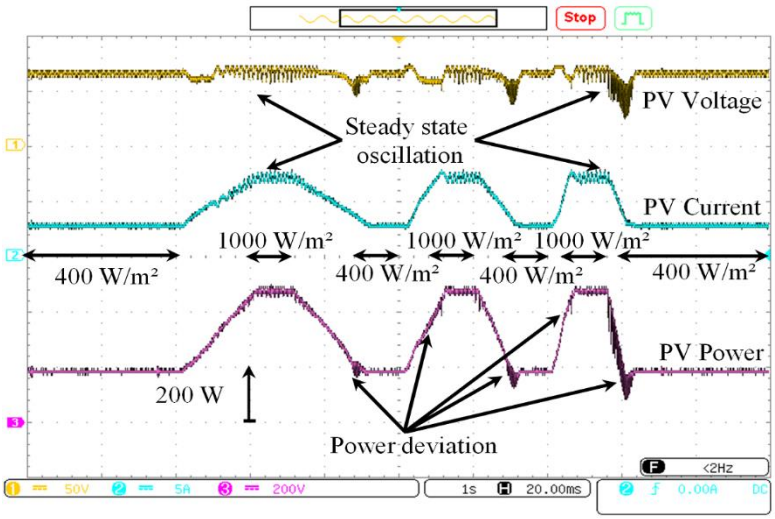

Figure 4.28: Experimental waveforms of the PV voltage, current and output power for ramp irradiance changes, using the conventional P&O.

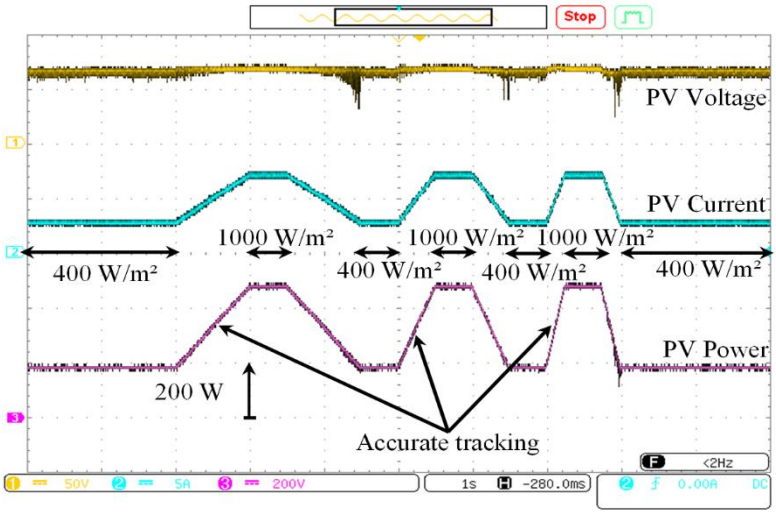

Figure 4.29: Experimental waveforms of the PV voltage, current and output power for ramp irradiance changes, using the current P&O based on MPC.

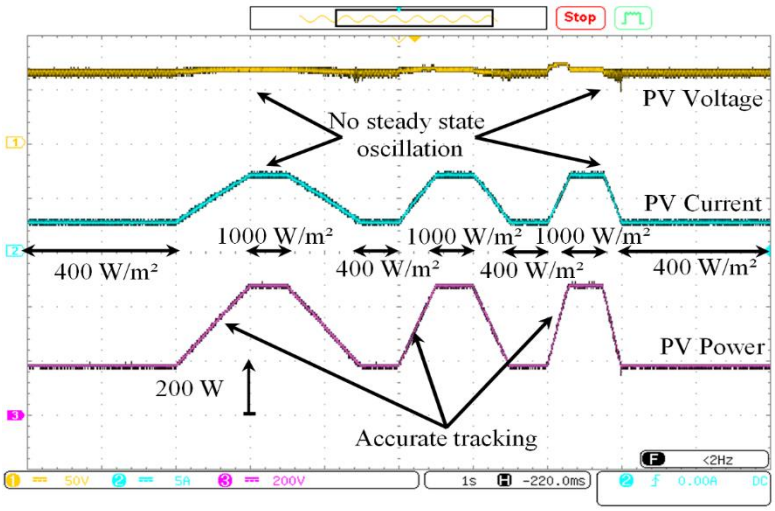

Figure 4.30: Experimental waveforms of the PV voltage, current and output power for ramp irradiance changes, using the variable current step size P&O based on MPC.

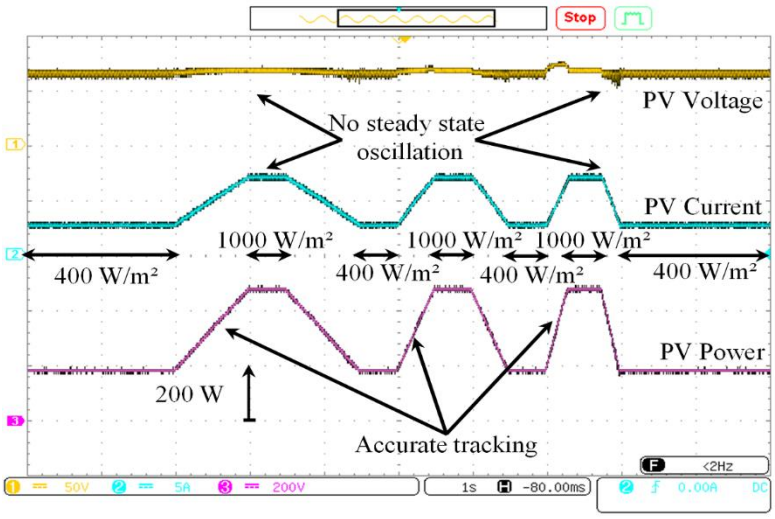

Figure 4.31: Experimental waveforms of the PV voltage, current and output power for ramp irradiance changes, using the FP&O based on MPC.

TABLE 4.5: Comparative issues between different MPPT algorithms.

Feature	Conventional P&O	Current P&O	Variable step size P&O	FP&O
Tracking speed time	High	Medium	Low	Low
Steady-state oscillation	Large	Small	Very small	Very small
Tracking accuracy	Bad	Good	Good	Good
Implementation complexity	Lower	Moderate	Moderate	Higher

4.8 CONCLUSION

This chapter presents design, simulation and experimental validation of MPPT algorithms for PV system by employing MPC current controller. The presented algorithms have been successfully simulated and implemented in real-time using dSPACE DS 1104 board for a laboratory bench based on PV emulator. Simulation and experimental results prove that the variable current step size P&O and FP&O algorithms based on MPC current controller have enhanced the PV system performance compared to both conventional P&O and current P&O employed with MPC algorithm. Comparative results show that the PV power oscillation and the tracking speed time of the MPP for the variable current step size P&O and FP&O algorithms have been considerably reduced.

REFERENCES

[4.1] Femia, N., Petrone, G., Spagnuolo, G., Vitelli, M., 2012. Power Electronics and Control Techniques for Maximum Energy Harvesting in Photovoltaic Systems. CRC Press.

[4.2] Femia, N., Petrone, G., Spagnuolo, G., Vitelli, M., 2005. Optimization of perturb and observe maximum power point tracking method. IEEE Trans. Power Electron. 20, 963–973.

[4.3] Hussein, K.H., Muta, I., Hoshino, T., Osaka, M., 1995. Maximum photovoltaic power tracking: an algorithm for rapidly changing atmospheric conditions. IEE Proc. Gener. Transnm. Distrib. 142, 59–64.

[4.4] de Brito, M.A.G., Galotto, L., Sampaio, L.P., e Melo, G.A., Canesin, C.A., 2013. Evaluation of the main MPPT techniques for photovoltaic applications. IEEE Trans. Ind. Electron. 60, 1156–1167.

[4.5] Elgendy, M.A., Zahawi, B., Atkinson, D.J., 2012. Assessment of perturb and observe MPPT algorithm implementation techniques for PV pumping applications. IEEE Trans. Sustain. Energy 3, 21–33.

[4.6] Pandey, A., Dasgupta, N., Mukerjee, A.K., 2008. High-performance algorithms for drift avoidance and fast tracking in solar MPPT system. IEEE Trans. Energy Convers. 23, 681–689.

[4.7] Harrag, A., Messalti, S., 2015. Variable step size modified P&O MPPT algorithm using GAbased hybrid offline/online PID controller. Renew. Sustain. Energy Rev. 49, 1247–1260.

[4.8] Ahmed, J., Salam, Z., 2015. An improved perturb and observe (P&O) maximum power point tracking (MPPT) algorithm for higher efficiency. Appl. Energy 150, 97–108.

[4.9] Killi, M., Samanta, S., 2015. Modified perturb and observe MPPT algorithm for drift avoidance in photovoltaic systems. IEEE Trans. Ind. Electron. 62, 5549–5559

[4.10] Kakosimos, P.E., Kladas, A.G., Manias, S.N., 2013. Fast photovoltaic system voltage- or current-oriented mppt employing a predictive digital current-controlled converter. IEEE Trans. Ind. Electron. 60, 5673–5685.

[4.11] Kollimalla, S.K., Mishra, M.K., 2014. A novel adaptive P&O MPPT algorithm considering sudden changes in the irradiance. IEEE Trans. Energy Convers. 29, 602–610.

[4.12] Shadmand, M.B., Balog, R.S., Abu-Rub, H., 2014. Model predictive control of PV sources in a smart DC distribution system: maximum power point tracking and droop control. IEEE Trans. Energy Convers. 29, 913–921.

[4.13] Bianconi, E., Calvente, J., Giral, R., Mamarelis, E., Petrone, G., Ramos-Paja, C.A., Spagnuolo, G., Vitelli, M., 2013. A fast current-based MPPT technique employing sliding mode control. IEEE Trans. Ind. Electron. 60, 1168–1178.

[4.14] Paz, F., Ordonez, M., 2014. Zero oscillation and irradiation slope tracking for photovoltaic MPPT. IEEE Trans Ind. Electron. 61, 6138–6147.

[4.15] Al Nabulsi, A., Dhaouadi, R., 2012. Efficiency optimization of a DSP-based standalone PV system using fuzzy logic and dual-MPPT control. IEEE Trans. Ind. Informa. 8, 573–584.

[4.16] Alajmi, B.N., Ahmed, K.H., Finney, S.J., Williams, B.W., 2011. Fuzzy-logic-control approach of a modified hill-climbing method for maximum power point in microgrid standalone photovoltaic system. IEEE Trans. Power Electron. 26, 1022–1030.

[4.17] Radjai, T., Gaubert, J.P., Rahmani, L., Mekhilef, S., 2015. Experimental verification of P&O MPPT algorithm with direct control based on Fuzzy logic control using CUK converter. International Transactions on Electrical Energy Systems, 25, 3492–3508.

[4.18] D'Souza, N.S., Lopes, L.A.C., Liu, X., 2010. Comparative study of variable size perturbation and observation maximum power point trackers for PV systems. Electric Power Systems Research 80, 296–305.

[4.19] Boukezata, B., Chaoui, A., Gaubert, J.–P., Hachemi, M., 2016. An improved fuzzy logic control MPPT based P&O method to solve fast irradiation change problem, J. Renew. Sustain. Energy 8, 04350–14.

[4.20] Zainuri, M.A.A.M., Radzi, M. A. M., Soh, A.C., Abd Rahim, N. , 2014. Development of adaptive perturb and observe-fuzzy control maximum power point tracking for photovoltaic boost dc–dc converter. IET Renew. Power Gener. 8, 183–194.

[4.21] El Khateb, A.H., Rahim, N.A., Selvaraj, J., 2013. Fuzzy logic control approach of a maximum power point employing SEPIC converter for standalone photovoltaic system. Procedia Environmental Sciences, 17, 529–536.

[4.22] Altin, Necmi, Ozdemir, Saban, 2013. Three-phase three-level grid interactive inverter with fuzzy logic based maximum power point tracking controller. Energy Convers. Manage. 69, 17–26.

[4.23] Mamarelis, E., Petrone, G., Spagnuolo, G., 2014. Design of a slidingmode-controlled SEPIC for PV MPPT applications. IEEE Trans. Ind. Electron. 61, 3387–3398.

[4.24] Rodriguez, J., Kazmierkowski, M.P., Espinoza, J.R., Zanchetta, P., Abu-Rub, H., Young, H.A., Rojas, C.A., 2013. State of the art of finite control set model predictive control in power electronics. IEEE Trans. Ind. Informa. 9, 1003–1016.

[4.25] Vazquez, S., Rodriguez, J., Rivera, M., Franquelo, L.G., Norambuena, M., 2017. Model predictive control for power converters and drives: Advances and trends. IEEE Trans. Ind. Electron. 64, 935–947.

Chapter 5

High-Performance Control Scheme for Photovoltaic Pumping System

5.1 INTRODUCTION

Water photovoltaic (PV) pumping systems without battery can provide a cost-effective use of solar PV energy. In this solution the role of batteries is substituted by fluid storage, and steady-state operation depends on the amount of available power. Firstly, the use of a DC motor was a standard. Currently, thanks to development of AC induction motor (IM) drive systems it is possible to use a more robust and less expensive motor for PV pumping application. The aim of this chapter is to show how to achieve an effective photovoltaic pumping system without batteries.

This chapter proposes an effective control scheme for a PV pumping system based on IM, where an improved P&O current based-MPPT is developed to generate a variable current step size in order to improve the performance of the conventional P&O, increase the stability of the MPPT under abrupt irradiance changes. Moreover, the proposed algorithm supported by an extra condition to protect the IM under load drops. The MPPT control includes a model predictive control (MPC) current controller, and the simplicity of implementation is nevertheless maintained. On the other hand, a Takagi-Sugeno (T-S) type fuzzy logic controller (FLC) is suggested to regulate and keep the DC-link voltage constant at the desired value

regardless the operation conditions. The torque command produced by the FLC can be directly applied to the predictive torque and flux control (PTC) algorithm, which eliminates the use of speed control loop. By adopting the PTC algorithm for IM drive, a significant flux and torque ripples reduction are achieved, when compared with the conventional direct torque control (DTC). Numerical simulations and real-time hardware in the loop (HIL) implementations have been done to confirm the performance improvement of the proposed control scheme.

5.2 STATE OF THE ART OF PHOTOVOLTAIC PUMPING CONTROL SCHEMES

In a continued effort to increase the efficiency, to decrease the cost and to improve the reliability performance of the PV pumping system, different configurations and control schemes have been proposed in the literature [5.1-26]. The PV pumping systems based on AC motors, particularly induction motors are often preferred because they make the pumping system more reliable, economical, and no need to the permanent maintenance [5.1]. The two typical configurations of a PV pumping systems using IM are single and dual stages [5.1]. In dual stages, the first stage is a DC-DC boost converter, in general from the PV module to a DC link (usually as a capacitor). This converter is used for boosting the PV voltage array and maximizing the power; the second one is for conversion of the PV power into a variable frequency power source. While, in the single stage, the DC-DC converter is not required, and a number of PV panels must be connected in a series arrangement. This method is impractical for fractional kilowatt rating (< 1 kW) PV system.

However, in such systems the generated PV energy must be properly regulated and maximized. Various control strategies have been suggested in the literature for tracking the maximum power point (MPPT) of PV array in water pumping application. Although these control strategies can achieve the same goals, such as high efficiency and fast speed under varying atmospheric (irradiance and temperature) conditions, their principles differ. The most conventional MPPT techniques are known as Perturb and Observe (P&O) [5.6-9] and incremental conductance (INC) [5.10-15]. Nonconventional MPPT techniques based on intelligent controller have been developed recently, such as fuzzy logic [5.16-20], artificial neural network [5.21-22], neuro-fuzzy [5.23], genetic algorithm [5.24] and variable structure MPP controller [5.25-26]. However, the conventional MPPT techniques suffer from high frequency oscillations, large steady-state errors and poor tracking of the MPP for sudden irradiance changes, and the major problem of the nonconventional MPPT techniques is the high computational burden which increases the controllers cost and complexity.

Nevertheless, the major issue in the battery-less PV pumping system with MPPT control is that the motor must absorb all the extracted power by the PV array even if there is no load demand [5.24]. Therefore, the occurrence of load drops due to any reason might lead to increase the motor voltage, which can may damage the motor. In order to avoid this issue, the authors in [5.24] designed an MPPT for a battery-less PV system based on DC motor to maximize the PV power under sudden irradiance changes and to protect the motor under different load conditions. The designed method has been successfully implemented using a Cuck converter, and compared with conventional MPPT algorithms.

In addition, the electromechanical power conversion in the PV pumping system must be with minimum losses for different climatic conditions. Different control drives for IM are presented in the literature; the most effective control methods used in PV pumping systems are constant *v/f* control [5.22], field-oriented control (FOC) [5.14] and direct torque control (DTC) [5.15, 25]. The greatest drawbacks of these control strategies are the sensitivity to parameters change of IM, and torque ripples, which lead to system power losses.

5.3 PHOTOVOLTAIC PUMPING SYSTEM DESCRIPTION

The overall schematic of the PV pumping system under study is shown in Figure 5.1. The PV modules convert the solar radiation into electrical energy, feeding an IM via a boost converter and a three phase two-level inverter. Therefore, the maximum of the PV generator power can be reasonably tracked by the boost converter, and fed to the IM through the inverter. The IM-side inverter regulates the DC-Link voltage and the power transfer between the DC-link and the utility IM. Finally, the mechanical energy is converted into hydraulic energy by the group IM-centrifugal pump.

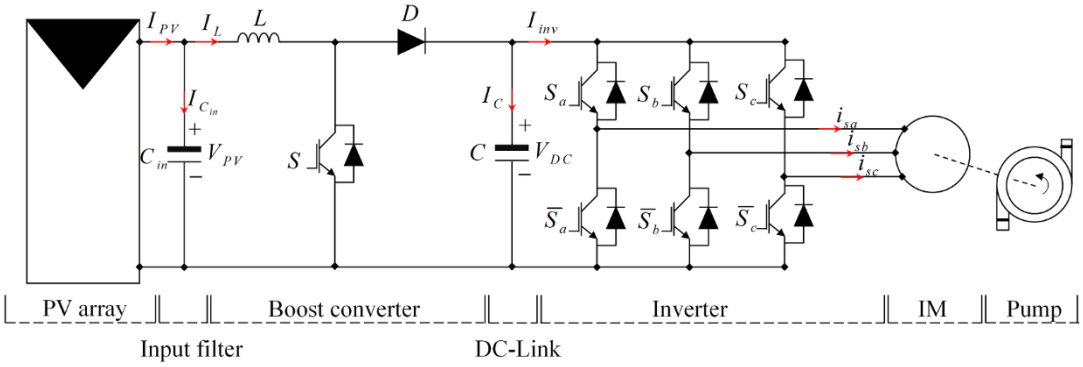

Figure 5.1: Schematic diagram of the PV pumping system.

5.4 CONTROL SCHEME PROPOSED

The complete control scheme based on the fuzzy logic and model predictive strategies for the proposed PV pumping water system is shown in Figure 5.2. In the proposed system, regulation is needed for:

- ❖ MPPT during all climatic conditions to improve PV energy conversion efficiency.
- ❖ DC-link voltage to ensure proper operation for the inverter.
- ❖ Electromechanical power conversion for IM drive.

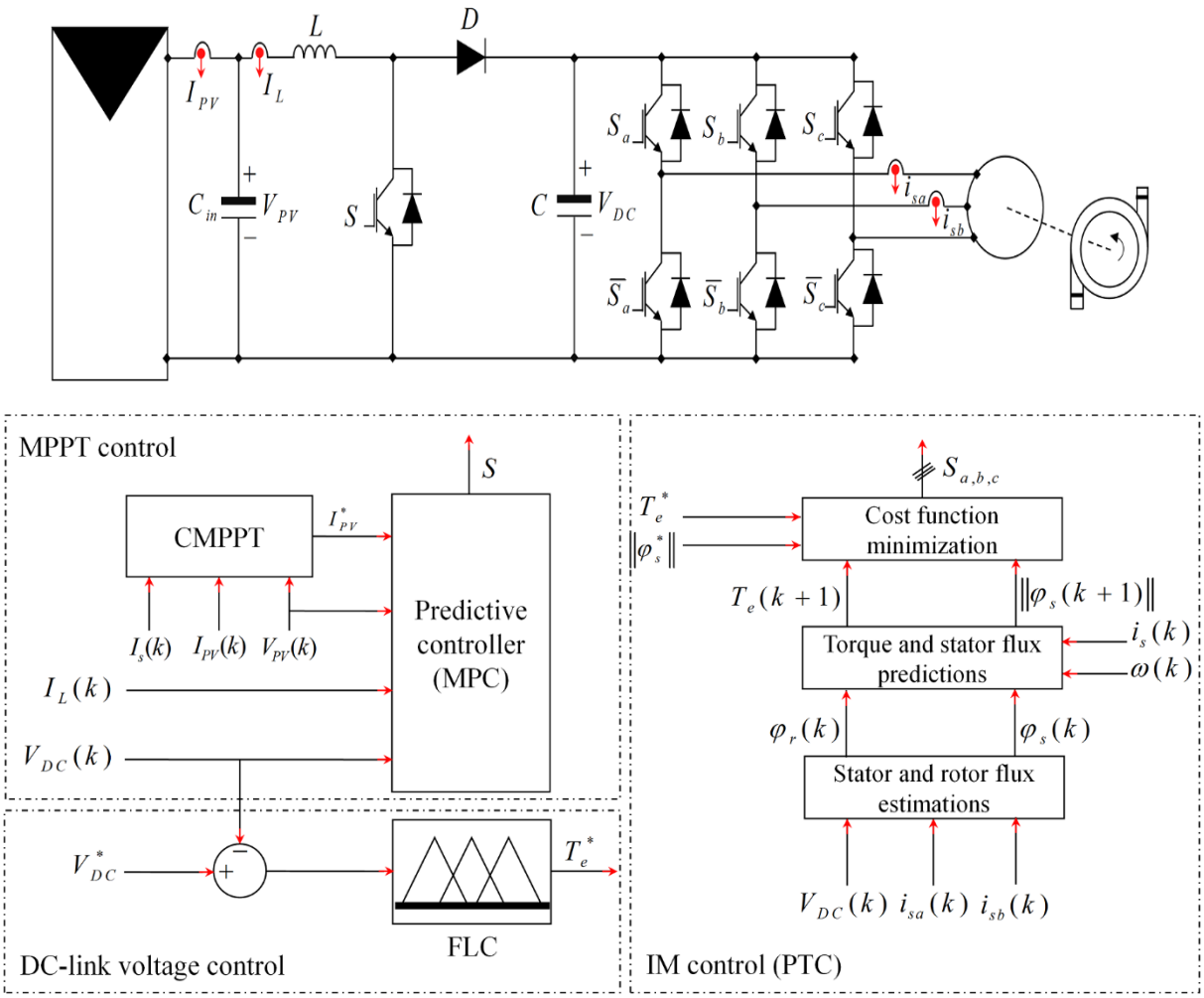

Figure 5.2: Proposed control scheme for PV pumping system.

5.4.1 MPPT Control

For the proposed MPPT control, an improved variable step size P&O based current MPPT (CMPPT) is used for extracting the optimum PV current and protecting the IM under sudden load drops. Therefore, an MPC current controller determines the optimal switching control for

the boost converter in order to regulate the PV current, by controlling the average input current of the boost converter.

5.4.1.1 Variable current step size perturb and observe algorithm

The P&O based-CMPPT is generally used with fixed current step size. This strategy works by perturbing the operation PV current, the perturbation effect is observed on the output power for deciding the direction of the next perturbation; if the present power is bigger than the previous, the perturbation remains in the same direction (the sign of the next perturbation is maintained), otherwise the direction is reversed. In this work, an improved variable current step size algorithm is proposed for the P&O based-CMPPT method; its objective is to find a simple and effective way to improve tracking accuracy as well as tracking dynamics. The current control is chosen to speed-up the tracking performance and to follow the right direction of the MPP under irradiance changing; due to the linear relationship between PV current and irradiance levels. The derivate of the PV power to voltage as (dP_{PV}/dV_{PV}) shown in Figure 4.3, is employed to determine the variable current step size, which is adopted to reduce the oscillation of the PV power in steady-state and accelerate the MPP tracking. The variable current step size is given as follows:

$$I_{in} = N\left|\frac{dP_{PV}}{dV_{PV}}\right| \tag{5.1}$$

where:

N: is the scaling factor that is tuned by the design to adjust the current step size.

Figure 5.3 illustrates the flowchart of the proposed algorithm. In order to ensure that the PV maximum power is provided during the sudden irradiance decrease, a simple loop is added to the main P&O based-CMPPT scheme. When a sudden irradiance occurs, the proposed algorithm is quickly able to detect it using a simple if statement through the predetermined current I_{set} and voltage V_{set} therefore, the modified algorithm is also required to reset the PV reference current for the upcoming MPPT period. Where, the stored value of I_{PV} is multiplied by a proportionality constant k_{opt}, which is used in FSCC algorithm, to achieve an approximate value of the optimum operating current. Thus, the PV system is able to track the MPP smoothly under sudden irradiance decreases.

In addition, unlike conventional MPPTs, the modified algorithm has provided a simple and effective way to protect the IM under load drops. A predetermined value $I_{s,\min}$, which represents the stator current root mean square (rms) value at the rated speed without load, is stored to

identify the existence of load drops. If the operation stator current rms I_s is smaller than the predetermined value, the PV reference current is set to zero in order to stop the PV power extraction; otherwise, the algorithm continues to track the MPP. Moreover, the proposed algorithm is supported by a numerical state machine to distinguish between the IM starting current and the load drop condition in the real-time implementation [5.24].

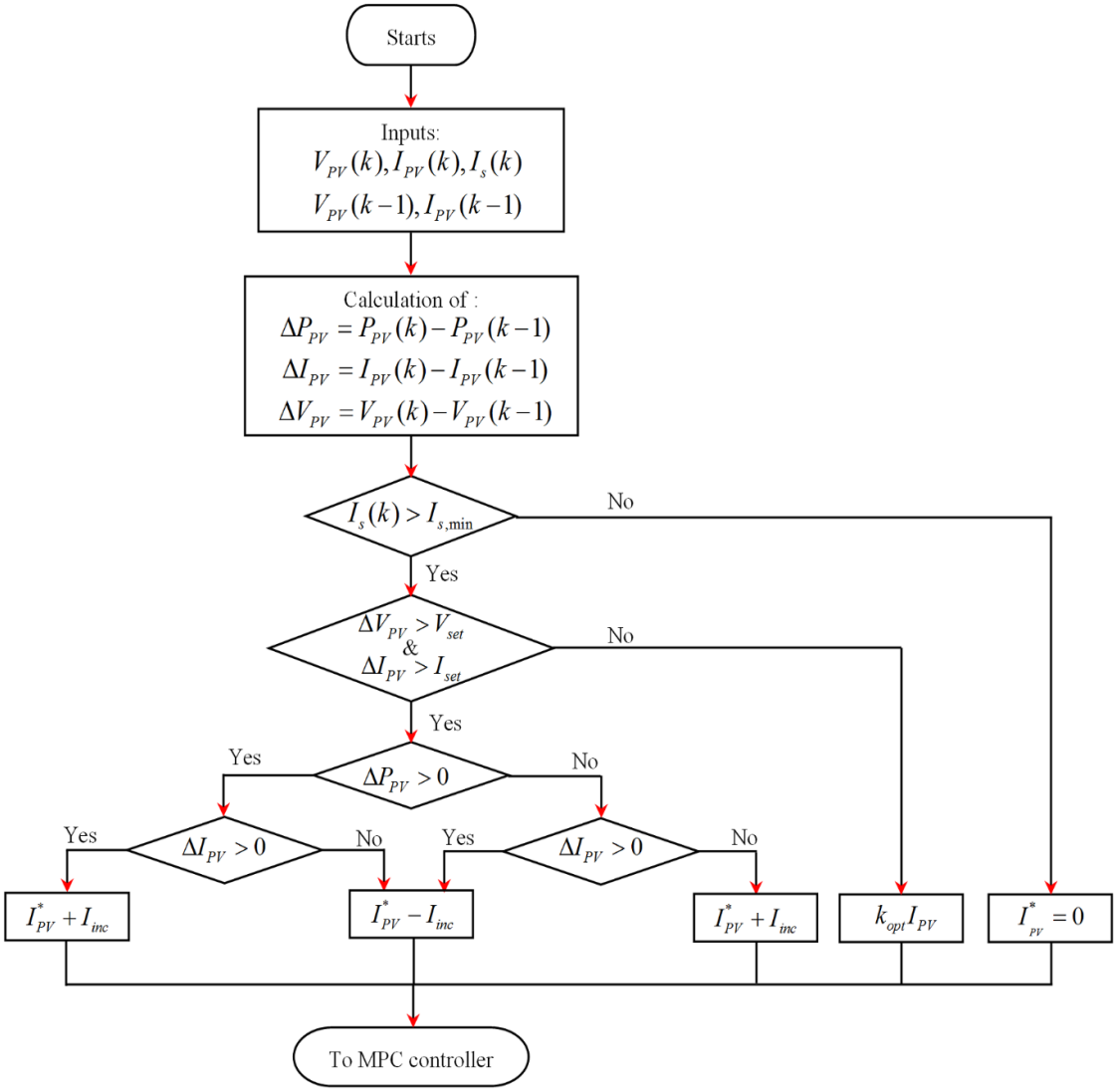

Figure 5.3: Flowchart of the proposed P&O CMPPT algorithm.

5.4.1.2 Model predictive current controller

The MPC is an advanced power converter control technique. The main idea of this control strategy is the prediction of the future behavior of the controlled variables. Moreover, micro-electronics development has facilitated the implementation of this methodology [5.27-28]. Then these predictions are used to generate the optimal control action. The boost converter is chosen to realize the MPPT. It is usually used in the PV systems due to some of its important

features, such as being simple, robust, and also it offers a continuous current at the input. The dynamic model of the boost converter is given in chapter 2 section 2.3. Therefore, the discrete equation of inductor current using Euler's formula can be expressed as follows:

$$I_L(k+1) = I_L(k) - (1-S)\frac{T_s}{L}V_{DC}(k) + \frac{T_s}{L}V_{PV}(k) \tag{5.2}$$

where:

T_s : is the sampling time used in the MPC algorithm.

The flowchart of the proposed MPC algorithm is presented in Figure 5.4. From the actual inductor current, this algorithm predicts the value during the next sampling instant using Euler discretization method, the measured inductor current, PV voltage and DC-link voltage. The prediction of inductor current $I_L(k+1)$ is obtained for both switch states, and the reference PV current I_{PV}^* from MPPT algorithm. Finally, a cost function is minimized and the appropriate switching state is selected at every sampling time according to the following quantity:

$$g_{S=1,0} = \left| I_{L,S=0,1}(k+1) - I_{PV}^* \right| \tag{5.3}$$

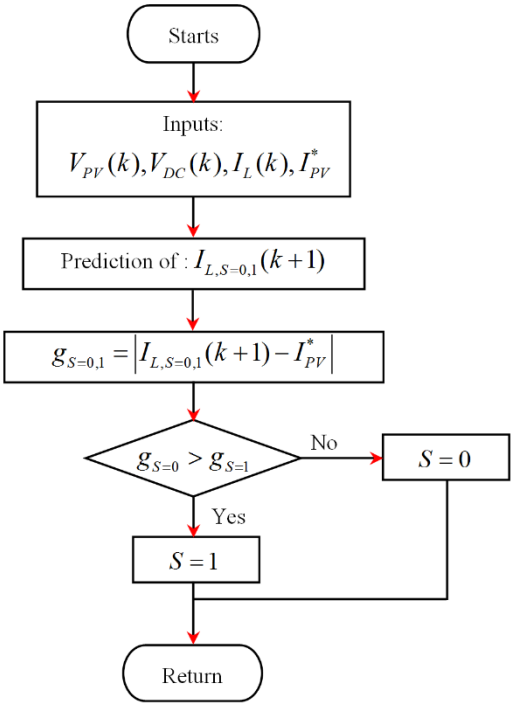

Figure 5.4: Flowchart of the MPC algorithm for current control.

5.4.2 Fuzzy Logic DC-Link Controller

Conventionally, a classical PI regulator is used to maintain a constant DC-link voltage at a reference value, and generates the torque reference regardless of operation conditions, for the

two stages PV pumping system [5.14, 25]. However, the fuzzy logic control is characterized by simple structure, robustness, and independence of the process model on the contrary to the conventional control. Therefore, in order to optimize performance, a T-S-type FLC is developed to control the DC-link voltage. The block diagram of the proposed FLC is shown in Figure 5.5. The error $e(k)$ and change of error $\Delta e(k)$ over a sampling period are considered as inputs of the FLC. The error is computed as the difference between the measured DC-link voltage $V_{DC}(k)$ and the desired reference V_{DC}^*:

$$e(k) = V_{DC}^* - V_{DC}(k) \tag{5.4}$$

The error change is calculated as:

$$\Delta e(k) = e(k) - e(k-1) \tag{5.5}$$

where:

Z^{-1}: represents the unit time delay.

The two inputs are fed into FLC unit for fuzzification after being adjusted by the normalization factors K_e and $K_{\Delta e}$, where these factors are optimally selected by means of simulation and experiments.

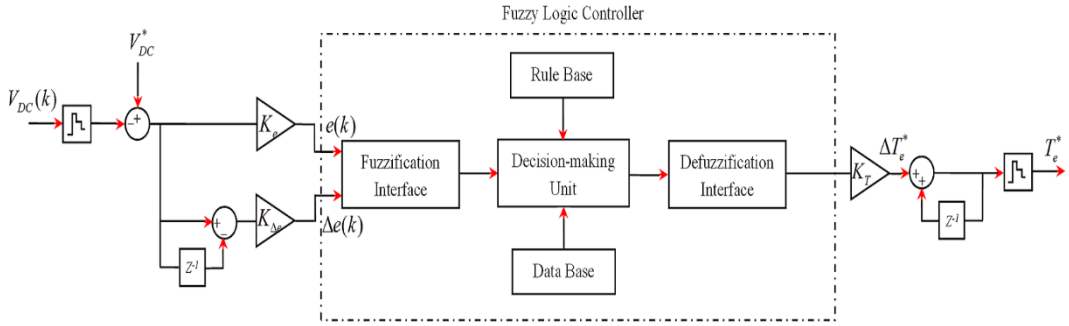

Figure 5.5: Block diagram of the proposed FLC.

Figure 5.6(a-b) represents the proposed normalized input membership functions in terms of linguistic variables, NB (Negative Big) to PB (Positive Big). Triangular and trapezoidal membership functions are chosen in order to reduce the computational complexity. After fuzzification, the fuzzy inference is carried out by using a T-S method which requires the least computation effort compared to other fuzzy inference methods [5.29-30]. The fuzzy rules used in the proposed FLC can be represented in a symmetric form, as illustrated in Table 5.1. The fuzzy rules can be formulated with IF-AND-THEN statements and a typical example is shown below:

If *e(k)* is NB **AND** $\Delta e(k)$ is NB **THEN** $\Delta T_e^*(k)$ is NB.

If *e(k)* is NB **AND** $\Delta e(k)$ is NS **THEN** $\Delta T_e^*(k)$ is NB.

…..

…..

…..

If *e(k)* is PB **AND** $\Delta e(k)$ is PS **THEN** $\Delta T_e^*(k)$ is PB.

If *e(k)* is PB **AND** $\Delta e(k)$ is PB **THEN** $\Delta T_e^*(k)$ is PB.

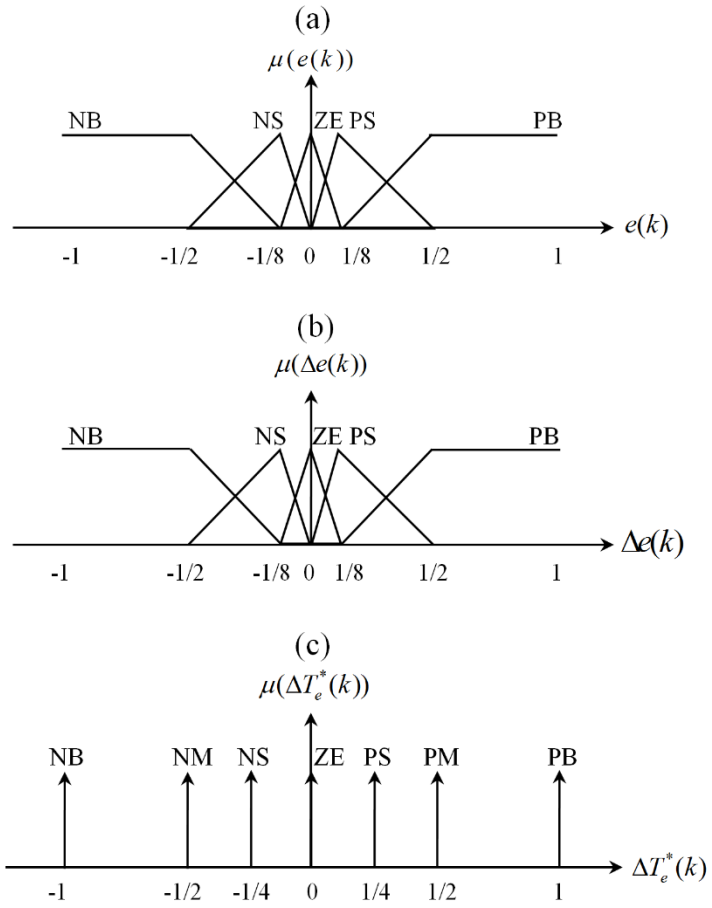

Figure 5.6: FLC membership functions. (a-b) Inputs, (c) Output.

Moreover, as presented in Figure 5.6(c), the zero-order T-S model is considered with seven fuzzy variables, i.e., NB (Negative Big), NM (Negative Medium), NS (Negative Small), ZE (Zero), PS (Positive Small), PM (Positive Medium) and PB (Positive Big). In the last step, a center weighted average algorithm is used in the defuzzification to convert the output fuzzy subset torque changes $\Delta T_e^*(k)$ into numerical value. The torque reference $\Delta T_e^*$is then produced as:

$$T_e^* = T_e^*(k) = T_e^*(k-1) + K_T \Delta T_e^*(k) \tag{5.6}$$

where:

K_T: is the scaling factor for denormalization of the FLC output, which can be optimally selected through simulation and experiments.

TABLE 5.1: Fuzzy rules base for DC-link controller.

			Δe(k)		
e(k)	**NB**	**NS**	**ZE**	**PS**	**PB**
NB	NB	NB	NM	NS	ZE
NS	NB	NM	NS	ZE	PS
ZE	NM	NS	ZE	PS	PM
PS	NS	ZE	PS	PM	PB
PB	ZE	PS	PM	PB	PB

5.4.3 Predictive Torque Control

The MPC-based control for the IM is presented in Figure 5.7. It is based on the computation of the required converter voltage vector to be applied during the next sampling time in order to minimize the flux and torque errors [5.31-34]. The torque reference is calculated by an FLC and, usually, the reference for the stator flux magnitude is set to a constant.

For the PTC operation, the estimation of stator and rotor flux is necessary. The stator flux φ_s can be calculated according to the dynamic IM model [5.31-34]:

$$\frac{d}{dt}\varphi_s = v_s - R_{ss} i_s \tag{5.7}$$

Also by using IM model, the rotor flux φ_r can be estimated by:

$$\varphi_r = \frac{L_r}{L_m}\varphi_s - \left(\frac{L_r L_s}{L_m} + L_m\right) i_s \tag{5.8}$$

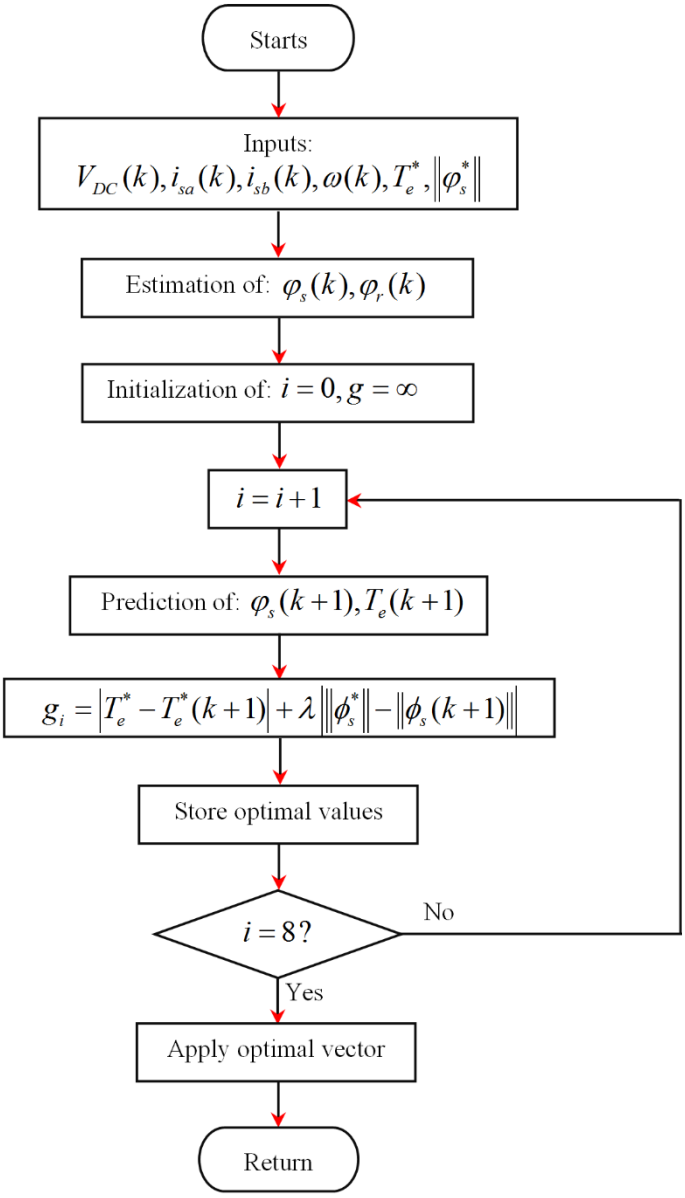

Figure 5.7: Flowchart of the PTC algorithm.

Based on this estimation, the future behavior of the controlled variable is predicted for the next sampling time (*k+1*). For the stator flux vector prediction $\varphi_s(k+1)$, the same voltage vector equation used for its estimation is discretized by Euler's formula:

$$\varphi_s(k+1) = \varphi_s(k) + T_s v_s(k) - T_s R_{ss} i_s(k) \tag{5.9}$$

The IM torque can be expressed by stator flux and current as follows:

$$T_e = \frac{3}{2} p \Im m(\varphi_s^* \cdot i_s) \tag{5.10}$$

Therefore, by considering the predicted values of the stator flux and current, the torque prediction can be calculated as follows:

$$T_e(k+1) = \frac{3}{2} p\Im m(\varphi_s^*(k+1) \cdot i_s(k+1)) \tag{5.11}$$

where:

$i_s(k+1)$ is the stator current prediction which can be expressed as in [5.34] by the following equation:

$$i_s(k+1) = \left(1 - \frac{T_s}{\tau_\sigma}\right) i_s(k) + \frac{T_s}{\tau_\sigma} \frac{1}{R_\sigma} \left[k_r \left(\frac{1}{\tau_r} - j\omega \right) \varphi_r(k) + v_s(k) \right] \tag{5.12}$$

where:

$$k_r = \frac{L_m}{L_r} \tag{5.13}$$

$$\tau_r = \frac{L_r}{R_r} \tag{5.14}$$

$$R_\sigma = R_{ss} + k_r^2 \tag{5.15}$$

$$\tau_\sigma = \frac{L_s}{R_{ss}} \left(1 - \frac{L_m^2}{L_s L_r} \right) \tag{5.16}$$

Finally, these predictions are evaluated by the following cost function:

$$g_i = \left| T_e^* - T_e^*(k+1) \right| + \lambda \left| \left\| \varphi_s^* \right\| - \left\| \varphi_s(k+1) \right\| \right| \tag{5.17}$$

where:

i: is the index of the stator voltage vector used to calculate the predictions of the controlled variables.

T_e^*: is the torque reference.

$\|\varphi_s^*\|$: is the stator flux magnitude reference.

λ: is the weighting factor, which ponders the relative importance of the torque versus the flux control. If the same importance is considered, this factor would be computed as the ratio between the magnitudes of the nominal torque and stator flux [5.32].

$$\lambda = \frac{T_{nom}}{\left\| \varphi_{s,nom}^* \right\|} \tag{5.18}$$

In conclusion, the voltage vector which minimizes the cost function will be applied to the inverter, during the next sampling period.

5.5 SIMULATION VERIFICATION

Simulations using MATLAB/Simulink® environment are conducted to test the proposed strategies. The model created in Simulink takes into account the full control system, including the different elements models of the PV pumping system. The PV panel consists of four 120 Wp PV modules connected in a 2 (series) × 2 (parallel), with the current-voltage and power-voltage characteristics of the PV array illustrated in Figure 2.6. An IM of 0.37 KW is used to drive the pump. The PV pumping system parameters are listed in Table 5.2. Sampling times are 1 ms, 0.5 ms and 50 µs for the MPPT, the FLC and the MPC controllers (MPC current controller and PTC algorithm) respectively. The flux stator is kept constant at its rated value 0.71 Wb. The reference for the DC-link voltage is constant and equal to 450 V. For the conventional control scheme, a conventionally fixed step size P&O algorithm based on PI controller is used to track the MPP of the PV panel, and a conventional DTC technique is applied to control the IM drive. The same conditions for the conventional and proposed control schemes are considered, which makes a fair comparison possible.

5.5.1 Sudden Irradiance Change

An irradiance profile with various sudden irradiance change is applied for different control schemes, where the irradiance is 1000 W/m² at the beginning, after 1.5 s, is decreased suddenly to 400 W/m², and then increased abruptly to 600 W/m², after more than 1 s, it is again increased suddenly to 800 W/m². The temperature is considered constant (25 °C).

Figures 5.8 and 5.9 present the simulated responses of the presented PV pumping system for the conventional and proposed control schemes, respectively. From top to bottom, the curves shown in Figures 5.8 and 5.9 are: (a) the considered irradiance profile, (b) PV voltage, (c) PV and inductor currents, (d) PV power, (e) DC-link voltage with its reference, (f) IM speed, (g) electromagnetic and load torques, (h) stator flux amplitude. First of all, the results confirm the poor tracking of the conventional P&O under sudden irradiance changes with a significant PV power oscillation in steady-state. On the other hand, the proposed MPPT offers a high tracking performance with an instantaneous effect on the PV current, which is correctly achieved, under sudden irradiance variations, where the PV pumping system is pursuing the MPP permanently, as depicted in Figure 5.10. Moreover, the proposed algorithm minimizes the frequency oscillation in the PV power. A comparative table regarding tracking speed, power oscillation in

steady-state with the main values obtained in simulation for the two MPPT is presented in Table 5.3. The comparative results demonstrate the excellent performance of the proposed MPPT.

TABLE 5.2: Parameters of the PV pumping system.

Boost converter	Nominal values
Inductance (L)	10 mH
Capacitance (C)	1110 µF
Input capacitance (C_{PV})	1110 µF
IM	**Nominal values**
Nominal power (P_{nom})	0.37 KW
Efficiency %	76.1%
Stator resistance (R_{ss})	20.2 Ω
Rotor resistance (R_r)	14.458Ω
Stator inductance(L_s)	0.982 H
Rotor inductance (L_r)	0.982 H
Magnetizing inductance (L_m)	0.921 H
Inertia (J)	0.00095 Kg.m²
Viscous friction coefficient (F)	1e-4 N.m/(rad/s)
Number of pole pairs (p)	2
Centrifugal pump	**Nominal values**
Pumping flow (Q)	0.08-0.58 liter/s
Pumping head	5-19.5 m

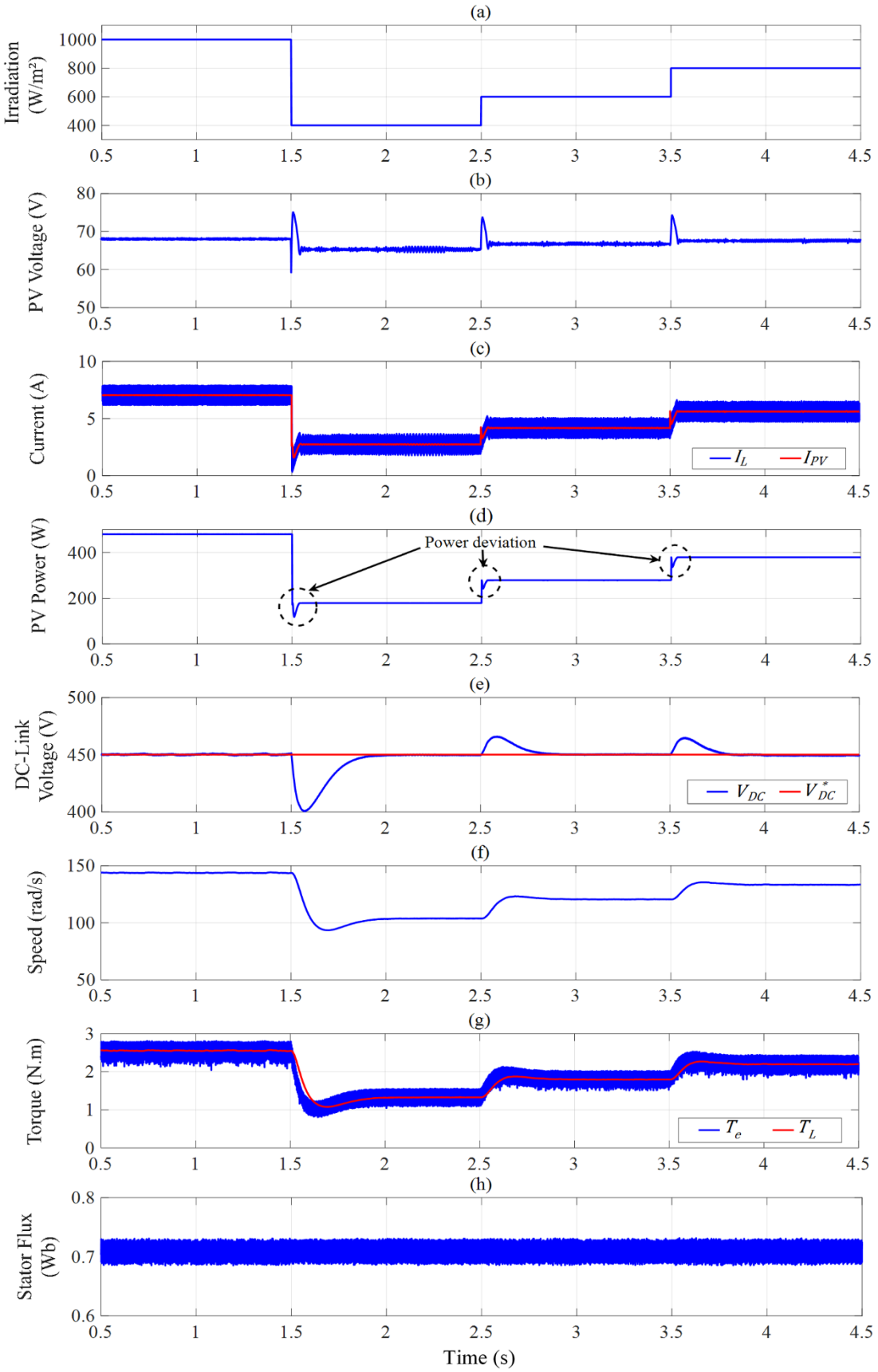

Figure 5.8: Simulation results of the PV pumping system with the conventional control scheme under sudden irradiance variations.

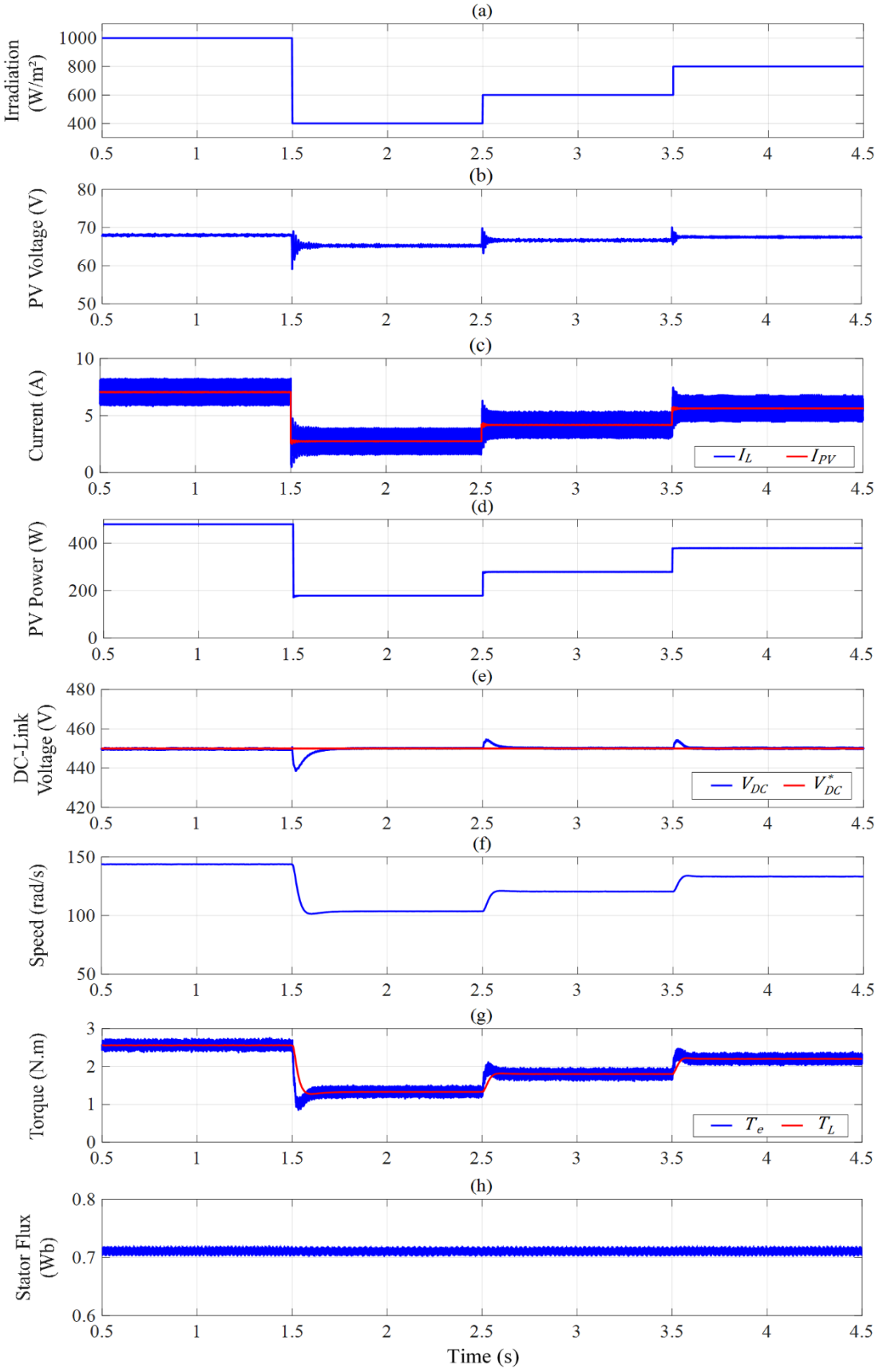

Figure 5.9: Simulation results of the PV pumping system with the proposed control scheme under sudden irradiance variations.

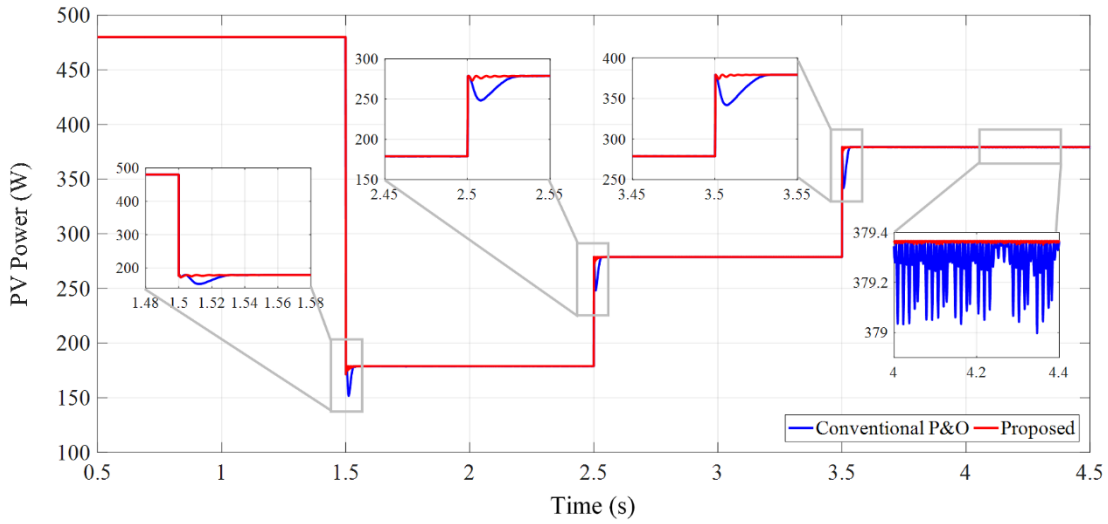

Figure 5.10: PV power waveforms for both conventional P&O and proposed MPPT under sudden irradiance variations.

TABLE 5.3: Comparison results for MPPT techniques.

Technique	Step decrease in irradiance 1000→400 W/m²		Step increase in irradiance 400→600 W/m²		Step increase in irradiance 600→800 W/m²	
	Tracking speed time (s)	Power oscillation (W)	Tracking speed time (s)	Power oscillation (W)	Tracking speed time (s)	Power oscillation (W)
Conventional P&O	0.061	0.48	0.042	0.35	0.042	0.24
Proposed MPPT	0.038	Less than 0.05	0.014	Less than 0.05	0.014	Less than 0.05

Moreover, the net DC-link voltage is regulated at its reference values by the proposed FLC for the conventional and proposed control schemes. As presented in Figure 5.11, the DC-link voltage tracks the reference with good accuracy and stability, regardless the irradiance variations for the two control schemes, which proves the effectiveness of the proposed FLC. Moreover, the overshoots and settling times in the proposed scheme are less than those found in the conventional scheme, as summarized in Table 5.4.

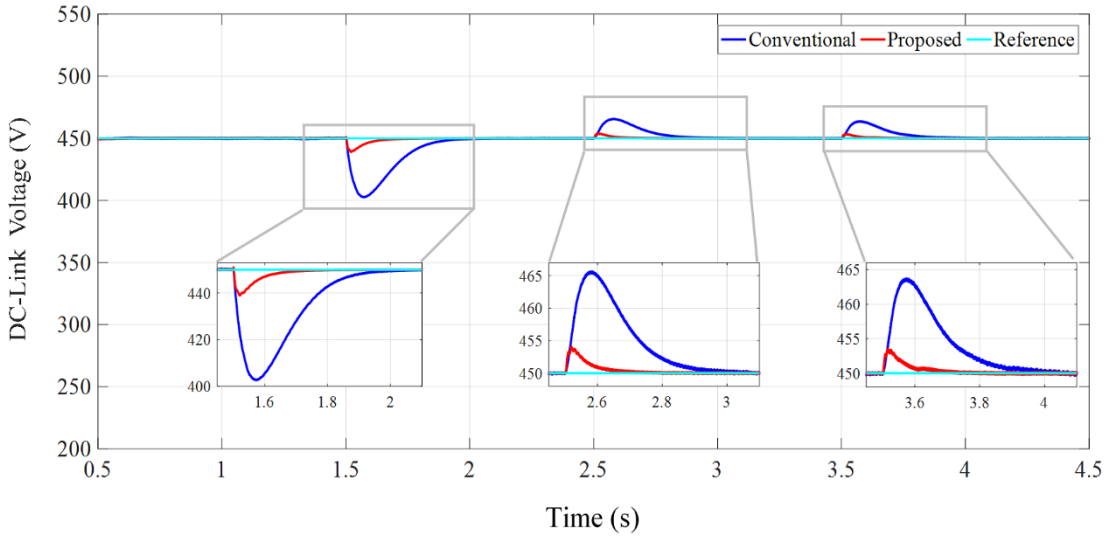

Figure 5.11: DC-link voltage waveforms for both conventional and proposed schemes under sudden irradiance variations.

TABLE 5.4: Comparison results for DC-link regulation.

Control scheme	Step decrease in irradiance 1000→400 W/m²		Step increase in irradiance 400→600 W/m²		Step increase in irradiance 600→800 W/m²	
	Overshoot (V)	Settling time (s)	Overshoot (V)	Settling time (s)	Overshoot (V)	Settling time (s)
Conventional	49.84	0.49	15.87	0.385	14.31	0.314
Proposed	11.60	0.26	4.66	0.157	4.25	0.11

On another side, the proposed control scheme using PTC proves high dynamic and static performances for IM drive, contrary to the conventional scheme (DTC). It is seen that the conventional scheme presents relatively large flux and torque ripples due to the harmonics in the stator currents, as illustrated in Figure 5.12. Furthermore, the electromagnetic torque and stator flux of direct PTC drive IM are controlled directly and rapidly in the proposed scheme. It is found that the stator flux exhibits smooth response and lesser ripple, and as a consequence, good current waveforms, as presented in Figure 5.13, which leads to good torque performance in steady-state (peak-to-peak torque ripple is always less than 0.2 N.m). A comparison summary in terms of current harmonics and torque ripple is presented in Figure 5.14 for different irradiance levels.

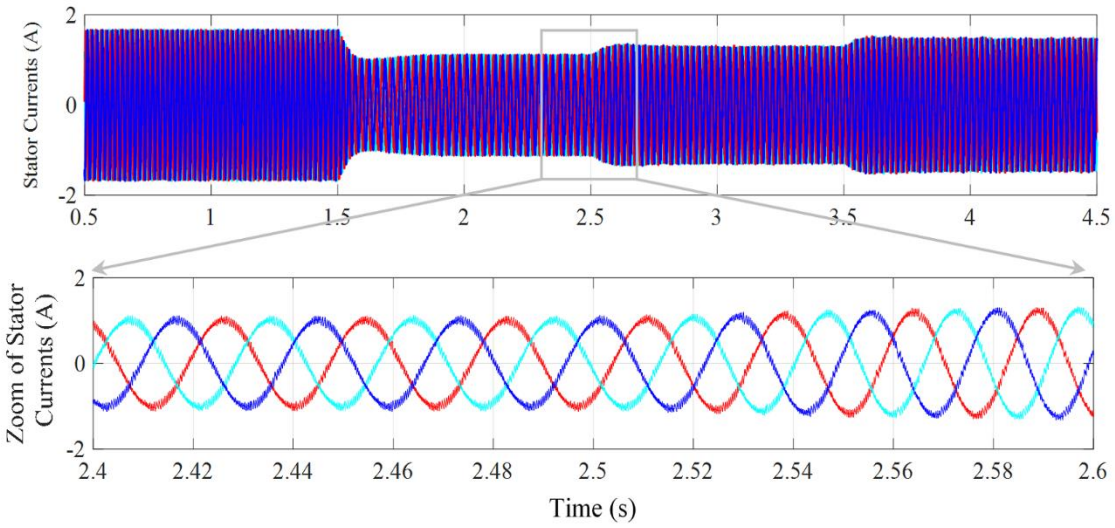

Figure 5.12: Stator currents with zoom waveforms for conventional scheme under sudden irradiance variations.

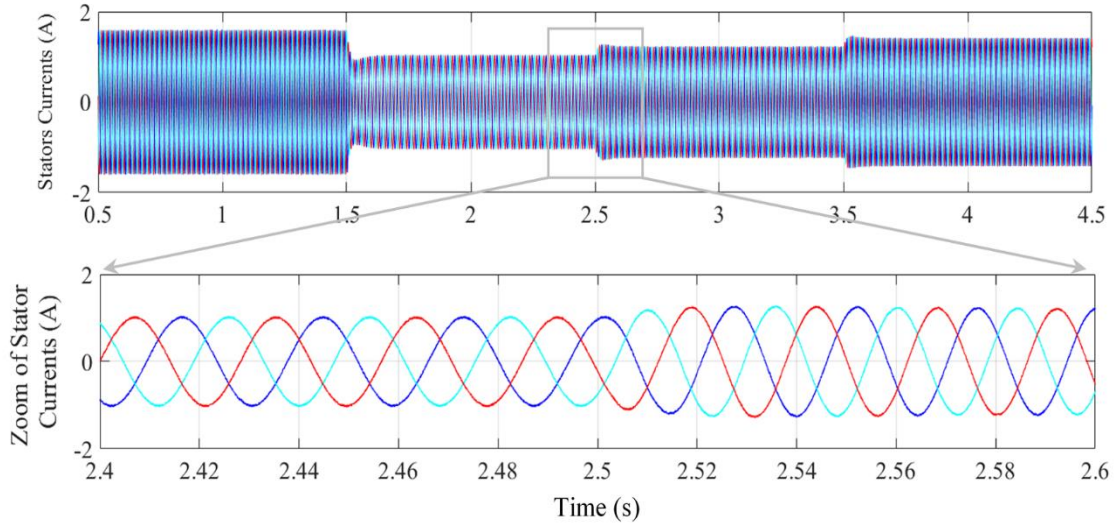

Figure 5.13: Stator currents with zoom waveforms for proposed scheme under sudden irradiance variations.

Figure 5.15 presents the hydraulic power and pump flow with the conventional and proposed schemes, for a hydraulic circuit with pumping head of 8.5 meters. It is clearly seen that the power conversion is more improved in terms of overshoot and speed response for the proposed scheme compared to the conventional one, which leads in improving the energy converted by the pump, as a consequence an increase of the pumped water quantity. Furthermore, Figure 5.15 illustrates how the sudden irradiance decrease negatively effects (decreased to zero over a time period of 0.19 s) the hydraulic power and the pump flow with

the conventional scheme. On another hand, it can be observed that the proposed scheme offers good performance in the case of sudden irradiance decrease.

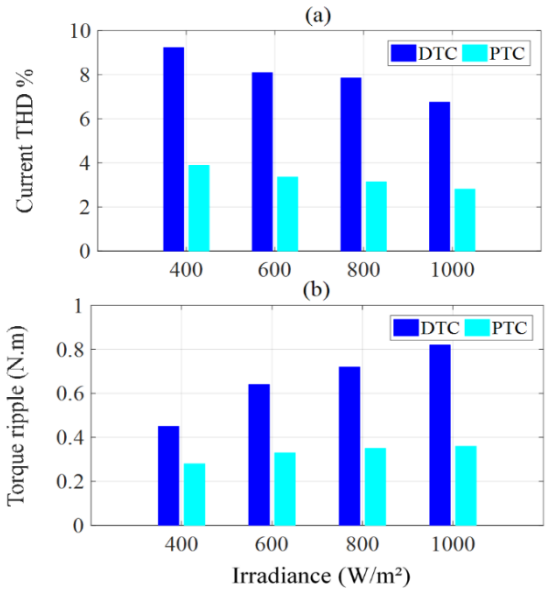

Figure 5.14: (a) Current THD and (b) torque ripple for conventional DTC and PTC under sudden irradiance variations.

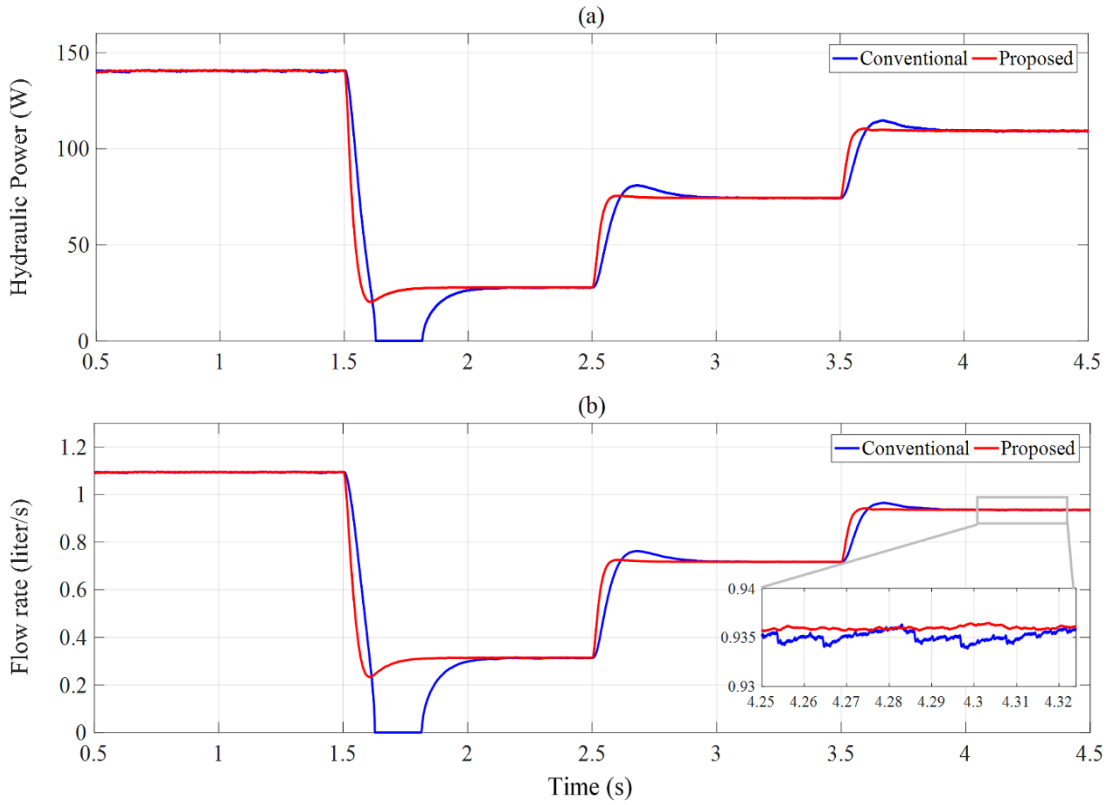

Figure 5.15: (a) Hydraulic power and (b) pump flow for conventional and proposed schemes under sudden irradiance variations.

5.5.2 Sudden Load Drop

To ensure that the proposed scheme is able to protect the IM under load drops. Both the conventional and proposed control schemes are examined for sudden loss of load.

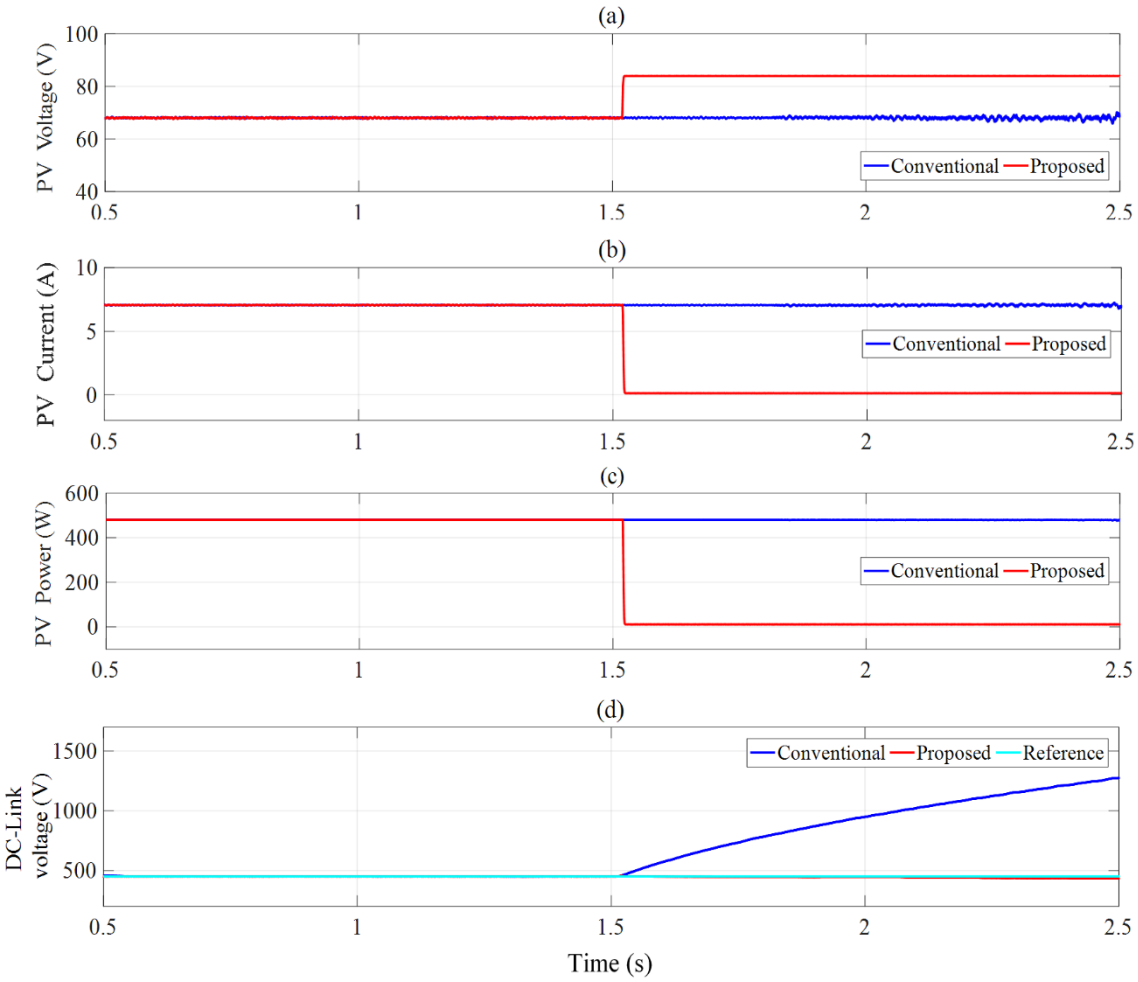

Figure 5.16: PV voltage, current, power and DC-link voltage waveforms for both conventional and proposed schemes under sudden load drop.

Figure 5.16 shows the simulation results for sudden loss of load. At the beginning, the irradiance is 1000 W/m² and the PV pumping system is normally operating under reasonable load. Both of the MPPT algorithms ensured that the PV modules operate at the MPP. Then, a sudden load drop occurs at instant 1.5 s (no load operation). It is clearly seen that the PV modules remain at the MPP with the conventional scheme, which leads to increase the DC-link voltage and can damage the IM, as shown in Figure 5.16(d). On the other hand, the proposed MPPT detected rapidly the load drop, and then kept on updating the PV reference current in order to protect the IM. As a consequence, the PV current and power decrease to zero, the DC-link voltage keeps stable and the PV voltage increases up to the open circuit voltage.

5.6 EXPERIMENTAL VERIFICATION

Experimental verification of the proposed control scheme and its MPPT control performance comparison with conventional scheme (based-on conventional P&O and DTC) are carried out on a hardware in the loop (HIL) system.

5.6.1 Platform Description

HIL experiments have been applied to evaluate real-time computational speed of the electronic control unit, embedded with the proposed controller. HIL experiments take in account the communication problems and controller computational limitation. Consequently, the results obtained through these experiments are considered more practical. As HIL system is more cost effective and faster than field/laboratory experiments, it is often performed in implementation of the power control systems.

In this study, a dSPACE system has been used for HIL implementation. The HIL system consists, in general, of an independent control-processing unit (CPU) to build the control algorithms, a real-time simulator to simulate the plant model and a communication channel between the simulator and the CPU [5.35]. For each sample time, the CPU obtains the state variables from the real-time simulator through the communication channel. From these state variables, the CPU computes the optimal control actions and drives it to the real-time simulator. The architecture of the HIL setup is presented in Figure 5.17.

The control and system parameters used in the HIL implementation are the same as those used in the simulations. The HIL results are recorded using the 500 MHz Instek oscilloscope and ControlDesk interface. Both the conventional and proposed control schemes are tested and compared under sudden irradiance and load changes, as in the simulations.

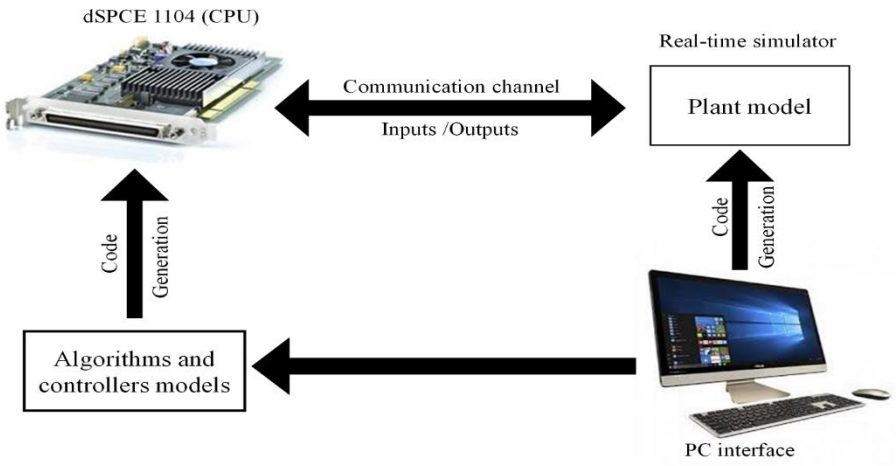

Figure 5.17: Schematic of the HIL setup

5.6.2 Real-Time Implementation Results

Figures 5.18, 5.19, 5.20 and 5.21 show and compare the MPPT performance of the proposed scheme with the conventional one. As it is expected, the proposed MPPT is able to achieve MPPs faster and has good dynamics with insignificant steady-state oscillations under sudden irradiance changes, compared to the conventional P&O algorithm. On the other hand, by using the modified variable step size P&O algorithm, it tracks the MPP more accurately under step decrease in the irradiance from 1000 W/m² to 400 W/m², as presented in Figure 5.21(b). As it is shown, the real-time HIL implementation of the proposed MPPT scheme confirms the simulation results.

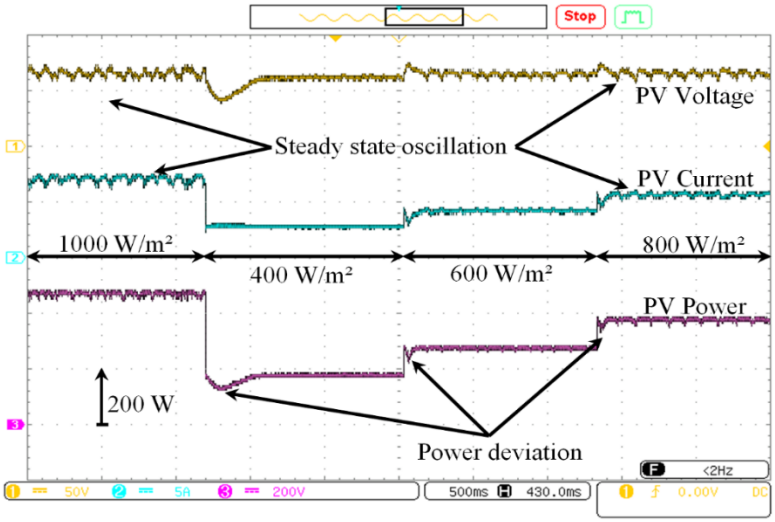

Figure 5.18: HIL responses of the PV voltage, current and power for conventional scheme under sudden irradiance variations.

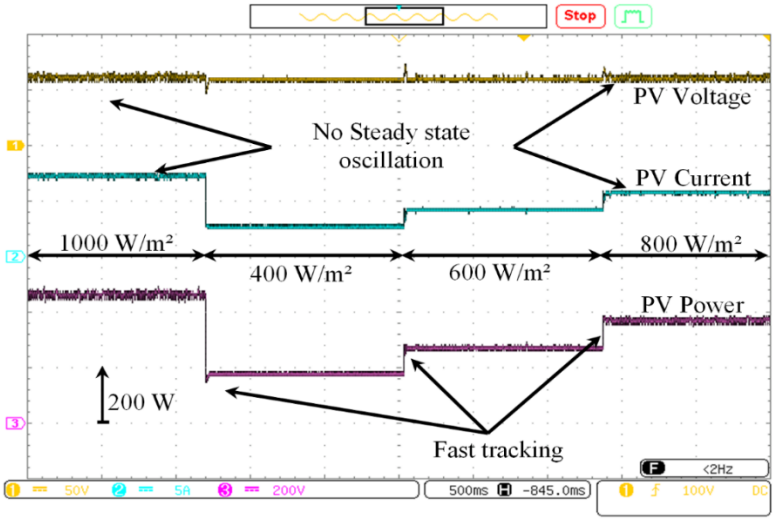

Figure 5.19: HIL responses of the PV voltage, current and power for proposed scheme under sudden irradiance variations.

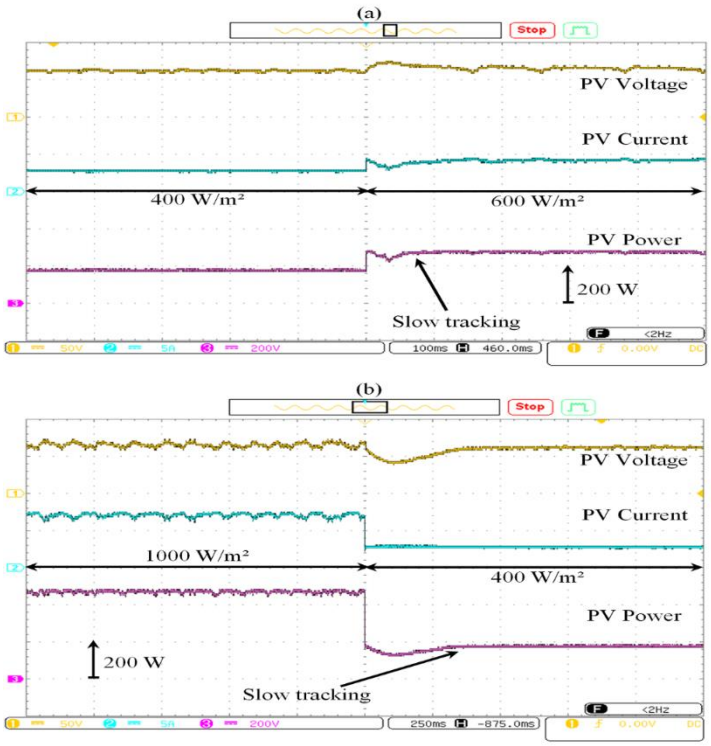

Figure 5.20: Zoom-in view of Figure 5.18 during (a) step increase in the irradiance level (400 W/m²–600 W/m²) and (b) step decrease in the irradiance level (1000 W/m²–400 W/m²).

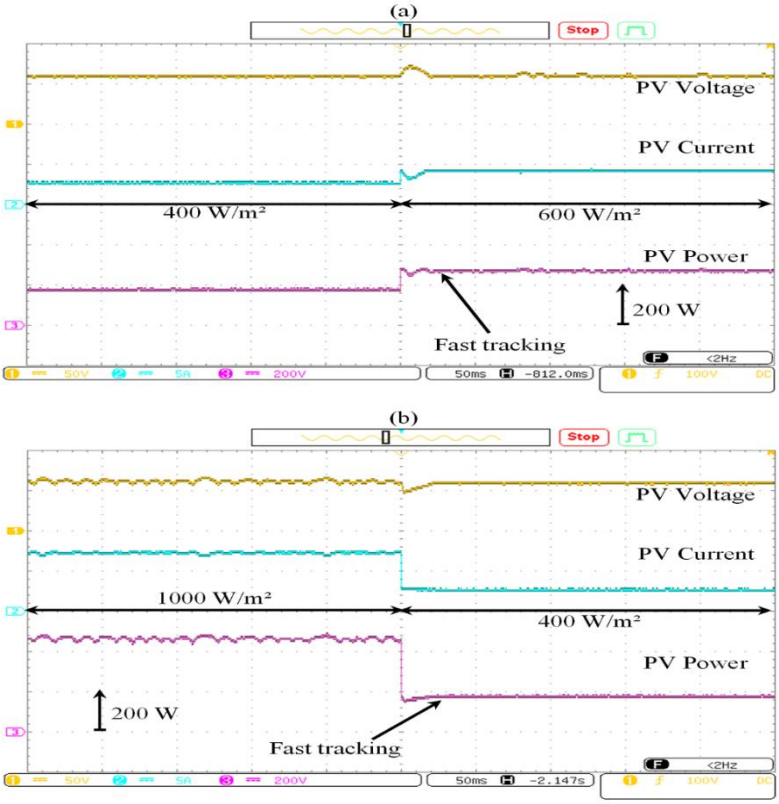

Figure 5.21: Zoom-in view of Figure 5.19 during (a) step increase in the irradiance level (400 W/m²–600 W/m²) and (b) step decrease in the irradiance level (1000 W/m²–400 W/m²).

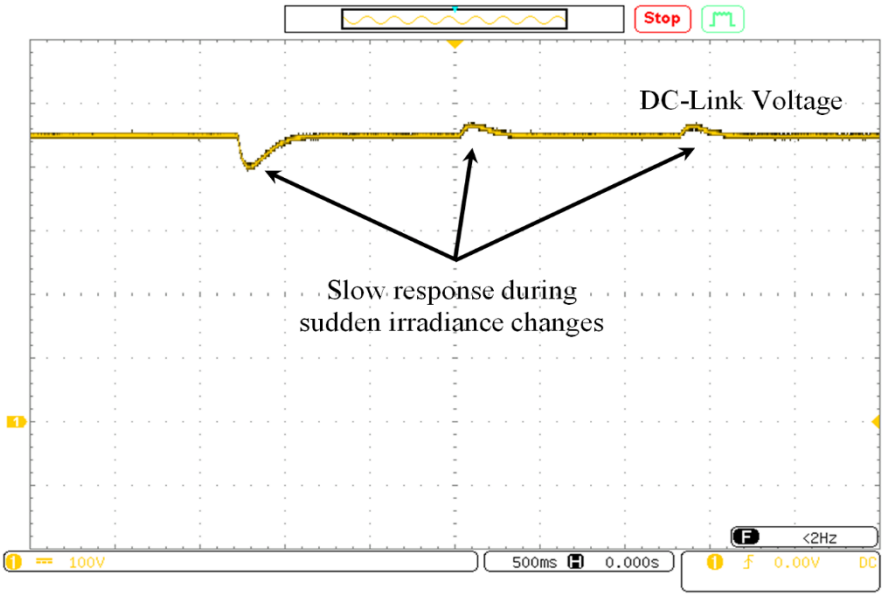

Figure 5.22: HIL responses of the DC-link voltage for conventional scheme under sudden irradiance variations.

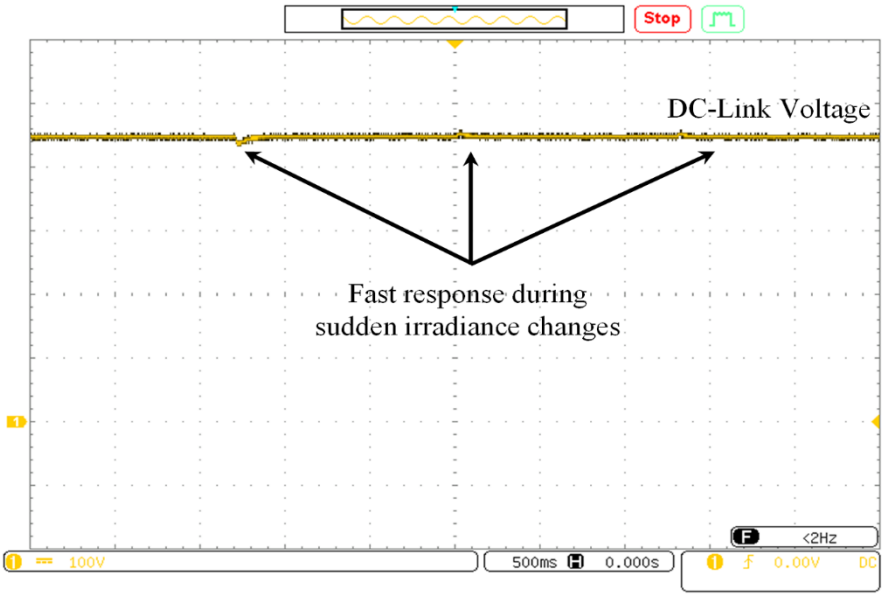

Figure 5.23: HIL responses of the DC-link voltage for proposed scheme under sudden irradiance variations.

Figures 5.22 and 5.23 present the HIL responses of the DC-link voltages when using the conventional and proposed schemes, where the DC-link voltage command is set to 450 V. It seen that the FLC in the proposed scheme tracks the desired voltage smoothly without steady-state error under sudden irradiance changes. While the conventional scheme has an overshoot and large settling time to arrive the desired voltage in comparison to the proposed scheme, when sudden irradiance variation occurs.

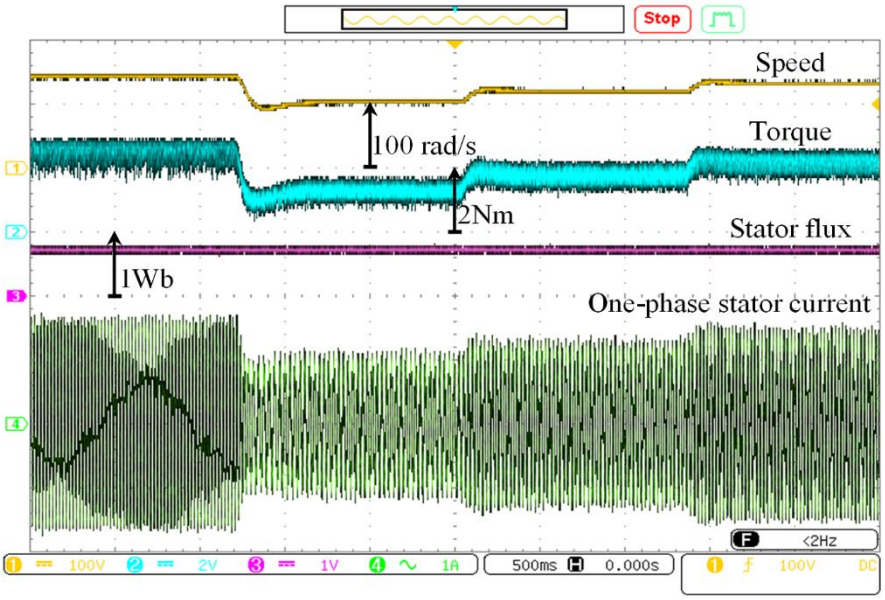

Figure 5.24: HIL responses of the speed, electromagnetic torque, stator flux amplitude and one-phase stator current for conventional scheme under sudden irradiance variations.

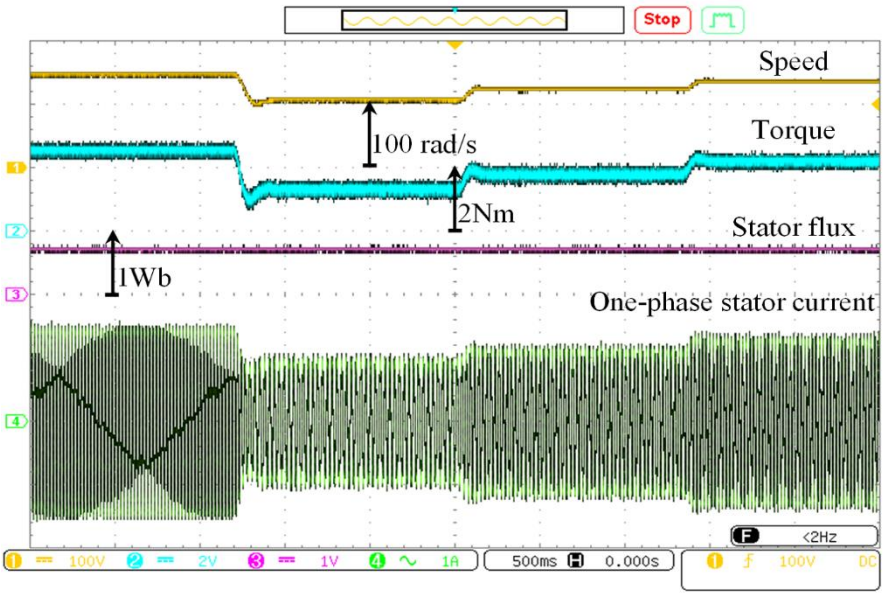

Figure 5.25: HIL responses of the speed, electromagnetic torque, stator flux amplitude and one-phase stator current for proposed scheme under sudden irradiance variations.

Figures 5.24 and 5.25 show the HIL responses of the speed, electromagnetic torque, stator flux amplitude and one-phase stator current for the conventional and proposed schemes. It is observed that the conventional DTC presents relatively large stator flux and torque ripples, also there are much current harmonics. On the other side, the stator flux and torque ripples are much reduced in PTC algorithm. In addition, Figures 5.26 and 5.27 demonstrate that small distortion of the stator current is achieved by using the proposed scheme.

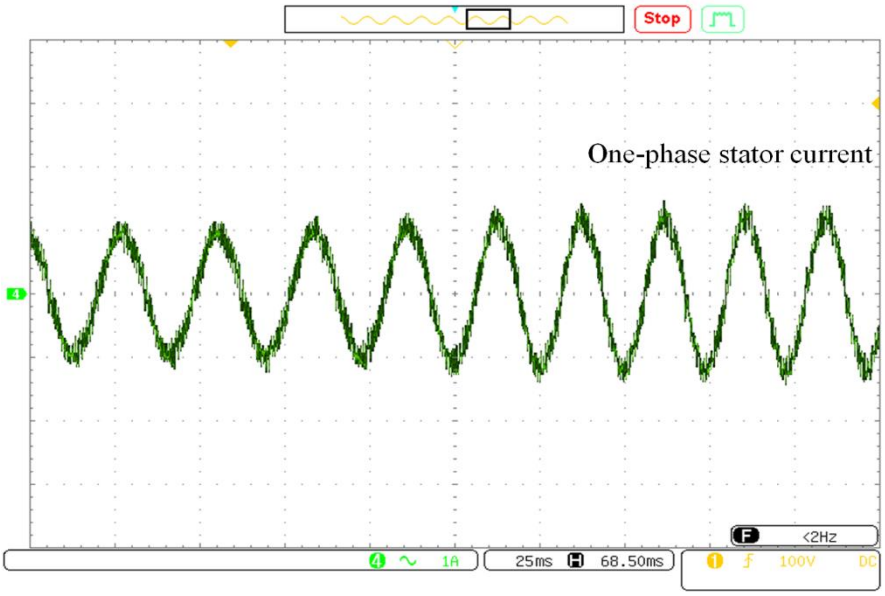

Figure 5.26: Zoom-in view of Figure 5.24 of one-phase stator current for conventional scheme under sudden irradiance variations.

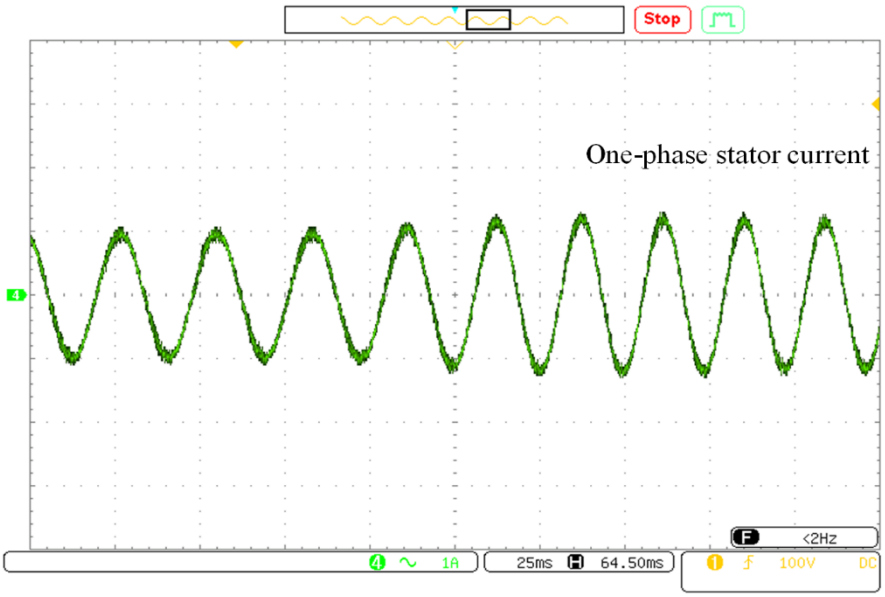

Figure 5.27: Zoom-in view of Figure 5.25 of one-phase stator current for proposed scheme under sudden irradiance variations.

The HIL responses of the hydraulic power and pump flow for the conventional and proposed schemes are shown in Figures 5.28 and 5.29. The parameters of the hydraulic circuit are the same as in the simulations. These HIL results are similar to the simulation results shown in Figure 5.15. In addition, there is a slight improvement in the pump flow with the proposed scheme. This improvement is clearly shown in the energy converted by the pump as well as the pumped water quantity for the long term. In this context, an irradiance profile over a time period

of 10 min similar to the precedent one is considered. The pumped water quantity of conventional and proposed schemes at various pumping heads are summarized in Figure 5.30 for simulation and HIL tests. It can be seen that the proposed scheme presents the highest pumped water quantity at all pumping heads.

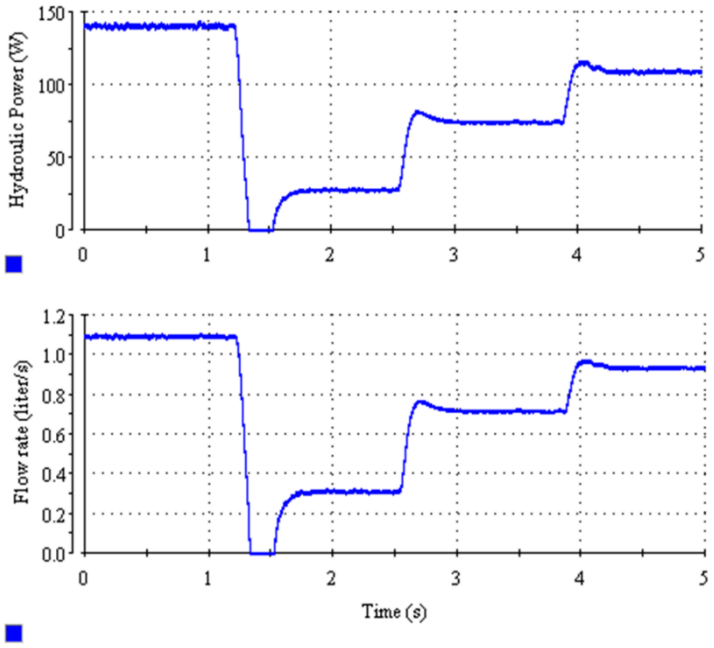

Figure 5.28: HIL responses of the hydraulic power and pump flow for conventional scheme under sudden irradiance variations.

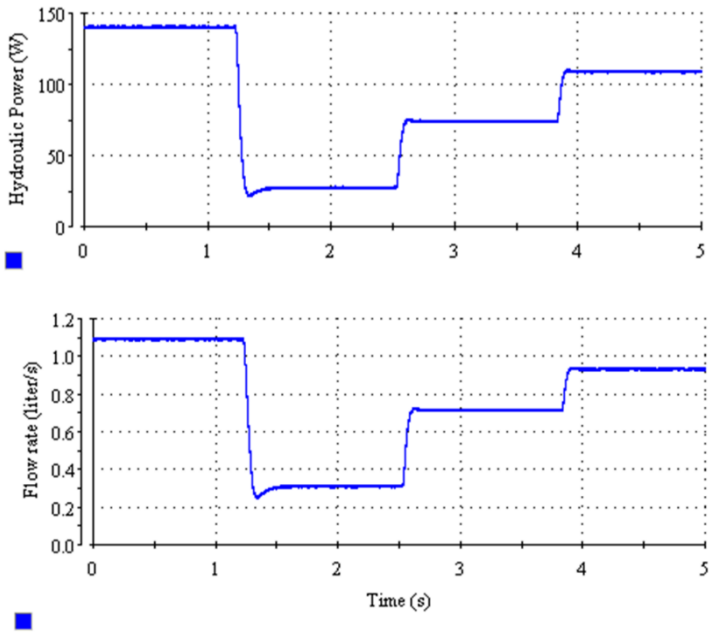

Figure 5.29: HIL responses of the hydraulic power and pump flow for proposed scheme under sudden irradiance variations.

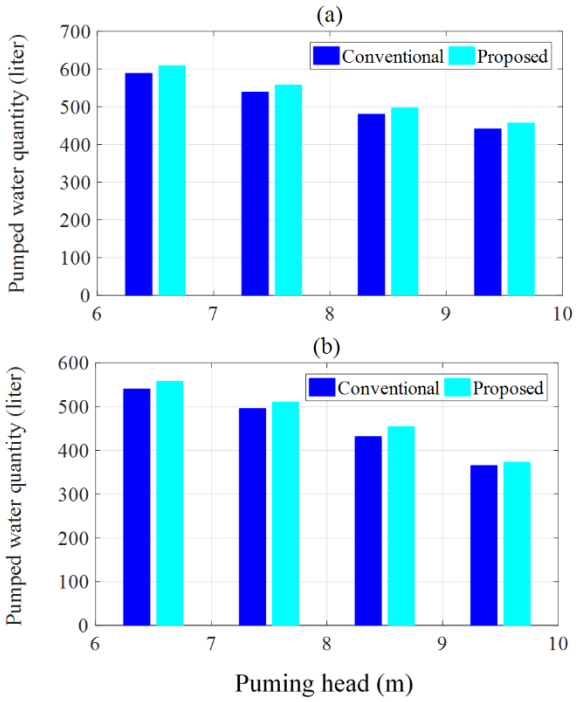

Figure 5.30: Pumped water quantity of conventional and proposed schemes at various pumping heads, during 10 min. (a) simulations, (b) HIL implementations.

Figure 5.31 shows the experimental results for sudden load drop with the proposed control scheme, where the results are similar to those in the simulation. The PV power waveform shows that the proposed algorithm stop tracking the MPP rapidly when a sudden load drop is occurred to protect the IM.

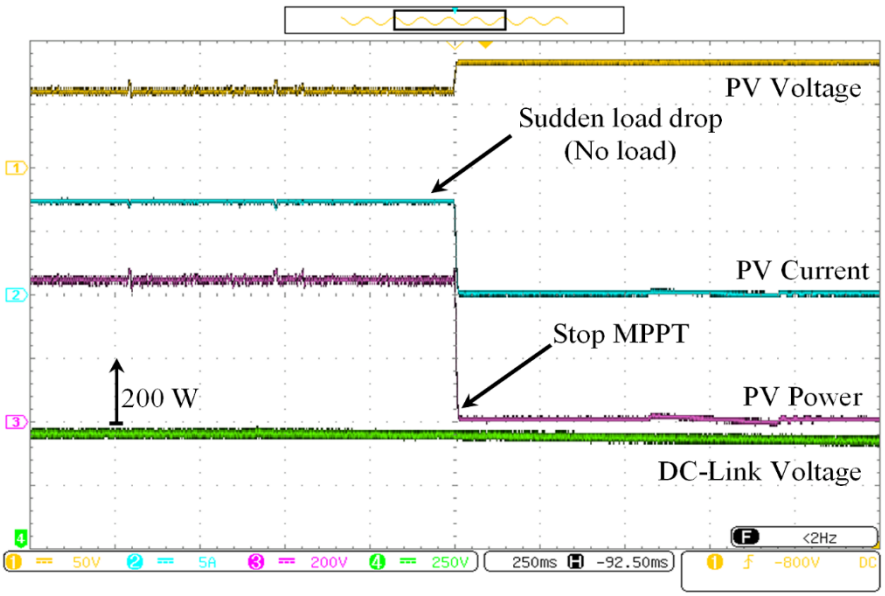

Figure 5.31: HIL responses of the PV voltage, current, power and DC-link voltage for proposed scheme under sudden load drop.

The whole system in the real-time HIL implementation demonstrates a satisfactory dynamic performance when the proposed scheme is used, which proves the effectiveness of the developed controllers and confirms the numerical simulation results obtained previously.

5.7 CONCLUSION

This chapter has proposed a high-performance control scheme for battery-less PV pumping system based on IM, with an improved variable step size P&O current-based MPPT. The proposed CMPPT is employed with MPC current controller. The control scheme uses a PTC algorithm to control the IM drive, with a T-S type FLC to maintain the DC-link voltage constant at the desired reference value.

The performance of the proposed scheme has been found better than that of the conventional one (based on conventional P&O and DTC). Furthermore, as compared to the conventional scheme, simulations and HIL results indicated that the proposed scheme could offer better performance and good robustness to sudden irradiance and load variations. Moreover, the PTC algorithm exhibits a fast torque response, low flux and torque ripples with an effective control for the net DC-link voltage.

Consequently, the proposed scheme offers more pumped water quantity for PV pumping water systems under variable pumping heads.

REFERENCES

[5.1] Periasamy, P., Jain, N.K., Singh, I.P., 2015. A review on development of photovoltaic water pumping system. Renew. Sustain. Energy Rev. 43, 918–925.

[5.2] Antonello, R., Carraro, M., Costabeber, A., Tinazzi, F., Zigliotto, M., 2017. Energy-efficient autonomous solar water-pumping system for permanent-magnet synchronous motors. IEEE Trans. Ind. Electron. 64, 43–51.

[5.3] Jain, S., Thopukara, A.K., Karampuri, R., Somasekhar, V.T., 2015. A single-stage photovoltaic system for a dual-inverter-fed open-end winding induction motor drive for pumping applications. IEEE Trans. Power Electron. 30, 4809–4818.

[5.4] Mohammedi, A., Mezzai, N., Rekioua, D., Rekioua, T., 2014. Impact of shadow on the performances of a domestic photovoltaic pumping system incorporating an MPPT control: A case study in Bejaia, North Algeria. Energy Convers. Manage. 84, 20–29.

[5.5] Betka, A., Attali, A., 2010. Optimization of a photovoltaic pumping system based on the optimal control theory. Sol. Energy 84, 1273–1283.

[5.6] Elgendy, M.A., Zahawi, B., Atkinson D.J., 2010. Comparison of directly connected and constant voltage controlled photovoltaic pumping systems. IEEE Trans. Sustain. Energy 1, 184–192.

[5.7] Packiam, P., Jain, N.K., Singh, I.P., 2013. Microcontroller-based simple maximum power point tracking controller for single-stage solar stand-alone water pumping system. Progr. Photovolt. Res. Appl. 21, 462–471.

[5.8] Elgendy, M.A., Zahawi, B., Atkinson, D.J., 2012. Assessment of perturb and observe MPPT algorithm implementation techniques for PV pumping applications. IEEE Trans. Sustain. Energy 3, 21–33.

[5.9] Ghosh, A., Malla, S.G., Bhende, C.N., 2015. Small signal modelling and control of photovoltaic based water pumping system. ISA Trans. 57, 382–389.

[5.10] Elgendy, M.A., Atkinson, D.J., Zahawi, B., 2016. Experimental investigation of the incremental conductance maximum power point tracking algorithm at high perturbation rates. IET Renew. Power Gener. 10, 133–139.

[5.11] Singh, B., Mishra, A.K., Kumar R., 2017. Solar powered water pumping system employing switched reluctance motor drive. IEEE Trans. Ind. Appl. 5, 3949–3957.

[5.12] Kumar, R., Bhim, S., 2016. Single stage solar PV fed brushless DC motor driven water pump. IEEE Trans. Ind. Appl. 52, 2315–2322.

[5.13] Kumar, R., Bhim, S., 2016. BLDC motor-driven solar PV array-fed water pumping system employing zeta converter. IEEE J. of Emerging and Selected Topics in Power Electron. 52, 1377–1385.

[5.14] Vitorino, M.A., de Rossiter, C.M.B., Jacobina, C.B., Lima, A.M.N., 2011. An effective induction motor control for photovoltaic pumping. IEEE Trans. Ind. Electron. 58, 1162–1170.

[5.15] Chergui, M.-I., Bourahla, M., 2013. Application of the DTC control in the photovoltaic pumping system. Energy Convers. Manage. 65, 655–662.

[5.16] Niapour, S.A.K.H.M., Danyali, S., Sharifian, M.B.B., Feyzi, M.R., 2011. Brushless DC motor drives supplied by PV power system based on Z-source inverter and FL-IC MPPT controller. Energy Conv. Manage. 52, 3043–3059.

[5.17] El-Khatib, M.F., Shaaban, S., El-Sebah, M.I.A, 2017. A proposed advanced maximum power point tracking control for a photovoltaic-solar pump system. Sol. Energy 158, 321–331.

[5.18] Benlarbi, K., Mokrani, L., Nait-Said, M.S., 2004. A fuzzy global efficiency optimization of a photovoltaic water pumping system. Sol. Energy 77, 203–216.

[5.19] Algazar, M.M., AL-monier, Hamdy, EL-halim, H.A., Salem, M.E.E.K., 2012. Maximum power point tracking using fuzzy logic control. Int. J. Electr. Power Energy Syst. 39, 21–28.

[5.20] Altas, I.H., Sharaf, A.M., 2008. A novel maximum power fuzzy logic controller for photovoltaic solar energy systems. Renew. Energy 33, 388–399.

[5.21] Elkholy, M.M., Fathy, A., 2016. Optimization of a PV fed water pumping system without storage based on teaching-learning-based optimization algorithm and artificial neural network. Sol. Energy 139, 199–212.

[5.22] Kulaksız, A., Akkaya, R., 2012. A genetic algorithm optimized ANN-based MPPT algorithm for a stand-alone PV system with induction motor drive. Sol. Energy 86, 2366–2375.

[5.23] Rahrah, K., Rekioua, D., Rekioua, T., Bacha, S., 2015. Photovoltaic pumping system in Bejaia climate with battery storage. Int. J. Hydrogen Energy 40, 13665–13675.

[5.24] Mohamed, A.A.S., Berzoy, A., Mohammed, O., 2017. Design and hardware implementation of FL MPPT control of PV systems based on GA and small-signal analysis. IEEE Trans. Sustain. Energy 8, 279–290.

[5.25] Achour, A., Rekioua, D., Mohammedi, A., Mokrani, Z., Rekioua, T., Bacha, S., 2016. Application of direct torque control to a photovoltaic pumping system with sliding-mode control optimization. Electric Power Compon. Syst. 44, 172–184.

[5.26] Farhat, M., Barambones, O., Fleh, A., Sbita, L., 2016. Variable structure MPP controller for photovoltaic pumping system. Trans Inst Measure Control 39, 1–10.

[5.27] Shadmand, M.B., Balog, R.S., Abu-Rub, H., 2014. Model predictive control of PV sources in a smart DC distribution system: maximum power point tracking and droop control. IEEE Trans. Energy Convers. 29, 913–921.

[5.28] Rodriguez, J., Kazmierkowski, M.P., Espinoza, J.R., Zanchetta, P., Abu-Rub, H., Young, H.A., Rojas, C.A., 2013. State of the art of finite control set model predictive control in power electronics. IEEE Trans. Ind. Informa. 9, 1003–1016.

[5.29] Sivanandam, S.N., Sumathi, S., Deepa, S.N., 2007. Introduction to fuzzy logic using MATLAB. Ed.Springer.

[5.30] Klir, G.J., Yuan, B., 1995. Fuzzy Sets and Fuzzy Logic: Theory and Applications. Prentice Hall.

[5.31] Rodriguez, J., Cortes, P., 2012. Predictive control of power converters and electrical drives. John Wiley & Sons.

[5.32] Rodriguez, J., Kennel, R.M., Espinoza, J.R., Trincado, M., Silva, C.A., Rojas, C.A., 2012. High-performance control strategies for electrical drives: An experimental assessment. IEEE Trans. Ind. Electron. 59, 812–820.

[5.33] Uddin, M., Mekhilef, S., Rivera, M., 2015. Experimental validation of minimum cost function-based model predictive converter control with efficient reference tracking. IET Power Electron. 8, 278–287.

[5.34] Wang, F., Li, S., Mei, X., Xie, W., Rodriguez, J., Kennel, R.M., 2015. Model based predictive direct control strategies for electrical drives: an experimental evaluation of PTC and PCC methods. IEEE Trans. Ind. Informa. 11, 671–681.

[5.35] Wilamowski, B. M., Irwin, J. D., 2011. The industrail electronics handbook, Taylor & Francis group.

Chapter 6

Conclusions

6.1 General conclusion

Photovoltaic (PV) energy represents a promising and motivating renewable energy technology for future electricity generation and recently acquired worldwide attention. In addition, the advantages of PV power, such as no fuel costs, no air pollution, and noiseless, have boosted the demand of this type of energy in many applications for example water pumping system in remote and isolation regions. However, the power generated from such systems depends not only on the climatic conditions, but also highly on the applied control technique. Therefore, MPPT (maximum power point tracking) control techniques become especially important for harnessing the maximum PV energy over a wide range of operating conditions. The standard MPPT algorithm in the industry is the perturb and observe (P&O) algorithm. Nevertheless, this method has some problems such as the power oscillations around the MPP (maximum power point) in steady-state, the slow response speed and the tracking in the wrong direction during fast changing of the environmental conditions.

In this thesis, two modified variable current step size P&O algorithms are proposed for maximum power point tracking of PV systems under sudden and ramp irradiance changes. The modified algorithms are performed to generate the PV output current reference. Then, a model predictive current controller is aimed to regulate the PV current according to the reference current. The advantages of the proposed algorithms were verified by MATLAB/Simulink® simulations and validated experimentally in real-time using a photovoltaic emulator. When compared with both conventional P&O and P&O employed with the model predictive current algorithm, the results of the proposed MPPT algorithms exhibit faster convergence speed, less

oscillation around the MPP under steady-state conditions, and no divergence from the MPP during varying weather conditions.

Moreover, a low-cost photovoltaic pumping system based on three phase induction motor (IM) without the use of chemical energy storage elements was studied. The PV generator-side boost converter performed the maximum power point tracking, while the IM-side two-level inverter regulated the net DC-link voltage and the developed electromagnetic torque by IM, which was coupled with a centrifugal pump. To improve system performance during sudden irradiance and load changes, an improved variable step size P&O algorithm was proposed. The proposed algorithm was based on a current control approach of the boost converter with a model predictive current controller to select the optimal control action. Moreover, predictive torque and flux control (PTC) was used to control IM drive, due to its advantages such as faster torque response, lower torque ripple, and simplicity of implementation. Furthermore, a T-S type fuzzy logic controller was developed in order to regulate the DC-link voltage, by producing the torque reference for PTC algorithm. To show the performance improvement of the proposed control scheme for PV pumping system, a complete simulation model was developed using MATLAB/Simulink® environment and confirmed through real-time hardware in the loop (HIL) system. The obtained results indicated the excellent performance of the proposed control scheme, which was much better than the conventional scheme based on conventional techniques (P&O algorithm and direct torque control (DTC)).

6.2 AUTHOR'S CONTRIBUTIONS

The major contributions of this research work can be summarized as follows:

- Two modified P&O algorithms based on model predictive current controller for MPPT of PV systems are proposed under sudden irradiance changes.
- Development of a photovoltaic emulator for testing and evaluation the proposed MPPT algorithms based on a flexible programmable source. The developed emulator shows a perfect reproduction of the PV array characteristics under different irradiance and temperature levels.
- An effective control scheme for battery-less PV water pumping system is proposed.
- An improved variable step size P&O CMPPT for PV pumping system is suggested to solve sudden changing irradiation problem as well as able to protect the IM under sudden load drops.
- A fuzzy logic controller is developed to regulate accurately the DC-link voltage and to produce the torque command without the use of the speed control loop.

- To improve the power quality and PV pumping system efficiency, a predictive torque and flux algorithm is used to control the IM drive.

6.3 FUTURE WORKS

The following future research works are suggested as an extension to the knowledge presented in this thesis:

- Improvement of the proposed MPPT algorithms to extract the global maximum power point under partially shaded PV system condition.
- Integration of the high-accuracy estimators or observers in the proposed control scheme for the PV pumping system can be improved the control performance and decreased the sensor number, which reduced the overall cost of the system.
- Application of the proposed control scheme philosophies to a two-stage grid-connected PV system.
- Investigation of the current source inverter (CSI) for PV pumping system. The optionality CSI voltage boosting capability allows a low-voltage PV array to be motor interfaced without the need of a transformer or an additional boost stage.
- Performance improvement of the predictive strategy. Despite many best features of MPC strategy, numerous challenges are described in the literature such as weighting factor selection and variable switching frequency nature.
- Implementation of the proposed control scheme using a field programmable gate array (FPGA) control board instead dSPACE platform. FPGA devices are generally cheaper than dSPACE system and are suited for high-speed demanding application.

List of Publications

The following list includes all the papers published by the author during his graduate studies. Papers designated by " ★ " are directly related with research results presented in this dissertation.

Journal Papers

★ [1] **Billel Talbi**, Fateh Krim, Toufik Rekioua, Saad Mekhilef, Abdelbaset Laib, Abdesslam Belaout, 2018. A high-performance control scheme for photovoltaic pumping system under sudden irraadaince and load changes. Solar Energy 159, 353–368. https://doi.org/10. 1016/j.solener.2017. 11.009 (Impact Factor: 4.018).

★ [2] **Billel Talbi**, Fateh Krim, Toufik Rekioua, Abdelbaset Laib, Hamza Feroura, 2017. Design and hardware validation of modified P&O algorithm by fuzzy logic approach based on model predictive control for MPPT of PV systems. Journal of Renewable and Sustainable Energy 9, 043503–14. http://dx.doi.org/10.1063/1.4999961 (Impact Factor: 1.135).

[3] Hamza Feroura, Fateh Krim, **Billel Talbi**, Abdelbaset Laib, Abdesslam Belaout, 2017. Finite-set model predictive direct power control of grid connected current source inverter. Elektronika ir Elektrotechnika 23(5), 36–40. http://dx.doi.org/10.5755/j01.eie.23.5.19240 (Impact Factor: 0.859).

[4] Hamza Feroura, Fateh Krim, **Billel Talbi**, Abdelbaset Laib, Abdesslam Belaout, 2017. Sensorless field oriented control of current source inverter fed induction motor drive. Revue Roumaine Des Sciences Techniques, Paper Accepted for Publication (Impact Factor: 1.036).

Conference Papers

[5] **Billel Talbi**, Fateh Krim, Abdelbaset Laib, Hamza Feroura, 20017. High-Accuracy Sliding Mode Observer for Boost Converter with MPC Switching Control. In: Proc. ICENT'17, M'sila, Algeria, Nov. 2017.

[6] Hamza Feroura, Fateh Krim, **Billel Talbi**, Abdelbaset Laib, 2017. Photovoltaic grid

connected current source inverter with resonance active damping method. In: Proc. ICENT'17, M'sila, Algeria, Nov. 2017.

[7] Abdelbaset Laib, Fateh Krim, **Billel Talbi**, Hamza Feroura, 2017. Current oriented MPPT based on fuzzy logic and predictive controllers for photovoltaic systems with SEPIC converter. In: Proc. ICENT'17, M'sila, Algeria, Nov. 2017.

[8] Abdelbaset Laib, Fateh Krim, **Billel Talbi**, Abbas Kihal, Abdeslem Sahli, 2017. Predictive control strategy for double-stage grid connected PV systems. In: Proc. ICEECA'17, Constantine, Algeria, Nov. 2017.

[9] Hamza Feroura, Fateh Krim, **Billel Talbi**, Abdelbaset Laib, 2017. Finite-set model predictive voltage control for islanded three-phase current source inverter. In: Proc. ICEE-B, Boumerdes, Algeria, Oct. 2017.

[10] Abdelbaset Laib, Fateh Krim, **Billel Talbi**, Hamza Feroura, 2017. Fuzzy logic maximum power point tracking through sliding mode current control for PV systems. In: Proc. IC-AIRES'17, Tipasa, Algeria, Oct. 2017.

[11] Hamza feroura, Fateh Krim, **Billel Talbi**, Abdelbaset Laib, Abdesslam Belaout, 2017. Finite-set model predictive direct power control of grid connected current source inverter. In: Proc. 21st international conference electronics, Palanga , Lithuania, Jun. 2017.

[12] Abdesslam Belaout, Fateh Krim, **Billel Talbi**, Hamza Feroura, Abdelbaset Laib, Semcheddine Bouyahia, Abderrazak Arabi, 2017. Development of real time emulator for control and diagnosis purpose of photovoltaic generator. In: Proc. ICSC'17, Batna, Algeria, May. 2017.

[13] Abdelbaset Laib, Fateh Krim, **Billel Talbi**, 2017. Simulation of variable step size incremental conduction MPPT through Predictive current control. In: Proc. ICESD'17, Adrar, Algérie, Feb. 2017.

[14] Abdelbaset Laib, Fateh Krim, **Billel Talbi**, 2016. An improved control for two-stage grid-connected photovoltaic systems. In: Proc. ICESTI'16, Annaba, Algérie, Nov. 2016.

★ [15] **Billel Talbi**, Fateh Krim, Abdelbaset Laib, 2016. An Improved Variable Step Size P&O

Current-Based MPPT Employing FSC-MPC for Sudden Irradiance change. In: Proc. Batna, CEE'16, Algérie, Oct. 2016.

[16] Abdelbaset Laib, Fateh Krim, **Billel Talbi**, 2016. Simulation of variable step size incremental conduction MPPT through sliding mode current control. In: Proc. Batna, CEE'16, Algérie, Oct. 2016.

[17] Hamza Feroura, Fateh Krim, **Billel Talbi**, 2016. A fuzzy logic control strategy for three phase current source inverter based on model predictive current control. In: Proc. Batna, CEE'16, Algérie, Oct. 2016.

★ [18] **Billel Talbi**, Fateh Krim, Hamza Feroura, 2015. Modified P&O algorithm by Takagi-Sugeno fuzzy logic approach for MPPT of PV systems. In: Proc. ICATS'15, Annaba, Algérie, Nov. 2015.

★ [19] **Billel Talbi**, Fateh Krim, Hamza Feroura, 2015. Predictive torque and flux control for three-phase induction motor. In: Proc. IECEC'15, Sétif, Algérie, Oct. 2015.

Other

★ [20] **Billel Talbi**, Fateh Krim, 2016. Conception et implémentation d'un système de pompage photovoltaïque. Participation in the UFAS1 Doctoriales dedicated to innovation, Sétif, Algérie, Mai. 2016.

Appendix: Real-Time Photovoltaic Emulator

The real-time photovoltaic (PV) emulator is a nonlinear power supply capable of producing the current-voltage (I-V) characteristic of the PV array. The PV emulator functions as a power source in the experimental test bench of the PV energy generating system to allow repeatable testing conditions. The PV emulator offers a convenient control of climatic conditions (irradiance and temperature) to allow faster and more efficient PV energy generation system testing.

In this thesis, the developed real-time photovoltaic (PV) emulator, as shown in Figure A.1, is achieved with a programmable power supply (APS-1102A GW Instek). The PV array model is implemented in real-time via dSPACE DS 1104 system through the Matlab/Simulink®. The operation of the developed real-time PV emulator is based on measuring the value of the output current from the analog port of the programmable power supply. Then, this measuring is insert to the implemented PV array model through the analog to digital port of the dSPACE interface. The mathematical model of PV array is constructed in away permit to give the voltage reference related to the measured current. Therefore, the implemented model will output reference voltage signal through the digital to analog port to the power supply to set its voltage related to the PV characteristic.

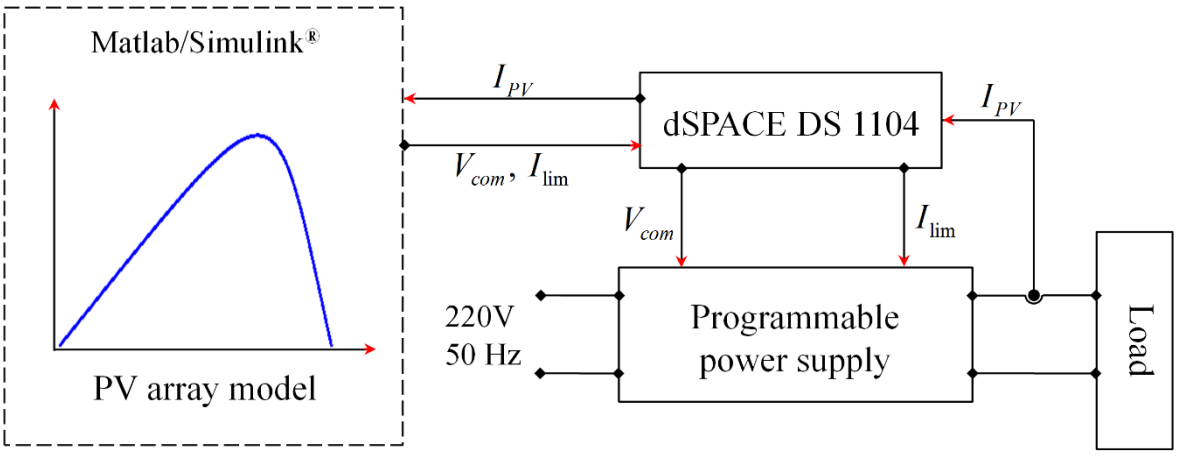

Figure A.1: Block diagram for the developed PV Emulator.

The PV emulator is implemented in the ControlDesk interface and allows real-time control of the climatic conditions. Figure A.2 shows the electrical behavior of the real-time PV emulator for the considered PV array (consist of four pb solar BP SX 120 modules, connected 2×2 in

series and parallel) under standard test conditions (STC), which means an irradiance of 1000 W/m² at 25°C temperature.

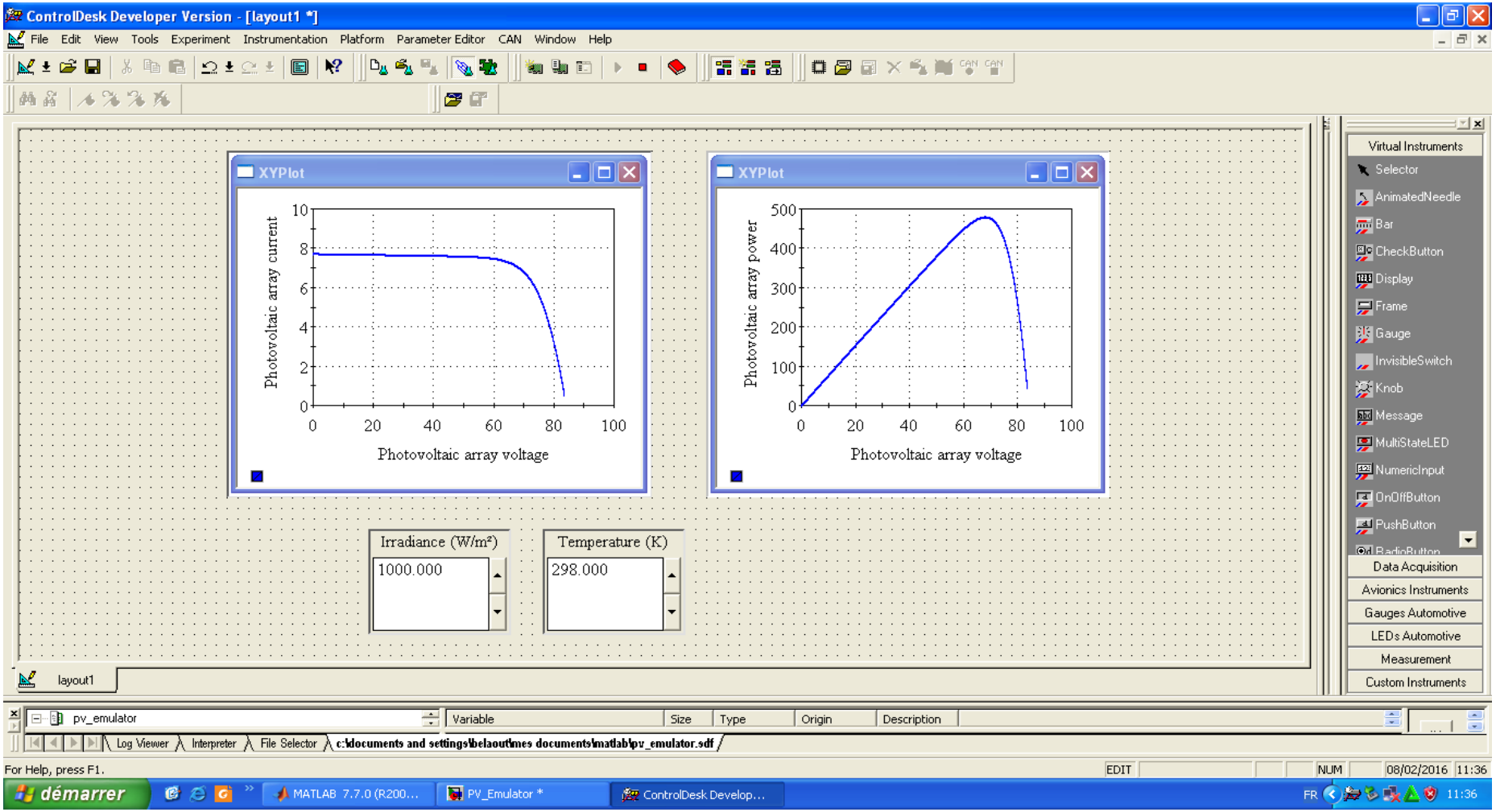

Figure A.2: Electrical behavior of the developed PV Emulator using ControlDesk interface.

Contribution à l'Amélioration de la Commande d'un Système de Pompage Photovoltaïque

Abstract :

This thesis is part of the research work dedicated for exploitation of solar photovoltaic energy. Due to the increasing energy demands, the use of photovoltaic energy has increased significantly in the worldwide, especially in remote and isolation regions. Off-grid photovoltaic systems, particularly water pumping system, is becoming more widespread. The use of photovoltaic energy as an energy source for water pumping is considered as one of the most promising areas of the photovoltaic applications. The photovoltaic pumping systems are basically operated in two ways, with or without battery bank. The study presented in this thesis focuses on the improvement photovoltaic power extracting for a battery-less pumping system. In this context, many researchers are committed to invent the algorithms for extracting the maximum energy from a photovoltaic array. It is the principle named maximum power point tracking (MPPT), which is the main object of our research. In the first, various MPPT strategies based on fuzzy logic and predictive control for an off-grid photovoltaic system with resistive load have been developed to improve the performance of the perturb and observe (P&O) algorithm under sudden irradiance changes. The different MPPT strategies have been simulated and verified experimentally using a laboratory bench based on the photovoltaic emulator. Afterwards, a high-performance control scheme have been developed for a photovoltaic pumping system based on three-phase induction motor, in order to maximize the delivered power by the photovoltaic array, to protect the motor under sudden load drops, to regulate the DC-link voltage and to minimize the electromechanical losses in the conversion chain. The developed control scheme is based on fuzzy logic and predictive control. In addition, this scheme has been confirmed through simulation and real-time hardware in the loop system. Simulations presented in this thesis are performed with MATLAB/Simulink® environment, and practical implementation in real-time has been done through a dSPACE DS 1104 system.

Keywords : Photovoltaic energy; Photovoltaic pumping system; MPPT; Fuzzy logic; Predictive control.

Contribution à l'amélioration de la commande d'un système de pompage photovoltaïque

Résumé :

Cette thèse s'inscrit dans les travaux de recherche menés sur l'exploitation de l'énergie solaire photovoltaïque. L'utilisation de cette énergie connaît une croissance significative dans le monde, devant la demande croissante d'énergie électrique, essentiellement pour les besoins des régions éloignées et isolées. Les systèmes photovoltaïques hors réseau, en particulier les systèmes de pompage d'eau, commencent à trouver de grandes applications. L'utilisation du photovoltaïque comme source d'énergie pour le pompage d'eau est considérée comme l'un des domaines les plus prometteurs d'application de l'énergie photovoltaïque. Les systèmes de pompage photovoltaïque se présentent fondamentalement de deux façons selon qu'ils fonctionnent avec ou sans un banc de batteries. L'étude présentée dans cette thèse se focalise sur l'optimisation de l'exploitation de l'énergie photovoltaïque dans un système de pompage sans utilisation des batteries. Dans ce contexte, de nombreux chercheurs se sont attachés à inventer des algorithmes permettant de récupérer le maximum d'énergie photovoltaïque c'est le principe nommé maximum power point tracker (MPPT) qui est l'objet principal de notre sujet. En premier lieu, diffèrent stratégies de commande MPPT basées sur la logique floue et la commande prédictive pour un système photovoltaïque hors réseau avec une charge résistive, ont été développées, simulées et validées sur un banc d'essai expérimentale fondé sur un émulateur photovoltaïque dont le but d'optimiser les performances de l'algorithme perturbation et observation (P&O) dans le cas de changement brusque d'irradiation. Par la suite, un schéma de commande pour un système de pompage photovoltaïque basé sur un moteur triphasé à induction est développé afin de maximiser l'énergie délivrée par le panneau photovoltaïque, de protéger le moteur durant les chutes soudaines de la charge, de régler la tension du bus continue et de minimiser les pertes de la conversion électromécaniques dans la chaine de conversion. Le schéma de commande développé est aussi basé sur la logique floue et la commande prédictive. De plus, ce schéma de commande est simulé et implémenté en temps-réel sur un banc hardware in the loop. La simulation de ces travaux a été mise en œuvre à l'aide du logiciel MATLAB/Simulink® et l'implantation en temps réel a été validée sous la plateforme dSPACE DS 1104.

Mots clés : Energie photovoltaïque; Système de pompage photovoltaïque; MPPT; La logique floue; La commande prédictive.

المساهمة في تحسين التحكم لنظام ضخ كهروضوئي

ملخص:

تصنف هذه الأطروحة ضمن أعمال البحث التي أجريت على استغلال الطاقة الشمسية الكهروضوئية. اذ ان استخدام واستغلال هذه الطاقة عرف انتشارا وتطورا هاما عبر دول العالم، وهذا نظرا للطلب المتزايد للطاقة الكهربائية وخاصة منها المناطق النائية والمعزولة. بدأت الأنظمة الكهروضوئية المفصولة عن الشبكة الكهربائية العامة في إيجاد تطبيقات كبيرة، ولا سيما انظمة ضخ المياه. ان استخدام الانظمة الكهروضوئية كمصدر للطاقة من اجل ضخ المياه تعتبر واحدة من أكثر المجلات الرائدة لتطبيق الطاقة الكهروضوئية. تصنف أنظمة الضخ الكهروضوئية الي نوعين اعتمادا على التخزين في البطاريات أو لا. تركز الدراسة المقدمة في هذه الرسالة على الاستفادة المثلى في استغلال الطاقة الضوئية في نظام الضخ الكهروضوئية بدون استخدام البطاريات. في هذا السياق، ركز العديد من الباحثين على اختراع نظام لتتبع نقطة الطاقة الأعظمية للنظام الكهروضوئي تحت تغير الإشعاع الشمسي وقد سمي تتبع نقطة الطاقة الأعظمية (MPPT). ويعتبر تطوير هذا النظام هو هدفا رئيسيا في موضوع بحثنا. أولا، تم تطوير عدة استراتيجيات مختلفة ل (MPPT) اعتمادا على تحكم المنطق الغامض والتحكم التنبئي لنظام الكهروضوئي خارج الشبكة الكهربائية مع مقاومة. تم التحقق من فعالية الاستراتيجيات المقترحة بواسطة المحاكاة الرقمية والتجارب التطبيقية على أساس المحاكي الكهروضوئي تحت التغير المفاجئ في الاشعاع الشمسي. فيما بعد، تم تطوير التحكم لنظام الضخ الكهروضوئية المزود بمحرك غير متزامن عن طريق تحقيق تتبع مثالي لأقصى قدر من الطاقة يمكن أن تسلمه اللوحة الشمسية، حماية المحرك خلال السقوط المفاجئ للحمولة، ضبط الجهد المستمر بين المحولين وتقليل خسائر التحويل الكهرو ميكانيكية في سلسلة التحويل .يستند مخطط السيطرة المطور أيضا على منطق التحكم الغامض والتحكم التنبئي. تم محاكاة هذا المخطط وتطبيقه في الزمن الحقيقي باستخدام بنظام hardwar in the loop. جميع هذه الأعمال تم التحقق من صحتها في منصات المحاكاة باستعمال برنامج ما تلاب وبعد ذلك تم تنفيذها في الواقع بتطبيق تجربي باستعمال البطاقة الرقمية dSPACE DS 1104 .

الكلمات المفتاحية : الطاقة الكهروضوئية; نظام ضخ كهروضوئي; MPPT; المنطق الغامض; التحكم التنبئ